Bistable surfaces activation by piezoelectric materials, application to haptic feedback

Taha Ajnada

université
PARIS-SACLAY

Activation de surfaces bistables par des matériaux piézoélectriques, application au retour haptique

Thèse de doctorat de l'Université Paris-Saclay

École doctorale n° 575 Electrical, optical, bio: physics and engineering (EOBE)
Spécialité de doctorat : Génie électrique
Unité de recherche : Université Paris-Saclay, CentraleSupélec, CNRS, Laboratoire de Génie Electrique et Electronique de Paris, 91192, Gif-sur-Yvette, France.
Référent : CentraleSupélec

Thèse présentée et soutenue à Gif-sur-Yvette, le 24/11/2021, par

Taha AJNADA

Composition du jury :

Lionel Petit Professeur, INSA de Lyon (LGEF)	Président
François Costa Professeur, Université Paris Est Créteil (SATIE)	Examinateur
François Pigache Maître de conférences HDR, INP-ENSEEIHT (LAPLACE)	Rapporteur
Frédéric Giraud Maître de conférences HDR, Université de Lille (L2EP)	Rapporteur
Yves Bernard Professeur, Université Paris-Saclay (GeePs)	Directeur de thèse
Laurent Daniel Professeur, CentraleSupélec (GeePs)	Encadrant

Thèse de doctorat

NNT: 2021UPAST106

Acknowledgements

I thank you, reader friend, for your interest in this work and I wish you find an answer.

I would like to express my gratitude to my supervisors Prof. Yves Bernard and Prof. Laurent Daniel who despite their responsibilities: Dean of Polytech Paris-Saclay and Head of the Chair of Automobile Mechatronics Faurceia respectively, were very available to take up my challenge: thank you for your guidance and encouragements throughout this work.

I want to thank Dr. François Pigache and Dr. Frédéric Giraud for having accepted to report on my thesis manuscript, for their precious remarks and professionalism in the reports.

I also thank Prof. Lionel Petit for having accepted to chair my thesis jury and Prof. François Costa for having participated and for his benevolence and his smile, magnificent sources of confidence for the great moment of the defence.

Many thanks to:

Abdellahi, Abderrahmane, Ali, Anderson, Bastien, Ghida, Ikram, Kangyi, Safae, Valentin... Abderraouf, Chaimae, Frédéric and Luiz... Sandrine for the moments of friendship, entreaide and respect that we shared in both the B_4 and C_2 corridors.

Eric, Laurent, Mahmoud, Mathieu, Maya, Romain, Xavier, for all the very interesting scientific discussions and convivial moments in the GeePs laboratory.

Sofiane Ghenna for accepting my internship on the subject of surface activation and for having initiated this adventure.

Mohammed Serhir. If the result of such a human adventure was just to meet such a person and have discussions with him and learn from his intellectual background, that would have been enough.

Ahmed Barry, to whom I owe a grace.

Abdelahaq, Abderrahmane, AbduLah, Anas, Anouar, Ayoub, Elkharchi, Hichem, Ibrahim, Oussama, Modar, Mustapha, Nouaamane, Saad, for the magnificent three years spent together on the Saclay plateau, with brotherhood, mutual respect and good humour.

Abdessamad, Ali, Hamza, Ismael, Youness and Zakaria for the example of fraternity and friendship that they give.

All childhood friends from my hometown Tissaf to have contributed to the construction of my personality.

My teachers since elementary school as well as my fellow competitors for their direct and indirect inspiration, advice and moral encouragement.

My family... Sisters and my brother for supporting the guy who I am.

My parents. Whom I work for to make proud.

Almighty God. AlhamduliLah.

Synthèse en français de la thèse

Introduction

Dans l'automobile, l'aéronautique et la médecine, l'ingénierie cherche à remplacer les systèmes mécaniques par des dispositifs électriques. Des matériaux dits intelligents, formant des capteurs ou des actionneurs, apparaissent avec leurs propriétés intrinsèques de transformation électromécanique pour répondre à ce besoin, notamment pour satisfaire des conditions spécifiques d'encombrement ou de dynamique.
En particulier, les **matériaux piézoélectriques** sont aujourd'hui d'une grande variété d'applications, dédiées à l'utilisation en faible et moyenne puissance. Parmi ces applications, il y a le **retour haptique**, qu'il soit un retour tactile ou un retour d'effort.
Lorsque nous interagissons avec un environnement virtuel, nous utilisons principalement un retour visuel et auditif. Des recherches ont été consacrées à l'ajout d'une sensation haptique à la **surface** touchée par la main ou plutôt par les doigts.
Afin de reproduire des sensations liées à la surface sous le doigt, nous avons cherché dans ce travail à exploiter la propriété de passage d'un état stable à un autre, de certains systèmes dits **bistables**, puisque cela peut générer un retour perçu par le doigt. Les moyens choisis pour **activer** le système bistable et donc générer un retour haptique sont les actionneurs piézoélectriques.

Ce manuscrit de thèse est composé de quatre chapitres :

Chapitre 1 : Introduction générale Un état de l'art est présenté sur la piézoélectricité, ainsi que sur les systèmes bistables, sur le domaine haptique et enfin sur l'utilisation des matériaux piézoélectriques pour actionner des systèmes bistables, pour des applications de retour haptique.

Chapitre 2 : Caractérisation des systèmes bistables Deux types de systèmes bistables sont modélisés, prototypés et caractérisés mécaniquement pour comprendre les niveaux de force caractéristiques qu'ils subissent en flambement et en basculement bistable.

Chapitre 3 : Modélisation de l'actionnement piézoélectrique Une étude paramétrique est réalisée sur les modèles analytiques d'actionnement statique des matériaux piézoélectriques, puis comparée à une étude paramétrique numérique pour conclure sur la validité des modèles de la littérature dans notre cas d'étude.

Chapitre 4 : Activation piézoélectrique de systèmes bistables Une preuve de concept de l'activation de systèmes bistables par actionnement piézoélectrique est réalisée, servant de validation expérimentale du travail de modélisation effectué au préalable dans les chapitre précédents.

Chapitre 1 : Introduction générale

Nous travaillons dans le contexte de l'industrie automobile. L'objectif est de concevoir une application qui génère du retour haptique au niveau du doigt, pour une intégration dans un tableau de bord de voiture.
L'application consiste en un système bistable, activé par des matériaux piézoélectriques afin qu'il puisse passer de son premier état d'équilibre stable au second, et par conséquent générer un effort ressenti par le doigt.
Toutes ces notions de piézoélectricité, de bistabilité et de systèmes haptiques seront développées dans ce premier chapitre.
L'objectif de ce chapitre est de présenter brièvement l'état de l'art des matériaux piézoélectriques, et notamment leurs lois de comportement. Ensuite, la notion de bistabilité, notamment en mécanique, sera présentée avec des exemples de compréhension. Ainsi, la notion d'haptique et de retour haptique sera élaborée avec des exemples d'applications existants dans l'industrie et dans la recherche. Une dernière partie sera consacrée au rassemblement de la bistabilité et des systèmes haptiques pour en faire l'application envisagée.

Introduction à la piézoélectricité

La piézoélectricité est une propriété cristalline intrinsèque de certains matériaux pour convertir l'énergie mécanique qu'ils reçoivent en énergie électrique, ou vice versa.
L'effet piézoélectrique peut se produire si le matériau cristallin est composé de particules chargées et peut être polarisé.
Le couplage entre les paramètres thermiques, élastiques et électriques d'un matériau peut être introduit formellement en utilisant l'approche thermodynamique.
En considérant les transformations isentropiques et isothermes, avec l'hypothèse de symétrie des tenseurs de contrainte et de déformation, le comportement piézoélectrique d'un matériau peut être présenté sous le format matriciel suivant :

$$\begin{array}{l} \\ \text{Actionneur} \\ \\ \\ \\ \\ \\ \text{Capteur} \\ \\ \\ \end{array} \overbrace{\left\{\begin{array}{c} \\ S_1 \\ S_2 \\ S_3 \\ S_4 \\ S_5 \\ S_6 \\ \hline D_1 \\ D_2 \\ D_3 \end{array}\right\}}^{} = \begin{array}{c} \overbrace{}^{\text{compliance}} \quad \overbrace{}^{\text{couplage}} \\ \left(\begin{array}{cccccc|ccc} s_{11}^E & s_{12}^E & s_{13}^E & 0 & 0 & 0 & 0 & 0 & d_{31} \\ s_{12}^E & s_{22}^E & s_{23}^E & 0 & 0 & 0 & 0 & 0 & d_{32} \\ s_{13}^E & s_{23}^E & s_{33}^E & 0 & 0 & 0 & 0 & 0 & d_{33} \\ 0 & 0 & 0 & s_{44}^E & 0 & 0 & 0 & d_{24} & 0 \\ 0 & 0 & 0 & 0 & s_{55}^E & 0 & d_{15} & 0 & 0 \\ 0 & 0 & 0 & 0 & 0 & s_{66}^E & 0 & 0 & 0 \\ \hline 0 & 0 & 0 & 0 & d_{15} & 0 & \varepsilon_{11}^T & 0 & 0 \\ 0 & 0 & 0 & d_{24} & 0 & 0 & 0 & \varepsilon_{22}^T & 0 \\ d_{31} & d_{32} & d_{33} & 0 & 0 & 0 & 0 & 0 & \varepsilon_{33}^T \end{array}\right) \\ \underbrace{}_{\text{couplage}} \quad \underbrace{}_{\text{permittivité}} \end{array} \left\{\begin{array}{c} T_1 \\ T_2 \\ T_3 \\ T_4 \\ T_5 \\ T_6 \\ \hline E_1 \\ E_2 \\ E_3 \end{array}\right\} \tag{1}$$

avec S_i et T_j les composantes des tenseurs de déformation et de contrainte (en Pa) dans la base des matrices respectivement (i, j = $1, 2, 3, 4, 5, 6$). D_k et E_l sont les composantes des vecteurs de déplacement électrique (en C/m^2) et de champ électrique (en V/m) respectivement (k, l = $1, 2, 3$). s_{ij}^E , d_{il} = d_{kj} (en raison de la symétrie géométrique du cristal) et ε_{kl} sont les composantes réduites des tenseurs de compliance élastique, de déformation piézoélectrique et de permittivité diélectrique respectivement.

Considérons une structure "S" dont l'axe principal est la direction 1. Nous nous intéressons à un couplage 31, où le matériau piézoélectrique est polarisé selon la direction 3. Nous considérons le couplage entre les quantités mécaniques axiales (S_1 et T_1) et les quantités électriques transversales (D_3 et E_3).
Avec ces considérations, nous pouvons déduire de la formulation matricielle de l'équation (1) les deux lois suivantes :

$$\begin{aligned} S_1 &= s_{11}^E T_1 + s_{12}^E T_2 + s_{13}^E T_3 + d_{31} E_3 \\ D_3 &= d_{31} T_1 + d_{32} T_2 + d_{33} T_3 + \varepsilon_{33}^T E_3 \end{aligned} \tag{2}$$

L'étude sera faite dans le cas particulier de la résistance des matériaux, concernant des structures de type poutre.

Les assertions suivantes seront détaillées dans le manuscrit.

Dans le cas de l'hypothèse des poutres concernant la structure "S", on assume que $T_2 = T_3 = 0$. La loi de comportement résultante, et que nous allons utiliser dans la suite de ce mémoire s'écrit sous la forme :

$$\begin{aligned} S_1 &= s_{11}^E T_1 + d_{31} E_3 \\ D_3 &= d_{31} T_1 + \varepsilon_{33}^T E_3 \end{aligned} \tag{3}$$

Introduction à la bi-stabilité

La stabilité est l'aptitude d'un système à rester dans un état donné. En mécanique, cet état correspond à un minimum de l'énergie potentielle du système. Lorsque la ou les forces extérieures sont relâchées, le mécanisme doit alors converger vers sa position dite stable.

Un système, qu'il soit mécanique, électrique, chimique ou autre..., peut avoir un état stable, tout comme il peut en avoir plusieurs.

Les systèmes bistables possèdent deux et seulement deux états d'équilibre stables, séparés par un état d'équilibre instable.
Les systèmes bistables présentent de multiples avantages. Ils peuvent rester dans deux positions d'équilibre à énergie interne non nulle, sans apport d'énergie et malgré les petites perturbations externes. Dans le domaine mécanique, grâce à cette capacité, ils trouvent des applications dans de nombreux dispositifs, tels que les interrupteurs, les vannes, les fermetures et les fermoirs....

Pour illustrer les caractéristiques statiques d'une structure mécanique bistable, nous présentons le système unidimensionnel de la Figure 1.

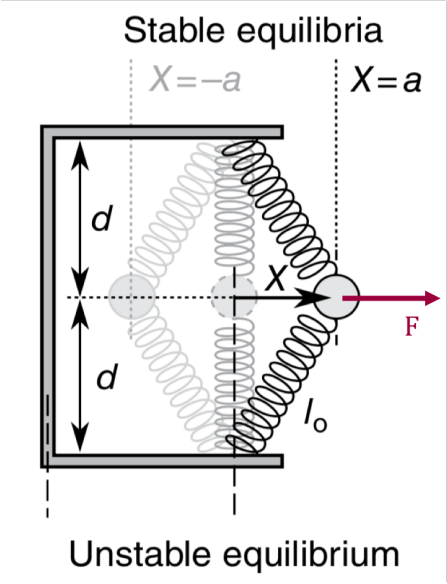

Figure 1: *Système bistable composé de ressorts, d'une masse et d'un cadre. Ici $l_o > d$ ce qui fait de la configuration centrale $X = 0$ une position instable d'équilibre statique [HW17]*

Pour ce système illustré, deux ressorts identiques de longueur l_o relient une masse à un cadre environnant d'une portée de $2d$.
Dans ce cas, où $l_0 > d$, les ressorts appliquent une force sur la masse inertielle. Ainsi, la masse ne peut pas être "facilement" maintenue dans la position centrale verticale.
Cette configuration à déplacement nul est une position d'équilibre instable, tandis que deux positions "faciles" à tenir, sans application de forces extérieures, existent symétrique-

ment de part et d'autre de la position centrale, à $X = \pm a$.

Le système masse-ressort et le cadre possèdent donc trois positions d'équilibre, dont deux et seulement deux sont faciles à tenir sans aucun effort extérieur. C'est la propriété des systèmes dits **bistables**. Cette propriété sera démontrée par une approche énergétique dans le mémoire.

Il existe plusieurs catégories de mécanismes bistables. Cinq grandes familles sont mentionnées ci-après [Caz09] : les mécanismes bistables multi-parties, les mécanismes bistables planaires pour MEMS, les mécanismes bistables pré-contraints, les mécanismes bistables à plaques préformées et les mécanismes bistables avec plaque anisotrope.

Introduction au retour haptique

Un dispositif haptique est une interface homme-machine, qui se place entre l'utilisateur humain et le domaine virtuel, afin d'enrichir la perception de l'utilisateur dans cet environnement par l'utilisation de capteurs cutanés et musculaires, en particulier ceux de la surface palmaire de la main.

Il existe deux types de sensations haptiques : le premier est le retour d'effort (ou retour kinesthésique), relatif aux muscles et aux articulations sollicités par les efforts et les déplacements, le second est le retour tactile qui concerne les capteurs sous-cutanés et recueille des informations sur les surfaces, la rigidité, les vibrations, la température, etc.

La classification du retour haptique est présentée dans la Figure 2.

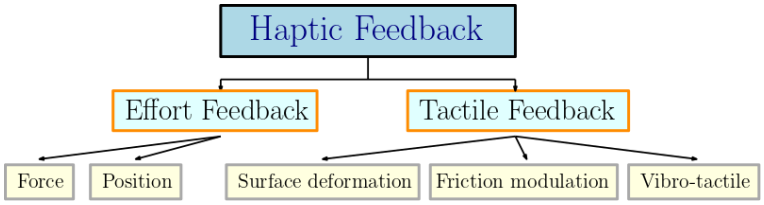

Figure 2: *Classification des catégories de retour haptique, adapté de [Kac20]*

Pour le second type, la famille des dispositifs qui explorent le retour tactile est basée sur la génération de sensations subtiles qui stimulent les mécanorécepteurs.
C'est le développement de ce type de retour haptique qui a servi aux appareils portatifs et aux écrans tactiles d'aujourd'hui. La plus connue est la propriété vibro-tactile.
D'autres applications existent, basées sur l'exploitation des propriétés de génération de friction ou de superposition de modes de déformation.

Le retour haptique qui nous intéresse dans ce travail est le premier type, à savoir le retour d'effort.
Il s'agit du retour de position, lorsqu'une force est appliquée au système puis relâchée, de sorte que le système revient à sa position initiale tout en étant libre. Il s'agit également

du retour d'effort, qui est un retour de position, avec la présence d'un effort tout au long du processus de pression puis de ressenti du retour.
L'appui ne doit pas non plus dépasser la capacité du système à fournir la force réactive de compensation pour revenir à l'état initial.

La bistabilité au service du retour haptique

Le système mécanique bistable, tel que décrit ci-dessus, possède deux configurations dans lesquelles, lorsqu'il n'est pas contraint, il est capable de rester stationnaire. Le mécanisme aura tendance à se déplacer lorsqu'il ne se trouve pas dans l'une de ces configurations.
Le passage d'un des états stables à l'autre, sous l'effet d'un actionnement externe, peut être exploité dans le domaine de l'haptique, comme retour de position ou retour de force (les deux types de retour d'effort). Cette commutation est communément appelée **snap-through**.

L'idée de ce travail de thèse est l'exploitation de la bistabilité et du basculement d'une structure flambée pour ressentir un retour haptique en l'actionnant avec des matériaux piézoélectriques (PZ).
La structure est donc la poutre flambée bistable et l'actionneur est un ou plusieurs patchs PZ.

L'application visée est un bouton avec retour d'effort ou retour de position en fonction des performances de l'actionneur. Une matrice de boutons indépendants sur une interface peut être imaginée à partir de ce bouton unique.
L'activation de ce système intégrera des aspects mécaniques et électriques : le passage de l'état haut à l'état bas se fait par l'application d'une force mécanique transversale (pression du doigt) et l'activation de l'état bas à l'état haut se fait par la mise sous tension électrique de l'actionneur PZ.

Chapitre 2 : Caractérisation des systèmes bistables

L'objectif de ce chapitre est d'étudier en détail deux types de structures bistables, en vue de leur utilisation ultérieure sous un actionnement PZ.
L'enjeu est de démontrer que les systèmes choisis sont bistables, puis de les caractériser mécaniquement pour comprendre leurs propriétés et les niveaux et emplacements d'effort qui doivent leur être appliqués pour exploiter leur bistabilité.

Les deux systèmes étudiés seront des poutres simples compressées axialement et des barrettes en forme de 'U' précontraintes latéralement. Le second système est une solution alternative pour dupliquer un dispositif bistable afin d'avoir une matrice de systèmes bistables qui fonctionnent indépendamment.

L'ensemble de l'étude est menée sous les hypothèses fondamentales de la résistance des matériaux (principe de Saint-Venant et hypothèse de Navier-Bernoulli).

Flambement des poutres

Le flambement est l'apparition brutale d'un changement de forme dans une direction différente de celle des charges appliquées.
Le flambement conduit souvent à la ruine des structures. Cependant, il peut être utilisé pour dissiper l'énergie ou créer des structures très flexibles.
Il s'agit d'un critère de conception pour les colonnes et les barres comprimées.
Ce phénomène est considéré comme une instabilité car il contient un équilibre instable, et est difficile à prévoir car il est très sensible aux imperfections géométriques et matériau, et aux conditions aux limites.

En ce qui concerne le processus d'obtention d'une poutre flambée, la configuration de base est une poutre élastique de longueur $(l_b + \delta)$ à double encastrement. La poutre a une extrémité fixe, l'autre extrémité peut se déplacer sous l'effet de l'application d'une force. Une force axiale P est appliquée à l'extrémité mobile. Cela entraîne le déplacement δ de cette extrémité, et par conséquent l'apparition d'un déplacement transversal D (Figure 3). Une fois que le déplacement D_0 souhaité est obtenu, le dispositif d'appui est fixé.

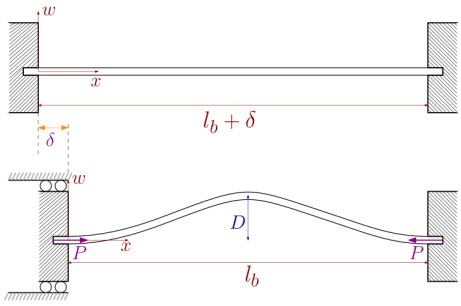

Figure 3: *Poutre doublement encastrée : processus d'obtention de la structure flambée*

On montre que le flambement apparaît quand l'effort axial P dépasse une valeur seuil donnée par :

$$P_{crit} = 4\pi^2 \frac{E_b I}{l_b^2} \tag{4}$$

avec E_b le module de Young de la poutre (en Pa) et I son moment quadratique (en m^4) donné par : $I = b\frac{t_b^3}{12}$, b étant la largeur et t_b l'épaisseur de la poutre.

Une force transversale $2R$ peut être ajoutée à force axiale fixe $P > P_{crit}$, comme montré sur la Figure 4.

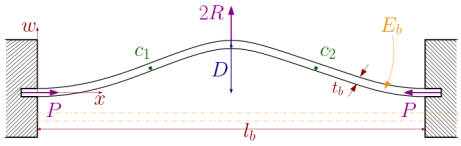

Figure 4: *Schéma 2D d'une structure flambée avec différentes forces impliquées et paramètres de la poutre*

Dans ce cas, une relation peut être retrouvée entre la force transversale $2R$, la force axiale P et le déplacement D [Tah00].

$$2R = \frac{P_{crit}}{\frac{1}{\pi^2} - \frac{4}{3}\left(\frac{D}{2l_b}\right)^2}\left[\frac{D}{2l_b}\left[1 + \frac{\pi^2}{2}\left(\frac{D}{2l_b}\right)^2\right] - \frac{P}{P_{crit}}\frac{D}{2l_b}\right] \tag{5}$$

Pour une valeur fixe de $P > P_{crit}$, qui fixe elle-même le déplacement transversal initial dû au flambement et que l'on note $D_0 \simeq 1\ mm$, on peut tracer la courbe ($2R = f(D)$) et analyser sa forme (Figure 5).

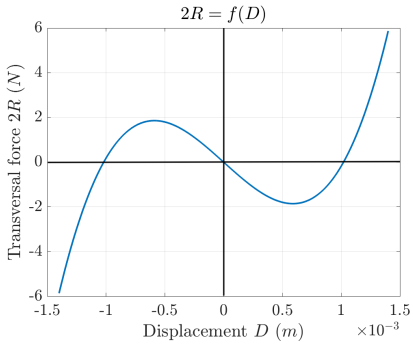

Figure 5: *Force transversale $2R$ en fonction du déplacement transversal D pour une poutre flambée avec une force axiale fixe $P > P_{crit}$*

Tout d'abord, le tracé a l'allure de la courbe classique des systèmes bistables mentionnée dans le chapitre 1. C'est un système qui passe d'un état d'équilibre stable à un autre, pendant la phase de rigidité négative (pente descendante sur le graphique).

La poutre flambée est bien un système bistable.

Pour valider cette conclusion, nous allons tracer plus tard l'énergie potentielle liée à la force transversale et au déplacement qu'elle induit en fonction de ce déplacement lui-même. On prévoit d'après ce qui a été présenté que cette courbe présentera trois optimums locaux, un maximum local et deux minimum locaux.

Barrette en forme de 'U' bistable

Les barrettes à cheveux exploitent le flambement dû à la flexion latérale des deux barres lorsqu'elles sont rapprochées (Figure 6).

Figure 6: *Barrettes à cheveux, un mécanisme bistable obtenu par précontrainte de deux barres en les rapprochant entre elles*

Il s'agit de systèmes bistables précontraints. Le même principe sera utilisé pour rendre bistables deux poutres reliées d'un côté et séparées par une fente au milieu, formant ainsi un 'U'.
Un premier travail de conception et de modélisation numérique a été réalisé pour assurer le flambement des barres en 'U' (Figure 7).

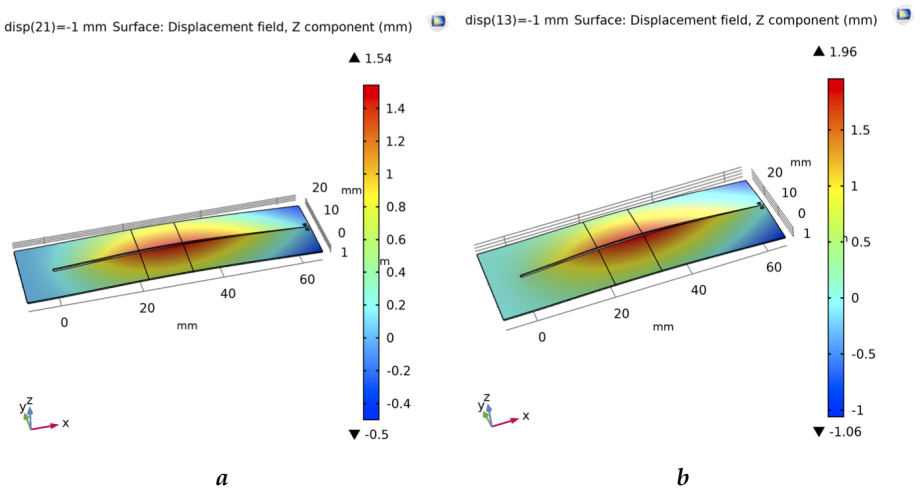

Figure 7: *Système en forme de 'U' flambé à contrôler en déplacement pour l'obtention de la courbe de bistabilité : (a) dimensions de* (70,10,0.3 mm) *et (b) dimensions de* (70,14,0.3 mm).

Nous nous sommes ensuite assurés que ces systèmes sont bistables. Sur cette base, des prototypes de poutres simples (pour la mesure et l'actionnement par des éléments PZ au chapitre 4) et de barres en forme de 'U' ont été fabriqués.
Puisque le système obtenu après flambement est bistable, nous pouvons en fabriquer plusieurs et les attacher entre les mors pour obtenir une matrice de systèmes bistables. Le problème d'avoir des poutres simples qui doivent être comprimées de la même manière pour être bistables n'existe plus. Les mors ne sont plus utilisés pour la compression, mais uniquement en tant que support.

Chapitre 3 : Modélisation de l'actionnement piézoélectrique

L'objectif de ce chapitre est d'évaluer le domaine de validité de deux approches analytiques principales pour modéliser l'effet statique d'un patch piézoélectrique (PZ) sur une poutre élastique.
L'enjeu est de démontrer que l'actionneur PZ peut être remplacé par un effort mécanique équivalent pur si certaines conditions géométriques et matérielles sont respectées.

La première approche remplace le patch PZ par deux forces opposées équivalentes et la seconde par deux moments opposés équivalents.

Étude paramétrique sur un cas simple : poutre encastrée-libre

Un choix a été fait. La modélisation de l'effet des matériaux PZ sur une structure sera faite pour un simple cantilever, où seul l'actionnement du PZ est impliqué, en l'absence de forces externes comme pour une poutre en flambement. Ensuite, ce modèle peut être utilisé sur d'autres structures (voir la transition de la Figure 8a à la Figure 8b).

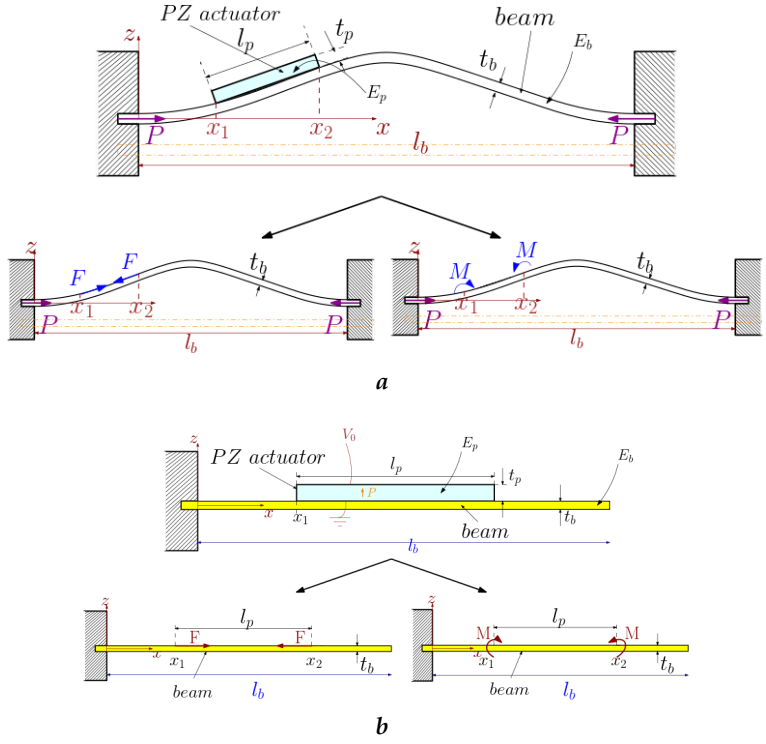

Figure 8: *Modèles de forces et de moments : (a) une poutre bistable flambée actionnée par un patch PZ et (b) une poutre encastrée-libre actionnée par un patch PZ*

Trois modèles équivalents d'actionnement piézoélectriques seront présentés.
F_1 suppose une déformation uniforme le long de la section du PZ et une variation linéaire de la déformation le long de la section de la poutre élastique, sans considérer la rigidité ajoutée par un patch PZ passif.
F_2 suppose une déformation uniforme le long de la section du PZ et une variation linéaire

de la déformation le long de la section de la poutre élastique, avec considération de la rigidité ajoutée par un patch PZ passif.
M suppose une déformation linéaire le long de la section du PZ et de la section de la poutre élastique, avec considération de la rigidité ajoutée par un patch PZ passif.

Les paramètres géométriques mis en jeu sont les épaisseurs t_b et t_p ainsi que les modules de Young E_b et E_p de la poutre et du PZ respectivement.

Une étude paramétrique (paramètres géométriques et paramètres matériaux) est effectuée sur le cas du patch PZ collé sur un cantilever, analytiquement et numériquement. L'étude numérique (logiciel de calcul par élément finis (FEM)) sert de référence à laquelle est comparé le résultat analytique des modèles F_1, F_2 et M. Le critère de comparaison est la valeur du déplacement de l'extrémité libre du cantilever.

Conclusion

La comparaison des modèles F_1, F_2 et M entre eux, et leur comparaison avec le calcul FEM, sur la base du déplacement de l'extrémité libre, peut se ramener à une comparaison de fonctions de deux variables: le ratio des épaisseurs $\frac{t_b}{t_p}$ et le ratio des modules de Young $\frac{E_b}{E_p}$.

L'erreur sur le déplacement libre normalisé entre chaque modèle et le résultat numérique peut être calculée. Nous avons imposé que le modèle analytique est valide si cette erreur ne dépasse pas 6%.

Pour résumer l'analyse, Figure 9 montre les domaines de validité des modèles analytiques F_1, F_2 et M, sur la base des résultats de l'analyse par FEM.

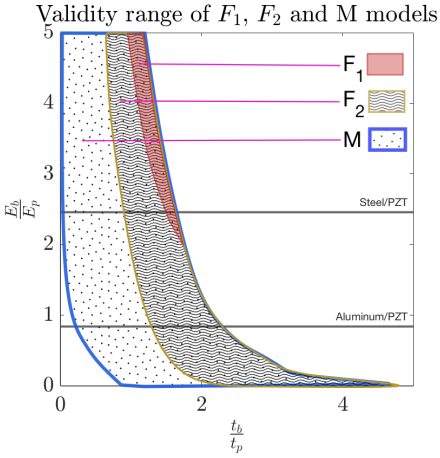

Figure 9: *Conclusion sur les domaines de validité des trois modèles analytiques, par rapport au calcul FEM*

Les résultats de la Figure 9 (i.e. les domaines de validité des modèles analytiques) seront commentés en détail dans la suite du mémoire.

Un résultat important pour la suite de notre étude est que le modèle M peut être appliqué (en particulier pour les cas des structures en acier et en aluminium). La seule exigence est d'être dans une zone de validité imposée par le calcul FEM. Cela concerne les rapports $0,1 \leq \frac{t_b}{t_p} \leq 2$ pour une poutre en acier et $0.5 \leq \frac{t_b}{t_p} \leq 2.5$ pour une poutre en aluminium.

Chapitre 4 : Activation piézoélectrique de systèmes bistables

L'objectif de ce chapitre est d'étudier analytiquement, par modélisation par éléments finis (FEM) et expérimentalement la faisabilité du passage d'un système bisatble d'un état d'équilibre à un autre en utilisant uniquement de l'actionnement piézoélectrique (PZ).
L'enjeu est de démontrer que les modèles de moment équivalent développés dans le chapitre précédent sont valables dans le cas d'un système flambé, et de mener une étude d'optimisation pour minimiser la tension requise pour faire passer la structure d'un état stable à l'autre, en ajustant la position du patch PZ. Cette étude sera réalisée analytiquement et par FEM.
Les positions intéressantes des patchs PZ sur une structure bistable seront exploitées pour réaliser un prototype expérimental qui servira à la validation.
Nous traiterons le cas des deux bistables sélectionnés : poutre simple compressée axialement et barres en forme de 'U' compressés latéralement.

Preuve de concept dans le cas d'une poutre bistable

Le matériau choisi pour les deux systèmes (poutre simple et barres en 'U'), qui sont bistables après précontrainte, est l'acier (acier XC75). Ce choix est dû à certaines études réalisées en laboratoire auparavant [Har12]. Elles ont conclu que le transfert d'effort entre la céramique PZT (NCE41) et la structure hôte est maximal, pour cette gamme de dimensions d'épaisseur, lorsque la structure est en acier.

La nature de la surface est très importante car elle détermine la qualité du collage. Il est donc nécessaire de préparer les surfaces.
La méthode utilisée est celle de la préparation des surfaces pour le collage des jauges de contrainte.

L'adhésif utilisé pour coller les actionneurs PZ aux structures est *Araldite*, un adhésif en pâte époxy à deux composants fourni par Huntsman International LLC.

On présente le cas de la poutre simple bistable actionnée par des patchs PZ. Les modélisations numérique et analytique de ce cas ont donné des résultats prometteurs en terme de tension de basculement. En effet, les tensions de basculement ne dépassent pas les

tensions de claquage des céramique PZT à disposition. Ce n'est pas le cas pour le basculement des barres en 'U'.

Conclusion

A partir de la configuration de poutre simple avec un ou deux patchs PZ collés dessus, nous comprimons axialement les poutres jusqu'au flambement. Le système obtenu est bistable.
Les patchs PZ sont ensuite alimentées en tension, avec des sauts de vingt volts. Cela permet d'avoir un aperçu du moment et de la mesure de la tension de passage d'un état stable à un autre. Cette opération est répétée avec différents points initiaux de tension d'alimentation, ce qui permet de tracer des barres d'erreur sur la tension. La possibilité de serrer la poutre en différents points nous permet de tester quelques points (tension, position), autour des points optimaux.
Une erreur sur la position du patch PZ de $1\ mm$ est ajoutée.
Figure 10 montre le résultat numérique des courbes de tension critique de basculement en fonction des positions du/des patch(s) PZ, ainsi que quelques points testés expérimentalement.

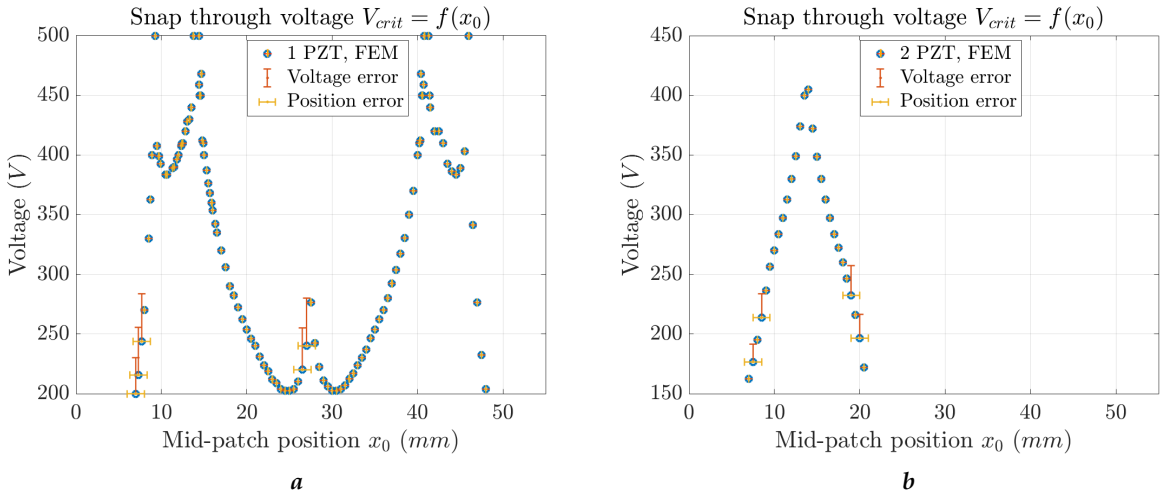

Figure 10: *Courbe numérique du snap-through avec des points validés expérimentalement : tension de basculement en fonction de la position du/des deux patch(s) PZ*

Dans le cas d'une seule céramique PZT collée sur la poutre en acier, Figure 10a montre que les erreurs sur la tension de commutation entre le modèle numérique et l'expérience ne dépassent pas 45 volts (entre $30\ V$ et $45\ V$).
Les erreurs sont principalement dues à la sensibilité du point de basculement, en particulier de la tension et de la position, aux conditions aux limites et au matériel utilisé pour appliquer les forces et appliquer la tension. La colle entre le PZT et la poutre, utilisée dans le banc d'essai et non prise en compte dans le modèle, est une source d'erreur également.

Dans le cas de deux céramiques PZT collées sur la poutre en acier, Figure 10b montre

que les erreurs sur la tension de commutation entre le modèle numérique et l'expérience ne dépassent pas 25 volts (entre $10\ V$ et $25\ V$).
Pour les mêmes raisons que dans le cas d'un seul patch PZ, les erreurs, cette fois relativement faibles compte tenu de l'utilisation de deux patchs PZ, s'expliquent par la sensibilité du point de basculement aux conditions aux limites et à l'équipement utilisé. La colle est aussi une source d'erreur.

Conclusions et perspectives

L'objectif de ce travail était de réaliser une étude de faisabilité pour répondre aux deux questions suivantes : la détection de contact et le retour haptique peuvent-ils être garantis avec une structure bistable actionnée par des matériaux piézoélectriques ? Quels sont les avantages de la duplication et de l'intégration d'un tel système dans un tableau de bord dans le domaine automobile ?

Pour répondre à la première question, le travail effectué concerne la modélisation, la compréhension, la conception et la preuve de concept de la capacité des actionneurs piézoélectriques à fournir un retour haptique, au moyen de la commutation d'un système bistable, menant à des applications automobiles utiles.
Pour la deuxième question, le concept a été proposé dans le cadre d'un brevet et une partie de l'étude de brevetabilité est présentée en annexe **??**.

Conclusions

Les principales contributions du travail effectué sont résumées ci-dessous :

- État de l'art prenant en compte les éléments qui construisent l'image globale du travail que nous voulons réaliser : piézoélectricité, bistabilité, et retour haptique.
- Proposition, conception et caractérisation de deux types de structures bistables.
- Benchmark sur les modèles analytiques piézoélectriques dans la littérature, et étude paramétrique pour conclure sur la validité de ces modèles en les comparant avec le calcul par éléments finis.
- Preuve de concept du basculement bistable à l'aide d'actionneurs piézoélectriques et validation expérimentale des niveaux de force et de tension impliqués.
- Un concept a été proposé pour générer du retour haptique, une application à intégrer dans le tableau de bord d'une voiture.

Perspectives

Une piste de perspectives pour le travail futur est de définir une bonne stratégie de transfert de technologie. Il s'agit d'un projet dont les résultats de recherche ont été démontrés

expérimentalement et pour lequel une preuve de concept sur une application cible a été établie.
Dans le jargon du transfert de technologie, il s'agit d'une maturité technique (niveau TRL 3-5). On imagine une application mais le marché n'est pas forcément totalement identifié. Un travail sur la maturité du marché reste à faire, afin d'identifier des spécifications supplémentaires pour le transfert de la technologie afin d'en faire un produit.

D'un point de vue technique, des perspectives d'études seront proposées à la fin de ce mémoire.

Contents

General overview

0.1 Introduction

The future of society depends on science and **research**. This has been understood and many have invested in exploiting this avenue, giving themselves the means to do so. It is a collective effort, which requires time and energy and whose reward is often not immediate. This is why, whether it is to lay the first stone or rather a continuation, it must be done in the best way.
In automobiles, aeronautics and medicine, engineering is seeking to replace purely mechanical systems with electrical devices. So-called intelligent materials, forming sensors or actuators, are emerging with their intrinsic transformation properties to meet this need, especially to satisfy specific space requirements or dynamic conditions.
In particular, **piezoelectric materials** have a wide variety of applications today, dedicated to low and medium power usage. Among these applications, there is **haptic feedback**, whether it is tactile or effort feedback.
When interacting with a virtual environment, we mainly use visual and auditory feedback. Research has been devoted to adding a **surface** haptic sensation, perceived by the hand and more specifically the fingers.
In order to reproduce surface-related sensations under the finger, the aim of this work was to exploit the property of switching from one stable state to another, of certain so-called **bistable** systems, since this can generate a feedback perceived by the finger. The means chosen to **activate** the bistable system and therefore generate haptic feedback are piezoelectric actuators.

0.2 Organisation of the manuscript

This thesis manuscript is composed of four chapters:

Chapter 1: General introduction A state of the art is presented on piezoelectricity, on bistable systems, on the haptic domain and finally a combination on the use of piezoelectric materials to actuate bistable systems, for haptic feedback applications.

Chapter 2: Characterisation of bistable systems Two types of bistable systems are presented, modelled and mechanically characterised to understand the characteristic force levels they experience.

Chapter 3: Modelling of piezoelectric actuation A parametric study is made on the analytical models of static actuation of piezoelectric materials, and then compared with a numerical parametric study to conclude on the validity of the literature models.

Chapter 4: Piezoelectric activation of bistable systems A proof of concept of bistable systems snap-through by piezoelectric actuation is performed, serving as an experimental validation of a modelling work carried out beforehand.

The thesis is multi-disciplinary and involves a wide range of knowledge in the field of electrical and mechanical engineering.
This project of surface activation by piezoelectric materials is the first in the framework of our team's research. We were able to get to grips with the subject and conduct a feasibility study of the operating principle of the targeted application. And it's not over, it's just the beginning...

This research work has resulted in a publication [Ajn+21] in JIMSS.

Chapter 1

General introduction

Contents

1.1 General context

This work is in line with the aim of using piezoelectric materials to design interactive systems, often referred to as "intelligent systems".
We work in an automotive industry context. This work is supported by the Automotive Mechatronics Chair, a cooperation between Faurecia, CentraleSupelec and Esigelec.
The goal is to design an application that generates haptic feedback at the finger level, for integration into a car dashboard.
The application consists of a bistable system, activated by piezoelectric materials so that it can switch from its first stable state to its second stable state, and consequently generate an effort felt by the finger.
All the notions of piezoelectricity, bistability and haptic systems will be elaborated in detail in this first Chapter.
The aim of this chapter is to briefly present the state of the art of piezoelectric materials, and in particular to demonstrate their behavioural laws based on thermodynamic, electrical and mechanical formalism. Then, the notion of bistability, especially in mechanics, will be presented with examples of understanding. Next, the notion of haptic and haptic feedback will be elaborated with examples of existing applications in industry as well as in research. A last section will be dedicated to the gathering of bistability and haptic systems to make applications.

1.2 Introduction to piezoelectricity

1.2.1 Principle of piezoelectric effect

Piezoelectricity is the process of using an intrinsic specific crystal property of a material to convert mechanical energy into electrical energy, or vice versa.
To present an anisotropic property such as piezoelectricity, a material should have its crystal structure with no centre of symmetry [RS74] [Def11].
Among the 32 existing crystalline classes shown in Figure 1.1, 20 are devoid of a centre of symmetry and exhibit the property of piezoelectricity.

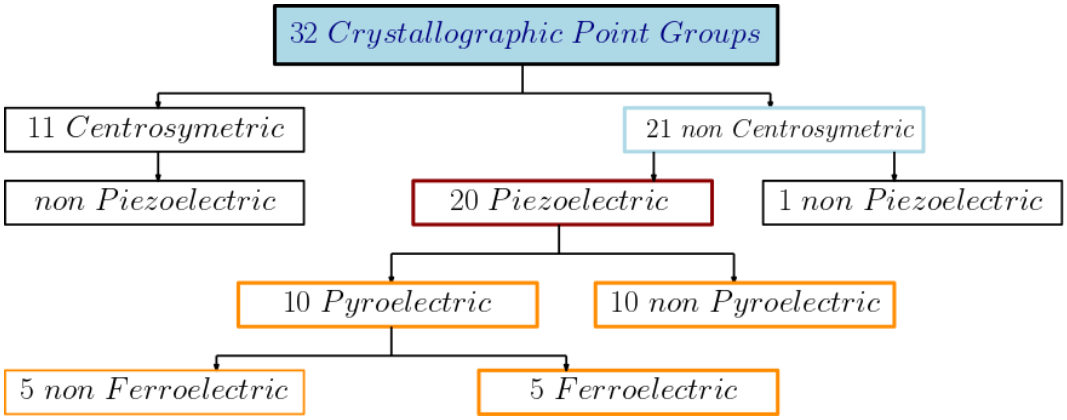

Figure 1.1: *Symmetry hierarchy for piezoelectricity [Def11]*

This sub-category of crystals with no centre of symmetry (piezo-crystals), possesses one or more crystallographic directional axes, and show piezoelectric effect along the directional axes. Of the 20 piezoelectric classes, 10 have one unique direction axis: they are called polar crystals as they show spontaneous polarisation. The spontaneous polarisation is temperature-dependent only. This effect is called Pyro-electricity. The Pyroelectric crystals for which the magnitude and direction of the spontaneous polarisation can be reversed by an external electric field have a ferroelectric behaviour.

The piezoelectric effect can occur if the crystalline material is composed of charged particles and can be polarised.

1.2.2 Coupling of thermal, electrical and mechanical properties

The coupling between the thermal, elastic and electrical parameters of a material can be introduced formally using the thermodynamic approach.

The involved quantities are:

- Stress field T, a second order tensor, with component T_{ij} in Pa.
- Strain field S, a second order tensor, with component S_{kl} without dimension.
- Electrical field E, a vector with component E_k in V/m.
- Electrical displacement field D, a vector with component D_i in C/m^2.
- Environmental temperature Θ, a scalar in K.
- Entropy density of the system Ξ, a scalar in $J/m^3/K$.

To lighten up the analysis, we often make the equivalence between tensor and components of the tensor.

Thermodynamic formalism

For an elastic dielectric material, the first law of thermodynamics gives the variation of its internal energy density U. If we consider the three contributions in this variation dU: the work of external forces, the work of applied electric field and the thermal energy brought to the dielectric material, the reversible (ensured by the second law of thermodynamics) change dU in the internal energy density is given by:

$$dU = T_{ij}dS_{ij} + E_i dD_i + \Theta d\Xi \tag{1.1}$$

where ($\Theta = \Theta_0 + \theta$) the temperature with Θ_0 its reference and θ a small variation. Einstein convention for all indices is used.

This formalism considers the quantities S_{ij}, D_i and Ξ, as variables, while the quantities T_{ij}, E_i and Θ ($\sim \theta$) are considered constant. Often, experiments are considered

isothermal, the electric field and the stress are independent and variable. Therefore, a formulation is needed to change the variables from the format (S_{ij}, D_i, Ξ) to the format (T_{ij}, E_i, θ). To do this, we define the free enthalpy G (Gibbs energy).

$$G = U - T_{ij}S_{ij} - E_iD_i - \Theta\Xi \tag{1.2}$$

From Equations (1.1) and (1.2), we express the variation of Gibbs energy as follows:

$$dG = -S_{ij}dT_{ij} - D_idE_i - \Xi d\theta \tag{1.3}$$

and therefore:

$$S_{ij} = -\left(\frac{\partial G}{\partial T_{ij}}\right)_{E,\theta} \quad D_i = -\left(\frac{\partial G}{\partial E_i}\right)_{T,\theta} \quad \Xi = -\left(\frac{\partial G}{\partial \theta}\right)_{T,E} \tag{1.4}$$

are expressions of strain tensor, electric displacement vector and entropy of the system components respectively. Subscripts indicate quantities kept constant.

Each of the partial derivatives in Equation (1.4) identifies a physical effect. For instance, piezoelectric effect could be presented by introducing the following third-rank tensor (in $C.N^{-1}$) definition:

$$d_{ijk}^{T,\theta} = \underbrace{\left(\frac{\partial S_{ij}}{\partial E_k}\right)_{T,\theta}}_{\text{indirect piezoelectric effect}} = -\left(\frac{\partial^2 G}{\partial E_k \partial T_{ij}}\right) = -\left(\frac{\partial^2 G}{\partial T_{ij} \partial E_k}\right) = \underbrace{\left(\frac{\partial D_k}{\partial T_{ij}}\right)_{E,\theta}}_{\text{direct piezoelectric effect}} = d_{kij}^{E,\theta} \tag{1.5}$$

considering the order in which derivatives are taken is irrelevant, Equation (1.5) demonstrates the thermodynamic equivalence of the direct and indirect piezoelectric effects.

To finally find expressions of strain field S, electrical displacement field D and entropy of the system Ξ, we write their total differentials first:

$$\begin{aligned}
dS_{ij} &= \left(\frac{\partial S_{ij}}{\partial T_{kl}}\right)_{E,\theta} dT_{kl} + \left(\frac{\partial S_{ij}}{\partial E_k}\right)_{T,\theta} dE_k + \left(\frac{\partial S_{ij}}{\partial \theta}\right)_{T,E} d\theta \\
dD_i &= \left(\frac{\partial D_i}{\partial T_{kl}}\right)_{E,\theta} dT_{kl} + \left(\frac{\partial D_i}{\partial E_k}\right)_{T,\theta} dE_k + \left(\frac{\partial D_i}{\partial \theta}\right)_{T,E} d\theta \\
d\Xi &= \left(\frac{\partial \Xi}{\partial T_{kl}}\right)_{E,\theta} dT_{kl} + \left(\frac{\partial \Xi}{\partial E_k}\right)_{T,\theta} dE_k + \left(\frac{\partial \Xi}{\partial \theta}\right)_{T,E} d\theta
\end{aligned} \tag{1.6}$$

To sum up, we express equations in (1.6) in an integrated form, assuming that dE and dT represent small deviations from the zero initial electrical and stress fields [Dam98] [Y91]:

$$\begin{aligned}
S_{ij} &= s_{ijkl}^{E,\theta} T_{kl} + d_{ijk}^{T,\theta} E_k + \alpha_{ij}^{T,E} \Delta\theta \\
D_i &= d_{ikl}^{E,\theta} T_{kl} + \varepsilon_{ik}^{T,\theta} E_k + p_i^{T,E} \Delta\theta \\
\Xi &= \alpha_{kl}^{E,\theta} T_{kl} + p_k^{T,\theta} E_k + \frac{c^{T,E}}{\theta} \Delta\theta
\end{aligned} \tag{1.7}$$

Other parameters, just like the third-rank tensor of piezoelectric coefficients (d_{ijk}) in Equation (1.5), have been defined and have each a physical significance:

- s_{ijkl} in $(m^2.N^1)$ is the four-rank elastic compliance tensor. An interesting tensor can be introduced based on the inverse relation between stress and strain tensors (in absence of electrical field and temperature variation): $T_{ij} = c_{ijkl}S_{kl}$. c_{ijkl} is the elastic stiffness tensor in $(N.m^{-2})$. T_{ij} and S_{kl} are symmetric by definition. Therefore, $s_{ijkl} = s_{jilk}$ and $c_{ijkl} = c_{jilk}$. It can be proven that s_{ijkl} is a symmetric tensor too ($s_{ijkl} = s_{lkji}$, idem for c_{ijkl}). Thus, the number of independent components of the elastic compliance (and stiffness) tensor is reduced from 81 to 36 to 21.

- α_{ij} in (K^{-1}) is the thermal expansion tensor, which defines the shape change of the matter in response to a change in temperature.

- ε_{ik} in $(F.m^{-1})$ is the dielectric permittivity of the material.

- p_i in $(C.m^{-2}.K^{-1})$ is the vector of Pyro-electric coefficients, which defines the change in spontaneous polarisation of the material with temperature.

- c in $(J.m^{-3}.K^{-1})$ is the heat capacity, an extensive property that present the heat to be given to a one gram mass of the material to produce a unit change in its temperature.

It's important to mention that Equations in (1.6) and (1.7) contain only linear terms and thus only linear effects. In the case of strong fields or strongly nonlinear material such as some ferroelectric materials, these relations must be extended to include higher-order terms [Dam98].

Piezoelectric formalism

Stress and strain tensors are symmetric. We take advantage of this property to write them in a matrix compressed format. It consists in replacing ij and kl by p and q according to changes in Table 1.1.

Table 1.1: *Tensor to matrix notations*

ij or kl	p or q
11	1
22	2
33	3
23 or 32	4
13 or 31	5
12 or 21	6

By considering isentropic and isothermal transformations, Equation (1.7) will therefore be written as follows:

$$\begin{aligned} S_p &= s^E_{pq} T_q + d^T_{kp} E_k \\ D_i &= d^E_{iq} T_q + \varepsilon^T_{ik} E_k \end{aligned} \tag{1.8}$$

Thus, under conditions of zero stress (resp. zero electric field), we obtain the pure piezoelectric strain (resp. charge). Equations in (1.8) are known as the **piezoelectric constitutive equations**.

The set of independent variables (T, E, θ) chosen for the derivation in Equations (1.6) is up to choice. Other thermodynamic potentials and combinations of independent variables give six remaining isotherm piezoelectric constitutive equations:

$$\begin{aligned} S_p &= s^D_{pq} T_q + g^T_{kp} D_k \\ E_i &= -g^D_{iq} T_q + \beta^S_{ik} D_k \end{aligned} \tag{1.9a}$$

$$\begin{aligned} T_p &= c^E_{pq} S_q - e^S_{kp} E_k \\ D_i &= e^E_{iq} S_q + \varepsilon^S_{ik} E_k \end{aligned} \tag{1.9b}$$

$$\begin{aligned} T_p &= c^D_{pq} S_q - h^S_{kp} D_k \\ E_i &= -h^D_{iq} S_q + \beta^S_{ik} D_k \end{aligned} \tag{1.9c}$$

with $i, k = 1, 2, 3$ and $p, q = 1, 2, 3, 4, 5, 6$.
New piezoelectric tensors: e,g and h have been defined. e contains stress or charge coefficients ($C.m^{-2}$ or $V.m.N^{-1}$), g contains strain or voltage coefficients ($m^2.C^{-1}$ or $N.V^{-1}.m^{-1}$) and h contains stress or voltage coefficients ($N.C^{-1}$ or $V.m^{-1}$).
It is important to mention that thermodynamics of piezoelectric materials shows an equivalence between piezoelectric coefficients of same type: $d^T = d^E$, $g^T = g^D$, $e^S = e^E$ and $h^S = h^D$. Thus, superscripts could be omitted [Dam98].

Depending on the nature of the problem faced, what the variables are, what is given and what is required, the constitutive equations of piezoelectricity (1.8) (1.9a) (1.9b) (1.9c) can be used indifferently.

Reduced constitutive laws

The idea of this paragraph is to reduce the behaviour laws in the case of beams. A way is to express the mechanical quantities along the beam axis and the electrical quantities along the direction of polarisation.

Let us take the (T, E) format given in Equation (1.8). First, we write its components using matrix notation. Due to crystal symmetries, piezoelectric coupling matrices have few non-zero elements [Pie01]:

$$\begin{array}{l} \\ \text{Actuation} \\ \\ \\ \\ \\ \\ \text{Sensing} \\ \\ \end{array} \overbrace{\left\{\begin{array}{c} S_1 \\ S_2 \\ S_3 \\ S_4 \\ S_5 \\ S_6 \\ \hline D_1 \\ D_2 \\ D_3 \end{array}\right\}}^{} = \overbrace{\left(\begin{array}{cccccc|ccc} s_{11}^E & s_{12}^E & s_{13}^E & 0 & 0 & 0 & 0 & 0 & d_{31} \\ s_{12}^E & s_{22}^E & s_{23}^E & 0 & 0 & 0 & 0 & 0 & d_{32} \\ s_{13}^E & s_{23}^E & s_{33}^E & 0 & 0 & 0 & 0 & 0 & d_{33} \\ 0 & 0 & 0 & s_{44}^E & 0 & 0 & 0 & d_{24} & 0 \\ 0 & 0 & 0 & 0 & s_{55}^E & 0 & d_{15} & 0 & 0 \\ 0 & 0 & 0 & 0 & 0 & s_{66}^E & 0 & 0 & 0 \\ \hline 0 & 0 & 0 & 0 & d_{15} & 0 & \varepsilon_{11}^T & 0 & 0 \\ 0 & 0 & 0 & d_{24} & 0 & 0 & 0 & \varepsilon_{22}^T & 0 \\ d_{31} & d_{32} & d_{33} & 0 & 0 & 0 & 0 & 0 & \varepsilon_{33}^T \end{array}\right)}^{\begin{array}{c}\text{compliance} \\ \text{coupling}\end{array} \quad \begin{array}{c}\text{coupling} \\ \text{permittivity}\end{array}} \overbrace{\left\{\begin{array}{c} T_1 \\ T_2 \\ T_3 \\ T_4 \\ T_5 \\ T_6 \\ \hline E_1 \\ E_2 \\ E_3 \end{array}\right\}}^{} \tag{1.10}$$

The available coupling modes are important in the design of actuation and sensing devices. Piezoceramics (PZT) are commonly used for actuation. For sensing applications, piezopolymers (PVDF) are used. As an example, the coupling matrices of PZT and PVDF could be written as follows:

$$d_{PZT} = \begin{pmatrix} 0 & 0 & 0 & 0 & d_{15} & 0 \\ 0 & 0 & 0 & d_{15} & 0 & 0 \\ d_{31} & d_{31} & d_{33} & 0 & 0 & 0 \end{pmatrix} \quad (d_{32} = d_{31}, d_{24} = d_{15}) \tag{1.11a}$$

$$d_{PVDF} = \begin{pmatrix} 0 & 0 & 0 & 0 & 0 & 0 \\ 0 & 0 & 0 & 0 & 0 & 0 \\ d_{31} & d_{32} & d_{33} & 0 & 0 & 0 \end{pmatrix} \quad (d_{15} = d_{24} = 0) \tag{1.11b}$$

That gives an idea of different modes of actuation and sensing: the in-plane mode (d_{31}, d_{32}), the thickness mode (d_{33}) and the shear mode (d_{15}, d_{24}).

Let us consider a structure whose main axis is direction 1. We are interested in a coupling 31, where the piezoelectric material is polarised along direction 3. We consider the coupling between the axial mechanical quantities (T_1 and S_1) and the transverse electrical quantities (E_3 and D_3).
With those considerations, we can deduce from the matrix formulation of the Equation (1.10) the following two laws:

$$\begin{aligned} S_1 &= s_{11}^E T_1 + s_{12}^E T_2 + s_{13}^E T_3 + d_{31} E_3 \\ D_3 &= d_{31} T_1 + d_{32} T_2 + d_{33} T_3 + \varepsilon_{33}^T E_3 \end{aligned} \tag{1.12}$$

Beam under linear elasticity assumption:

The beam case is the one where the dimensions of the sections along axes 2 and 3 of the material are comparable. The length along axis 1 is assumed to be infinite. The stresses are then equal to zero in directions 2 and 3:

$$T_2 = T_3 = 0 \tag{1.13}$$

In this case, the three-dimensional behaviour law reduces to the following expression:

$$\begin{aligned} S_1 &= s_{11}^E T_1 + d_{31} E_3 \\ D_3 &= d_{31} T_1 + \varepsilon_{33}^T E_3 \end{aligned} \tag{1.14}$$

This is the result using the piezoelectric tensor d. Another way to express an equivalent result is to use the tensor e, where the couple (S,E) is involved (Equation (1.9b)). This makes it possible to find simple relationships between the various piezoelectric tensors and coefficients, including compliance and stiffness (s^E and c^E), in the case of beam structure.

Plate under linear elasticity assumption:

This is the case when the thickness (along 3) is small compared to the width (along 2) of the elastic sample. The length (along 1) and width are of the same order of magnitude. It is assumed in this case that there is no stress in the transverse direction 3 and that the displacements are blocked in the directions 2 and 3:

$$T_3 = 0, \qquad S_2 = 0 \tag{1.15}$$

In this case, the three-dimensional behaviour law "in d" reduces to the following expression [Duc09]:

$$\begin{aligned} S_1 &= \overline{s}_{11}^E T_1 + \overline{d}_{31} E_3 \\ D_3 &= \overline{d}_{31} T_1 + \overline{\varepsilon}_{33}^T E_3 \end{aligned} \tag{1.16}$$

where $\overline{s}_{11}^E$, $\overline{d}_{31}$ and $\overline{\varepsilon}_{33}^T$ are piezoelectric tensors components with modifications taking account of conditions in Equation (1.15):

$$\overline{s}_{11}^E = s_{11}^E \left(1 - \nu_{12}^2\right), \qquad \overline{d}_{31} = d_{31} \left(1 + \nu_{12}\right), \qquad \overline{\varepsilon}_{33}^T = \varepsilon_{33}^T - \frac{d_{31}^2}{s_{11}^E} \tag{1.17}$$

ν_{12} is Poisson's ratio of the material in the plane 12.

Electrostriction

Electrostatic forces acting in dielectric environment in general, including ferroelectric and piezoelectric materials, produce not only an electrical response (polarisation) but also a

mechanical response.
A mechanical nonlinear strain appears. This is electrostriction: a quantity that varies according to even powers of the applied electric field (thus, doesn't depend on its sign), mainly the second order [EF90].
If an electric field E is applied on a material, the electrostrictive strain S is defined by:

$$S_{ij} = M_{ijkl} E_k E_l \tag{1.18}$$

where M_{ijkl} (in $m^2.V^{-2}$) are tensor components and are called electrostrictive coefficients.

Alternatively, the electrostrictive effect can be expressed, for a linear material or in a linear limit for non linear materials, in terms of the vector of induced polarisation:

$$S_{ij} = Q_{ijkl} P_k P_l \tag{1.19}$$

where Q_{ijkl} and M_{ijkl} are related by:

$$M_{ijmn} = \chi_{km} \chi_{ln} Q_{ijkl} \qquad \text{(because } P_i = \chi_{ij} E_j\text{)} \tag{1.20}$$

and χ ($F.m^{-1}$) is the second-rank tensor known as the dielectric susceptibility of the material.

The electrostrictive effect is a property of all materials, regardless of the symmetry.

In our study, the materials concerned are PZT. For these materials, the longitudinal and transverse electrostriction coefficients (Q_{3333} and Q_{1133}) do not exceed $0.1\ m^4C^{-2}$ [WL85] [ZWG85]. The electrical polarisation in our samples does not exceed $10^{-9}C.m^{-2}$ in the static case. The deformation induced by electrostriction is of the order of 10^{-19}, a too small strain value to be taken into account.

In the course of our study, we will remain within the framework of the linear piezoelectricity formalism, with beam or plate hypotheses, depending on the situation and the problem treated.

1.2.3 Advantages of piezoelectric materials

The common characteristics of piezoelectric devices are listed in this paragraph.
First of all, response times are low (below $1ms$). The materials can therefore be exploited at high frequencies [Zha+04]. It is the property that is exploited, for example, in the case of fuel injection in automotive industry. It also means that a wide range of speeds can be exploited.

The stress levels that the materials can withstand are high [BTS21]. This makes it possible, for example, to generate high forces or torques in complete and compact systems that incorporate piezoelectric materials.

Electromechanical conversion is intrinsic and it is simple to generate the electric field necessary for the conversion, this leads to compact and lightweight devices with simple structures [POH15]. The above statement, combined with the exploitable speeds and stress levels, suggests devices with high power-to-weight ratio.
The use of these materials, e.g. in travelling wave motors, leads to actuators with low rotational speeds [Zha+05]. This property eliminates the need to use gearboxes for high torque and low speed applications.
The small displacements generated (under high voltage levels) lead to good controllability of the actuators and high resolution, reaching the nanoscale [SLZ21], with very fast response times, below $1ms$.
The electromechanical transformation is increasingly improved [TMM14]. It takes place silently and with a negligible magnetic field (compared to conventional solutions).
Operation at cryogenic temperatures is possible even if the performance of the actuators is lower at low temperatures. PZ materials can operate at high temperatures without failure. Their usage temperature range is though limited by their Curie point T_C, being about $160°C - 350°C$ for ferroelectric ceramics [SY11]. The lifetime of these materials is relatively long, with very low consumption, especially in static use.
Finally, piezoelectric materials use under vacuum or in clean rooms is permitted due to their composition [Shc+18].

1.2.4 Applications of piezoelectricity

Piezoelectric materials have a wide range of applications. They exist in many various forms: PZT Ceramics, PVDF polymer films, ElectroMechanical Films and PZT fibers, each exhibiting different characteristics, advantages and drawbacks depending on the application.
There are three main areas of application of piezoelectricity depending on the effects employed [Maa17]:

- Devices using direct effect (sensors): microphones, sensors, energy harvesting systems, lighting systems...
- Devices using the reverse effect (actuators): loudspeakers, sonar, micro-positioners, motors, injectors...
- Devices using both effects: filters, time base, active sensors, ultrasonic transmit/receive probes...

Specific examples:

As piezoelectric actuation property is more challenging in terms of scientific research than sensor's, Figure 1.2 presents some specific applications of the piezoelectric effect.

- Quartz watch: very precise with its piezoelectric heart beating 32,768 times a second, for the matter of non-audible frequency and the power of 2 ($32,768 = 2^{15}$) for obtaining 1 second using 15 logic flip-flops.

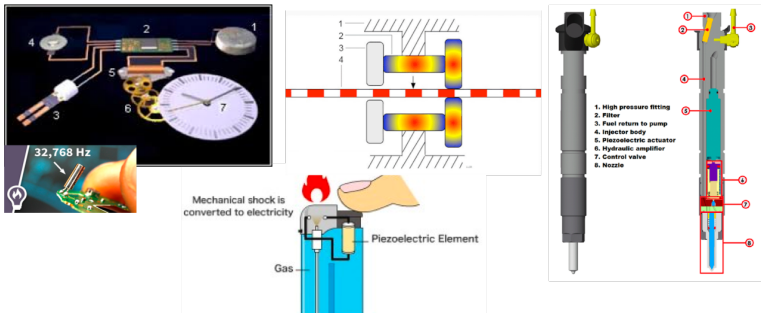

Figure 1.2: *Examples of piezoelectric systems based on actuation function*

- Piezo lighter: creating the spark with a piezoelectric material that turns on the gas.
- Inchworm: could be used in automotive application, under the car seat or on the headrest for a straight and controlled translation (not yet the case).
- Piezo injectors: According to Bosch, who introduced piezo injectors to the industry, a piezo actuator acts up to 5 times faster than a standard injector solenoid and the motion is frictionless. The greatest advantage of piezo injectors is the rate and precision in which fuel can be delivered, since the actuator can be rapidly activated and deactivated.

The applications of piezoelectricity are multiple and find their places in all fields. We are more interested in this work in actuators and sensors for haptic applications (Figure 1.3).

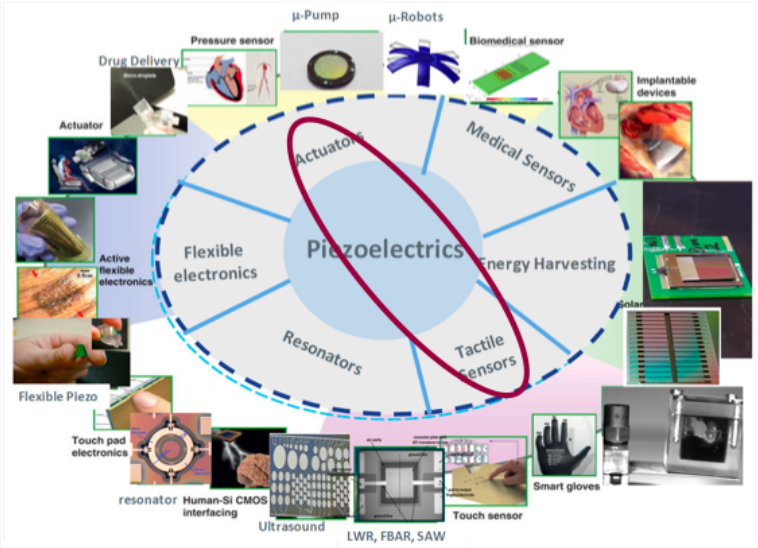

Figure 1.3: *Piezoelectric materials and systems: a wide range of applications* [1]

[1] https://www.tyndall.ie/

1.3 Introduction to bi-stability

The stability is the ability of a system to remain in a given state. In mechanical engineering, this state corresponds to a minimum of the potential energy of the system. When external force(s) is/are released, the mechanism must then converge to its so-called stable position.
A system, whether mechanical, electrical, chemical or other..., can have one stable state or several. Bistable systems have two and only two stable equilibria, separated by an unstable equilibrium state.

1.3.1 Bistability in mechanics

Bistable systems have multiple advantages. One of the relevant advantages is their ability to stay in two positions without power input and despite small external disturbances. In mechanical field, thanks to this ability, they have applications in many devices, such as switches, valves, closures, clasps, etc.

To illustrate static characteristics of a bistable mechanical structure, we introduce the one dimensional system in Figure 1.4.

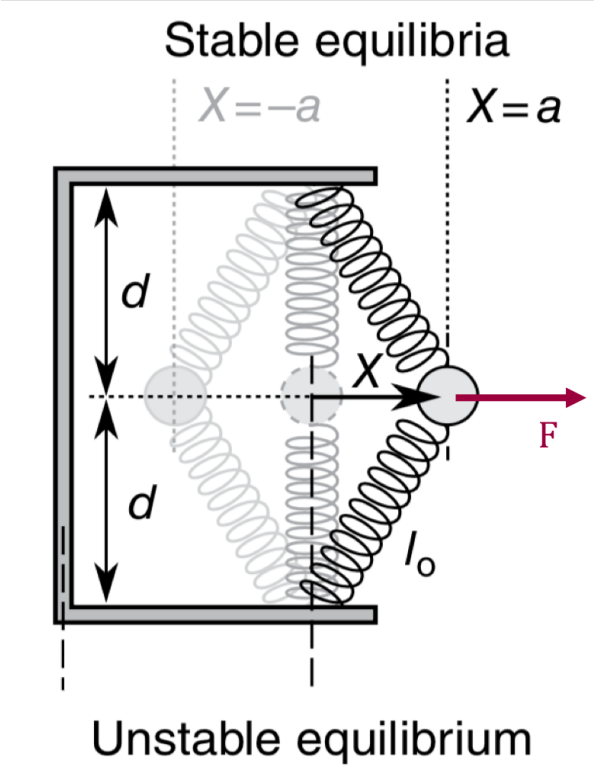

Figure 1.4: *Bistable system composed of springs, mass, and frame. Here $l_o > d$ which makes the central configuration $X = 0$ an unstable position of static equilibrium [HW17]*

For this system, two identical springs of lengths l_o connect a mass to a surrounding frame of span $2d$.

In this case, where $l_0 > d$, the springs exert a force on the inertial mass. Thus, the mass can't be "easily" maintained in the vertical central position.
This zero displacement configuration is an unstable equilibrium position, while two "easy" to hold positions, without external forces application, exist symmetrically on either side of the central position, at $X = \pm a$.
The system mass-spring and the frame has therefore three equilibrium positions, two and only two of them are easy to be hold without any external effort. This is the property of so-called **bistable systems**. This property is further demonstrated by an energetic approach.

Let's consider first a force F in the same direction as the transverse displacement X. The application of such a force changes the position X of the mass. The starting point is the equilibrium position $X = +a$. If $F > 0$, X increases. Otherwise, X decreases and can move to negative values. Figure 1.5a illustrates the force F as a function of the mass position variation (displacement X).

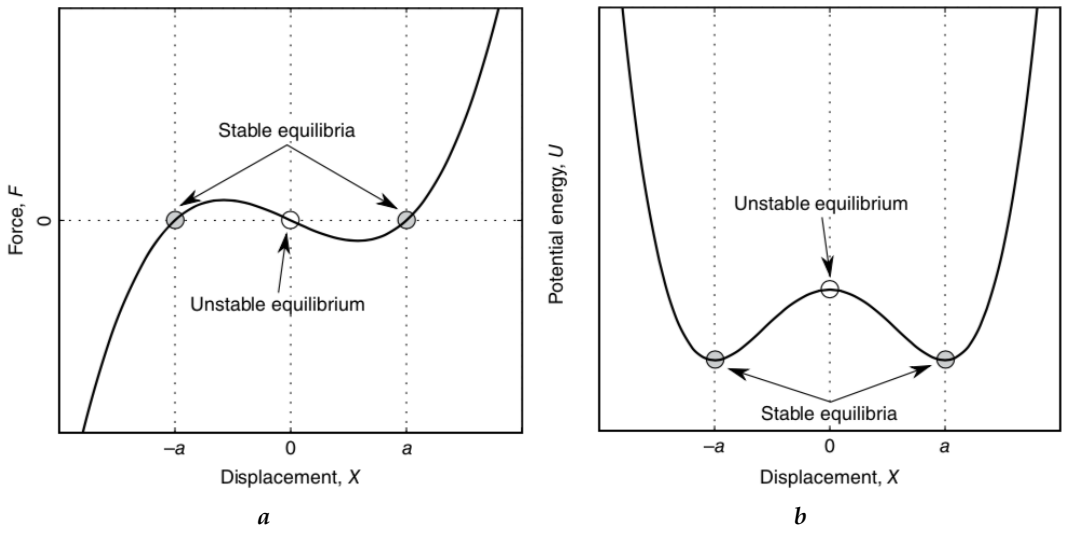

Figure 1.5: *Dependence of (a) transverse force (in same direction as X displacement) and (b) its related potential energy on the displacement position of the frame lumped mass [HW17]*

This sub-figure 1.5a shows that the transverse force F is zero when the mass is in one of the equilibrium positions ($X = 0$ or $\pm a$).
To demonstrate that these are indeed equilibrium positions, and to see which are stable, we define the potential energy of the system, related to the force F as follows:

$$U = \int F.dX \tag{1.21}$$

Figure 1.5b shows that the potential energy U is *locally maximised* at the central position of the mass $X = 0$. A local maximum of the potential energy defines an unstable equilibrium position. Thus, $X = 0$ is unstable.
In contrast, potential energy U is *locally minimised* at the adjacent positions $X = \pm a$, they

are therefore stable equilibrium positions.

To sum-up, the energy study carried out shows that the system has three equilibrium positions, **two** of them are stable, the third is unstable. Hence, it is a **bi**-stable system.

The system studied in this paragraph is called the "double spring", an historical and basic bistable system [HW17].

1.3.2 Bistable systems categories

Several categories of mechanisms with bistable positions exist. Five main families are mentioned below [Caz09]: Multi-part bistable mechanisms, Planar bistable mechanisms for MEMS, Pre-stressed bistable mechanisms, Bistable mechanisms with preformed plates and Bistable mechanisms based on anisotropy.

Multi-part bistable mechanisms

The principle of such a mechanism is the existence of two stable states, guaranteed by the existence of an assembly of elements including a spring. The two states are separated by a configuration jump, and the transition between the two states is made by means of an additional part.

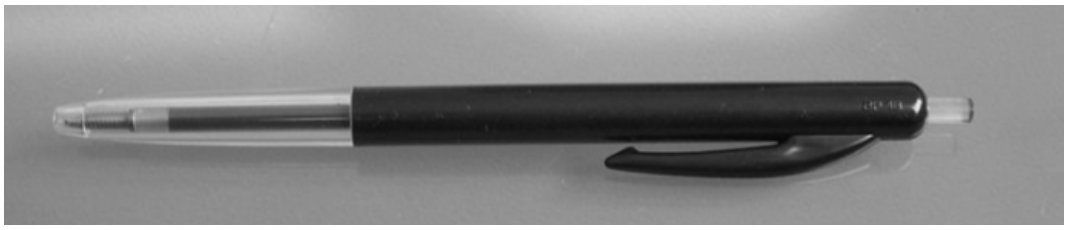

Figure 1.6: *Bic pen, a bistable mechanism by assembling multiple activation parts*

A typical example is the bic pen (Figure 1.6). In this case, the state jump is achieved by moving a small side piece. In other cases, a rotating part is used. A spring provides the stability of the two stable configurations.

Planar bistable mechanisms for MEMS

Known by the acronym MEMS, micro-electro-mechanical systems such as relays, valves, threshold switches and memory cells find in bistable systems an efficient solution. One crucial advantage of those systems in MEMS devices, as mentioned before, is their ability to apply a contact force without the need for continued actuation power.
In the MEMS literature, three main families of bistable mechanisms have been reported [QLS04]: latch-lock mechanisms [HKV99] [SFC98], hinged multi-segment mechanisms [Jen+01] [KP98], and residual-compressive-stress buckled beam or membrane mechanisms [Van98] [YK95] [Wag+96].
This category of bistable systems concerns plan mechanisms. Some of the known examples are given in Figures 1.7, 1.8 and 1.9.

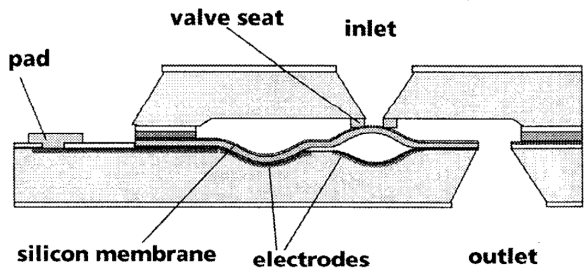

Figure 1.7: *Schematic cross-section of a bistable micro-valve [Wag+96]*

Figure 1.7 presents a MEMS application: the micro-valve. It is based on the principle of bistable electrostatic actuator with pneumatic coupling.
For a quick presentation of the principle of this coupling, the membranes operate in counteraction. If one electrode is pulled down electrostatically, the other is pushed up pneumatically, and vice versa.

Figure 1.8 presents a bistable switching micro-relay structure for DC signals.
The bistable frame structure can be used to design the holding force of the contact with minimal impact on actuator requirements.
The frame also allows control over the necessary force and displacement of actuation almost independent of relay requirements [KP98].

Figure 1.9 presents a snap-action bistable micro-mechanisms.
Known applications include micro-switches, addressable MEMS-based pixel arrays and optical micro-filters.
The bistability in this case comes from buckling or a similar phenomenon like bending.
Those mechanisms are limited to two dimensions. They can be produced by cutting techniques without any final assembly. We find many, for instance, manufactured in silicon.

Pre-stressed bistable mechanisms

There are other types of systems with the property of bistability. Among these there are plate mechanisms with a pre-stress.

Figure 2.17 presents two types of pre-stressed bistable mechanisms: the electrical circuit breaker (sub-figure (a)) and the hair clip (sub-figure (b)).

The circuit breaker, being an asymmetrical bistable mechanism, is operated in the tripping direction by a thermal bimetallic strip, and then manually reset in the other direction.

The hair clip is manually operated.
This type of structures, in particular the 'U' system (hair clip), will be elaborated on and studied in detail in Chapter 2. Its advantages compared to a simple beam will also be mentioned.

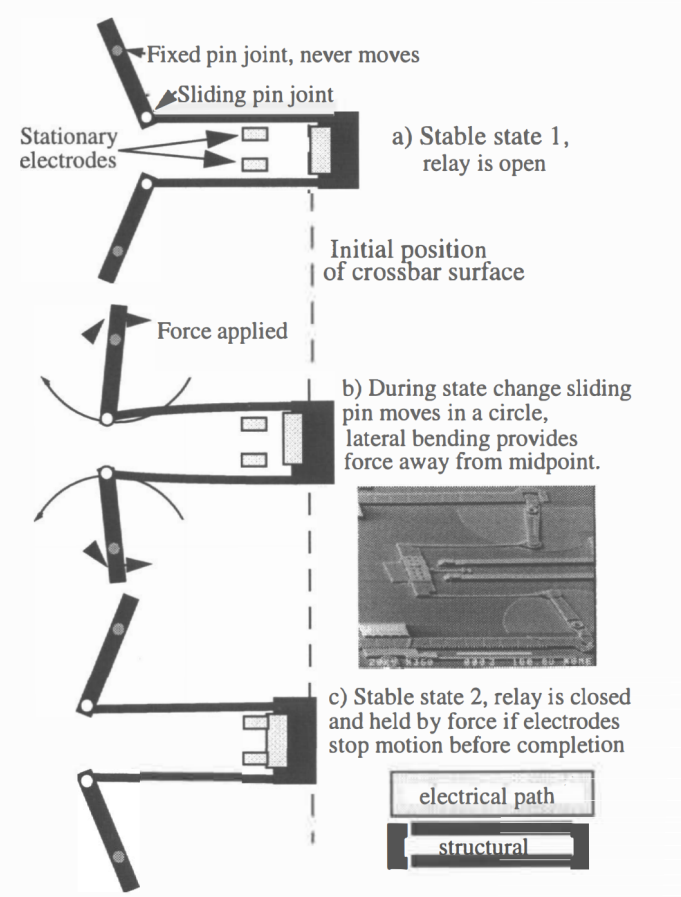

Figure 1.8: *Bistable action in the relay frame holds the device in an open or closed state without actuation [KP98]*

Bistable mechanisms with preformed plates

Other bistable systems use pre-formed plates (Figure 1.11).

These systems make it possible to do away with the pre-stress of previous mechanisms.

The click-clack box is a very interesting application inspired by bistability. The principle is simple and the idea is ingenious (Figure 1.12). It has been patented since the 1920s.

By operating the preformed part transversely or axially, we manage to open or close the box.

Bistable mechanisms with anisotropic plates

Last family of bistable systems that we mention is the one that uses anisotropic plates (Figure 1.13).

Same as preformed plates, these systems make bistability possible to do without the pre-stress like it's the case in previous mechanisms.

[2] https://www.swissplastics-cluster-event.ch/web/wp-content/uploads/2018/05/Badaoui_JT2018.pdf

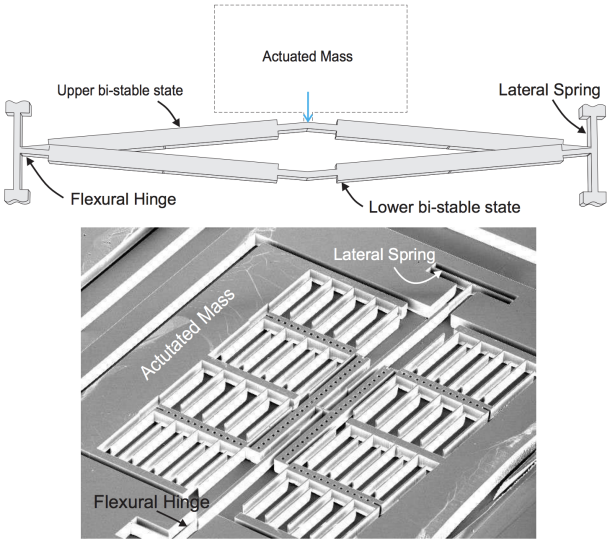

Figure 1.9: *Truss-like micro-switch based on two slightly bended beams [CS04]*

The trouser clip, on the other hand, exploits the anisotropic property of the materials of which it is made. It is often used for structures that can be rolled up and unfolded [GG04], such as the wings of light aircraft or laptop screens [NSG08].

1.3.3 Discussion

In the context of our work, we need a system that is centimetric in size (the size of a button) and simple to implement.

As our application of the bistable system is aimed at haptic feedback, especially on the automotive dashboard where several buttons coexist, the chosen mechanism must be housed within a matrix of bistable structures, independent and able to be operated independently.

Systems that exploit buckling seem to be a promising solution, as they are not complicated to realise and they use only two dimensions: they are classified as planar bistable mechanisms at the beginning of this section.

In Chapter 2 we will present the buckling phenomenon, how it is obtained, the resulting structure, why it is bistable and how it can be used to create haptic feedback. An attempt to prototype an array of independent bistable structures will also be presented.

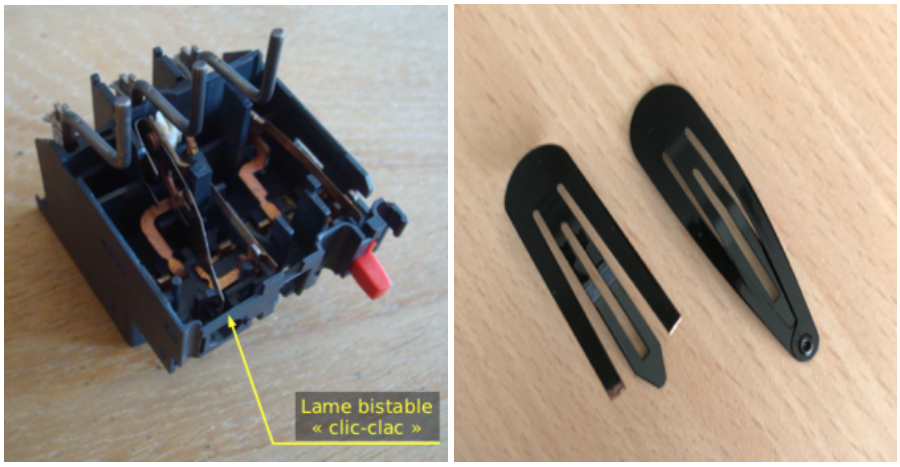

a *b*

Figure 1.10: *Bistable mechanisms by pre-stressing a monolithic plate: (a) a Schneider circuit breaker and (b) a hair clip*

Figure 1.11: *Bistable click-clack box, a mechanism that uses a preformed plate*

1.4 Introduction to haptic feedback

1.4.1 The sense of touch: neural basis

The sens of touch is one sign, among many others, of the greatness and perfection of the human body.
With the help of the sense of touch, we make many exploratory movements, and this allows us to encode many properties of surfaces and objects.
The texture of a surface is felt through the shear forces applied to the skin, when a lateral movement is made by touch.
The hardness or softness are felt when we apply pressure with the touch to deform or twist an object.
Static contact allows us to feel the temperature of a body.
To measure the weight of an object, holding it can be a sufficient approach.
The overall or exact shape of an object can be felt by wrapping it in the hand or by following its contours.
The parts of the human skin that are responsible for these perceptions and through which

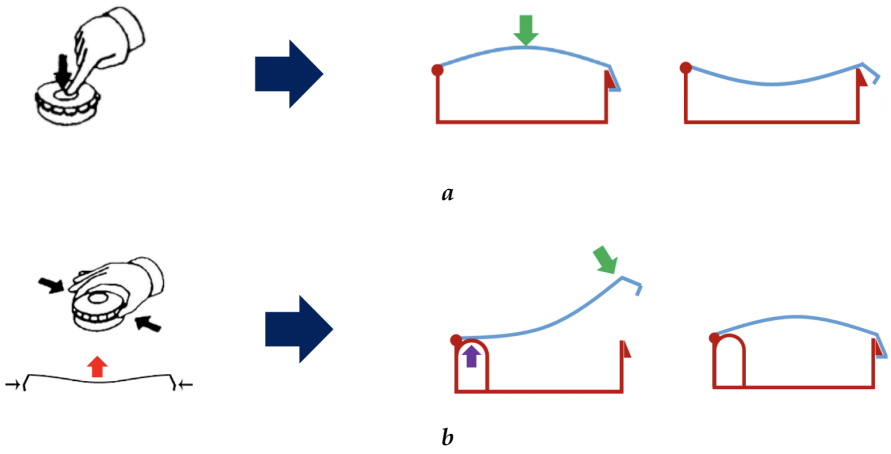

Figure 1.12: *The opening (a) and closing (b) principle of the click-clack box* [2]

Figure 1.13: *Two trouser clips, one open (left) and one closed (right), a bistable plate mechanism that uses the anisotropy*

encoding takes place are called mechanoreceptors. These are the four receptors presented in Figure 1.14: Meissner corpuscles, Pacinian corpuscles, Merkel cell and Ruffini ending.

Mechanoreceptors act as mechanic-electric transducers that transform mechanical information (pressure, vibration, shear, etc.) into nerve impulses that are transmitted to the brain.

The four mechanoreceptors are classified according to their frequency pass band (Fastly Adaptative -FA- and Slowly Adaptative -SA-) [JV77] [Kac20]:

(FA I) Meissner corpuscles: are located between the dermis and the epidermis. Their spatial density is 140 units per cm^2. They have a weak receptive field, hence the number I after FA type. This allows them to provide a precise spatial location of the stimulated object. However, they are insensitive to static deformation and low frequency vibrations. With their sensitivity of between $10\ Hz$ and $100\ Hz$, they detect the vibrations of an object sliding against the skin for instance, which then allows the holding force to be adjusted.

(FA II) Pacinian corpuscles: are located in the deep dermis, with a density of 30 units per cm^2. Their receptive field is relatively wide (type II), with a frequency sensitivity range between $40\ Hz$ and $1\ kHz$. These mechanoreceptors detect vibrations, especially those that are spatially extended.

(SA I) Merkel cell: are located between the dermis and the epidermis. Their spatial density is 70 units per cm^2. Their receptive field is more restricted than Meissner's

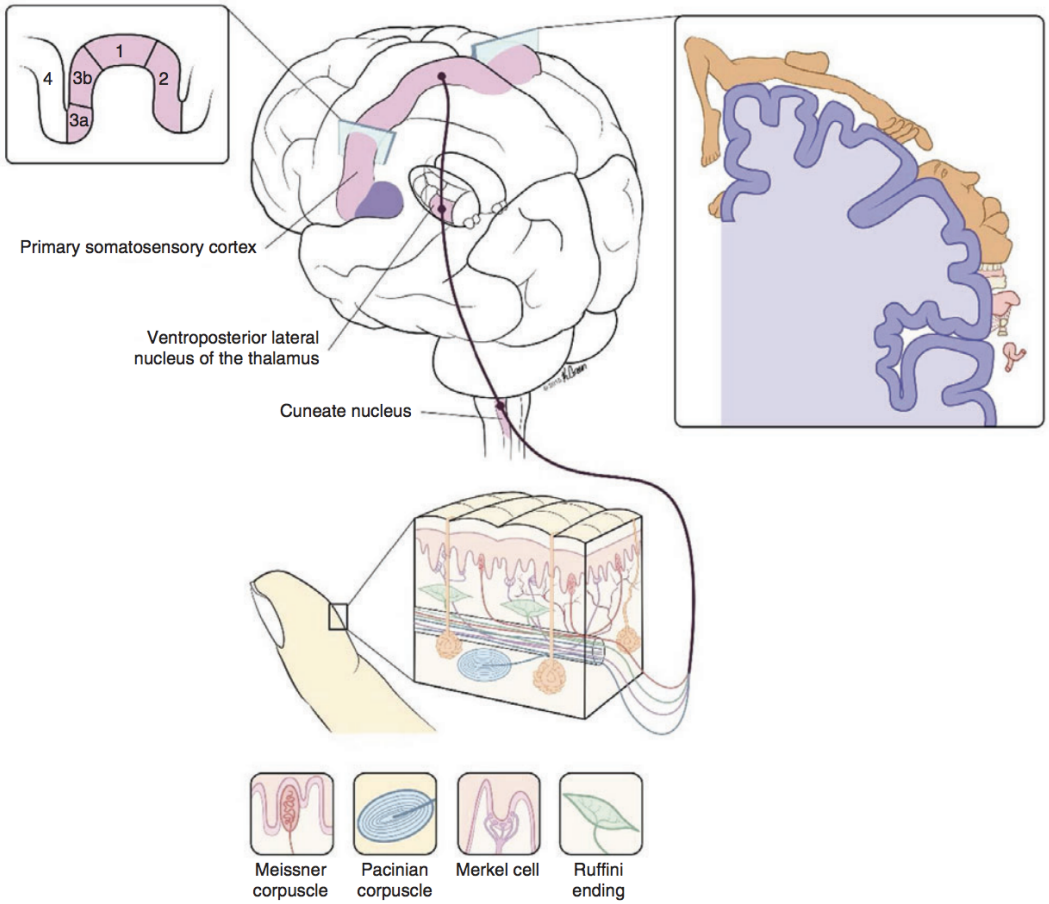

Figure 1.14: *Tactile skin sensors: the four types of low-threshold mechanoreceptors of the hand palmar surface and brain transmission channels [GB18]*

(type I). They detect static stimuli, whether it concerns shape, deformation or temperature, etc.

(SA II) Ruffini ending: are located in the dermis. Their spatial density is low (10 units per cm^2). They have a very large receptive field (type II). They are characterised by their particular sensitivity to shearing of the skin and to the sliding of objects against it.

The sense of touch is therefore armed with numerous sensitive mechanoreceptors distributed over the skin.
Without this sense, it is difficult for us to perform the most basic activities of daily life, such as buttoning a shirt, turning a doorknob or feeling the deformation of a surface, etc. In order to interact effectively with technology interfaces through the sense of touch, scientists have developed a discipline they call **Haptic**.

1.4.2 Haptic feedback

A haptic device is a human-machine interface, which is placed between the human user and the virtual domain, in order to enrich the user's perception in this virtual environ-

ment through the use of skin and muscular sensors, in particular those of the hand palmar surface.

There are two types of haptic sensation: the first is the effort feedback (or kinaesthetic feedback), relating to the muscles and joints solicited by efforts and displacements, the second is the tactile feedback which concerns the subcutaneous sensors and gathers information on surfaces, stiffness, vibration, temperature, etc.
The classification of haptic feedback is presented in Figure 1.15.

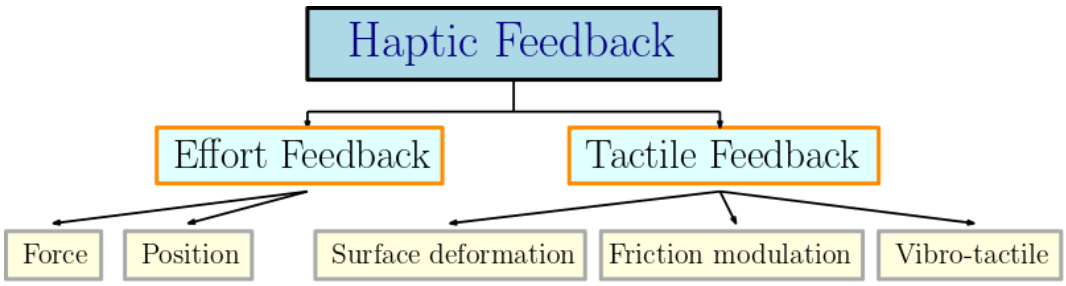

Figure 1.15: *Classification of haptic feedback, adapted from [Kac20]*

For the second type, the family of devices that explore tactile feedback is based on the generation of subtle sensations and then stimulating the mechanoreceptors.
It is the development of this type of haptic feedback that has served today's handheld devices and touch screens. The best known is the vibro-tactile property.
Other applications exist based on the exploitation of friction generation properties or superposition of deformation modes.
Examples of these technologies with their references will be presented after the next subsection.

The haptic feedback that interests us in this work is the first type, namely effort feedback.
This concerns the position feedback, when a force is applied to the system and released, so the system returns to initial position while being free. It also concerns force feedback, which is a position feedback, with the presence of a system reaction effort all along the process of pressing and return to initial position.
Nor should the pressing exceed the capacity of the system to provide the compensating reactive force to return to the starting state.

1.4.3 Criteria and needs of the haptic domain

The majority of haptic interfaces are intended for use with the hands and fingers. This is due to our current manual activity and the high density of sensors in these organs [Hay01].
To realise these tactile feedback functions, the techniques adopted use quasi-static or vibratory, thermal, or indentation devices to approximate as closely as possible the sensory information returned by a real object.
Effort feedback interfaces must provide variable effort to the user, counteract the user's

partial movement or prevent movement altogether.

A scale of our faculties to perceive an external stimulus can be given, and thus estimate the forces necessary to perceive a feedback or even the transcription of a virtual environment (Table 1.2).

Perception levels of the human hand		
Minimum perceptible angle variation	finger	2.5°
	wrist	2.0°
Variation perception of	stiffness of an object	22%
	weight	10%
	contact force	5% to 15%
Maximum controllable force		50N to 100N
Typical maximum force of devices		5N to 15N
Resolution of a force control		approx. 0.04N

Table 1.2: *Data on human manual perception [Pig05]*

The tactile feedback must meet considerations of simplicity for the handling, also of safety to avoid confusing the user. This must therefore be limited in both speed and force, either by the control or by the capabilities of the actuators.

1.4.4 Current haptic feedback technologies

Examples of simple common haptic devices include game controllers, joysticks and steering wheels, etc.
The interesting addition is to feel a feedback. This allows and generates human-machine interaction.
Talking about human-machine interaction today makes us think first of virtual reality (VR).
The development of haptic feedback devices is a need in the context of the VR industry.
VR has its origins with Ivan Sutherland in 1965 with his concept proposal of "the ultimate display" [WAN+19].
The three main features of VR are immersion, interaction and imagination. They remain criteria that haptic feedback must meet.
Today's haptic feedback devices try to address all of those specifics to ensure quality human-machine interaction.
Below are some examples of haptic feedback devices (tactile and effort feedback).

Tactile feedback devices

As mentioned at the beginning of this section, tactile feedback generally manifests itself in surface deformation, friction modulation and vibro-tactile effect.
The first type to be presented in the context of tactile feedback devices is the one based on mechanical vibrations. This is the most common method used in touch screens [WAN+19]. To produce vibro-tactile simulations, several actuation technologies are used: rotating eccentric masses, magnets or piezoelectric actuators, etc.

Hayward *et al.* [HC00] presented a vibro-tactile interface exploiting transverse and lateral skin deformations. Based on piezoelectric ceramics, the vibration is used as an information feedback to the finger (Figure 1.16).

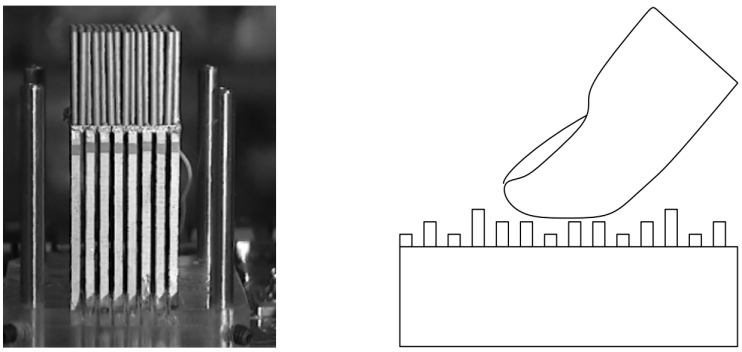

Figure 1.16: *Typical tactile display based on piezoelectric technology vibration, principle of vibro-tactile simulation [HC00] [Ghe16]*

This is the principle used on touch screens when touch vibration is activated.
There are several methods for making the system vibrate locally or globally, including multimodal superposition, time reversal and last but not least phase-shifted acoustic pulses presented in Figure 1.17.

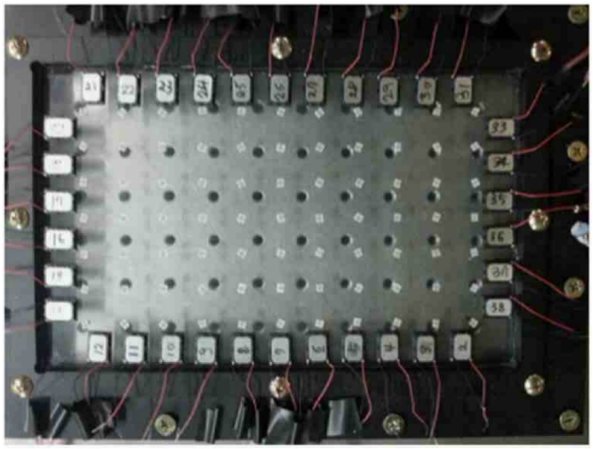

Figure 1.17: *Transparent vibro-tactile interface based on the acoustic pulse method [WI15]*

Friction modulation can also be exploited to produce a tactile effect.

In 1995, Watanabe and Fukui [WF95] developed a rectangular plate vibrated by a piezoelectric actuator at the resonant frequency of the whole system. As a result, they noticed that the surface becomes smoother to the touch when the ultrasonic vibrations are activated (Figure 1.18).

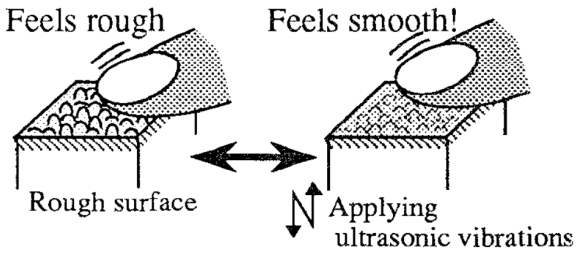

Figure 1.18: *Concept of controlling the tactile sensation of surface roughness [WF95]*

We can then, as Winfield *et al.* [Win+07] demonstrated in 2007, simulate different textures using friction modulation.

In 2016, Ben Messaoud *et al.* [MBL16] virtually simulated textiles such as velvet, cotton or polyester based on their smoothness and roughness (Figure 1.19). Vezzoli *et al.* [Vez+16] set up a touch feedback tablet on which an eigen mode of a glass plate was excited (Figure 1.20).

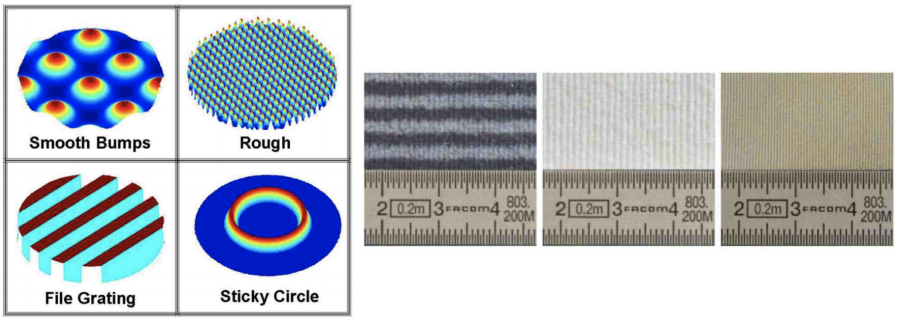

Figure 1.19: *Different types of simulated textures as well as the simulated fabrics [Win+07] [Kac20]*

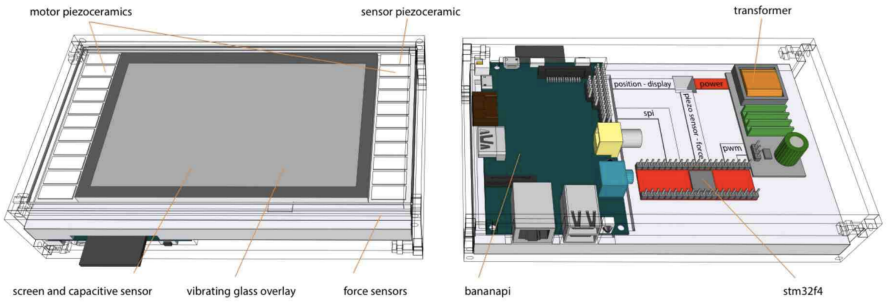

Figure 1.20: *Ultrasonic vibration-based touch interface with a 5-inch display to simulate textures: E-vita [Vez+16]*

The third type of tactile feedback mentioned is surface deformation. This is the simplest way to generate a tactile sensation, and the intuitive example is the Braille code. Among these techniques, we distinguish between pin arrays, electrode arrays, pneumatic chamber arrays and magneto-rheological liquid (Figure 1.22) arrays.
Devices based on these surface deformation techniques are shown in Figure 1.21.

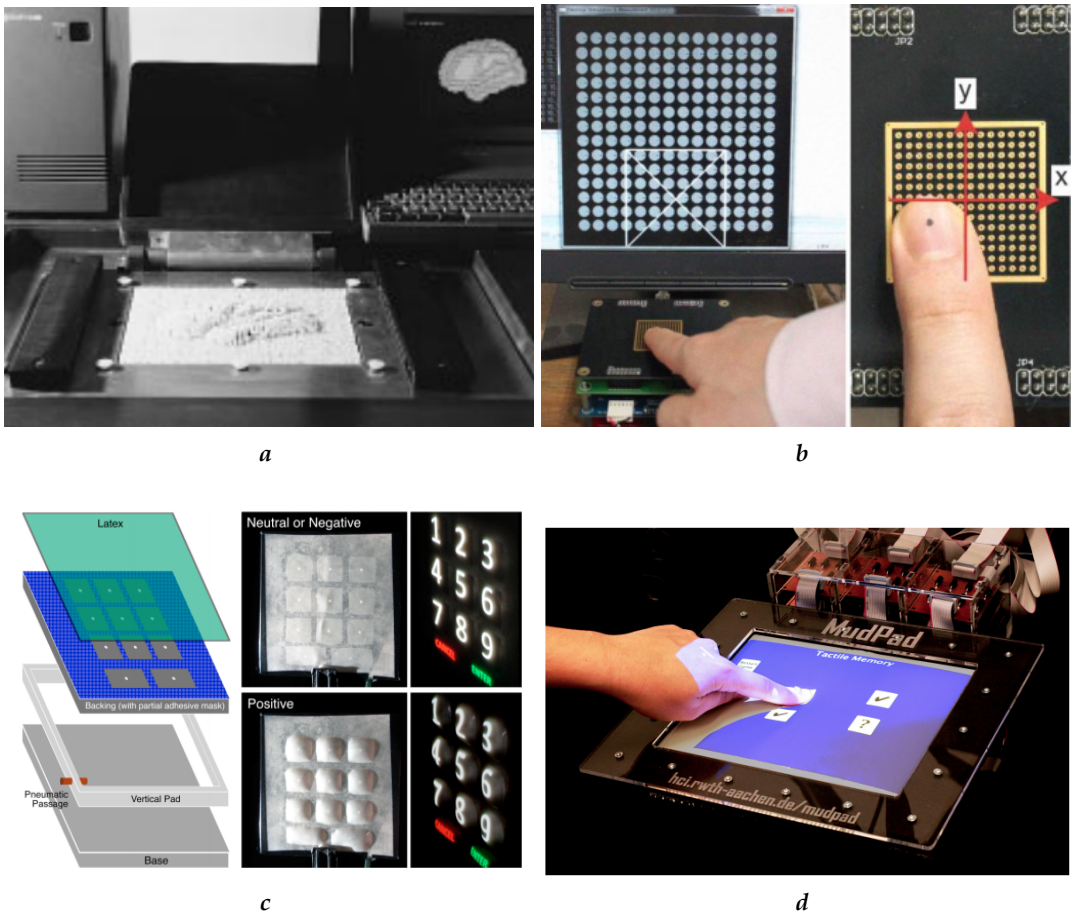

Figure 1.21: *Devices based on surface deformation techniques: (a) tactile display device presenting a relief image of the cerebral cortex using a pin network [SSM98], (b) Electro-tactile display with an array of electrodes structure [Kaj11], (c) ATM-like tactile display using pneumatic chamber, provides the sensation of a contiguous hard surface when neutrally or negatively pressurised [HH09], (d) Mudpad: a system based on exploring Magneto-rheologic Fluid properties, it provides localised haptic feedback independently at multiple points [JKB10]*

Effort feedback devices

Kinesthetic (effort feedback) devices generally consist of sensors to sense position, application of force, etc. and actuators to provide an action to the user, whether in a real or a virtual world.
They can be worn on the user as gloves or as an exoskeleton in context of virtual reality applications (Figure 1.23). Otherwise, they are non-portable, positioned on a fixed sup-

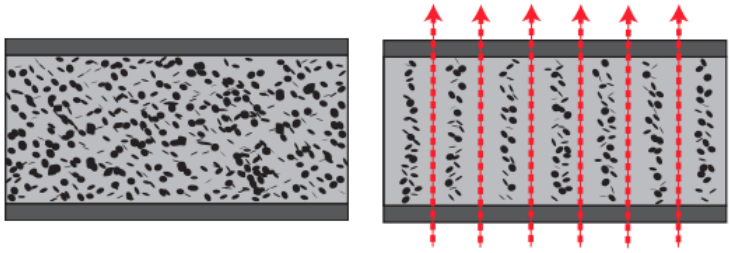

Figure 1.22: *Magneto-rheologic fluid under the influence of a homogeneous magnetic field. (left) Off state: free flowing particles within the carrier fluid, (right) On state: particles arrange along the flux lines [JKB10]*

port or a simple desk.

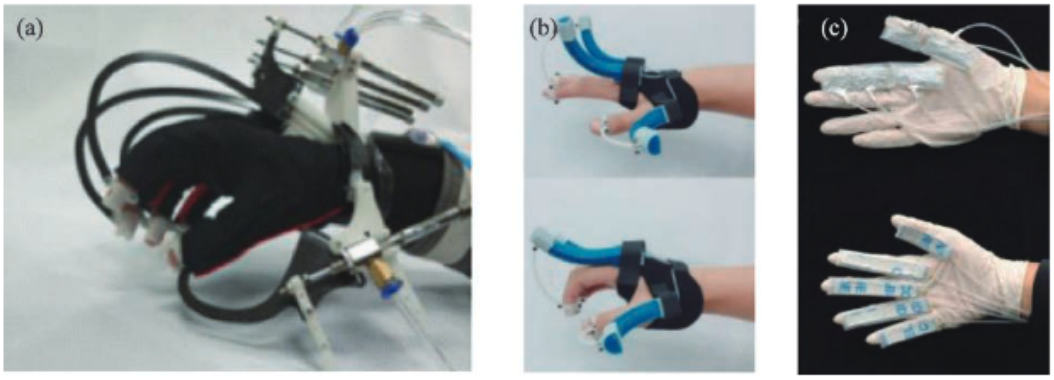

Figure 1.23: *Haptic feedback gloves using (a) Pneumatic-driven rigid actuators, (b) Fiber-reinforcement soft actuators, (c) Layer jamming soft actuators [WAN+19]*

The desktop mouse can be considered as a haptic feedback (position feedback) system with two degrees of freedom.
There are others with more than two degrees of freedom. They provide force feedback that allows, for instance, to feel collisions and contacts in a virtual world.
Dental surgery or mechanical assembly and maintenance simulators (Figure 1.24 and Figure 1.25) use this type of technology, which makes it possible to perceive the characteristics of the virtual objects being handled.

Discussion

1.5 Bi-stability to the service of haptic feedback

The bistable mechanical system, as described earlier, has two configurations in which, when unconstrained, it is able to remain motionless. The mechanism will tend to move forward when it is not in one of these configurations.
Switching from one of the stable states to the other, under the effect of an external actuation, can be exploited in the field of haptics, as position feedback or force feedback

Figure 1.24: *Force feedback simulator setup for dental surgery: comparison between handling the real instrument and the haptic stylus [CPT09]*

(both types of effort feedback). The switching is commonly known under the name of **snap-through**.

1.5.1 IPMC: the system itself is bistable

A possible first type of applications, that makes bistability to the service of haptics, is the bistable beam of Ionic Polymer-Metal Composite (IPMC).
IPMC is an ionic polymer like Nafion or Flemion whose surfaces on both sides are plated with a noble conducting material (like gold) as electrodes (Figure 1.26). It bends when a voltage (electric field) is applied between the electrodes.

IPMC is polymer based, it is therefore lightweight and can be cut out easily in any shapes.

To have multiple degrees of freedom to a beam of IPMC, we segment electrodes on the surface of the IPMC, which allows the control of each segment individually. This could be used in a case of an array of beams, if we want multiple strips of IPMC in one system. This case will be presented later in this section.

An interesting example of IPMC bistable devices, whose bistability could be exploited for haptic feedback, is the artificial muscle presented by Rossiter *et al.* [RSM06].

[3] https://www.qwant.com/?client=ext-chrome-sbt=imagesq=IPMC+ionic+polymer

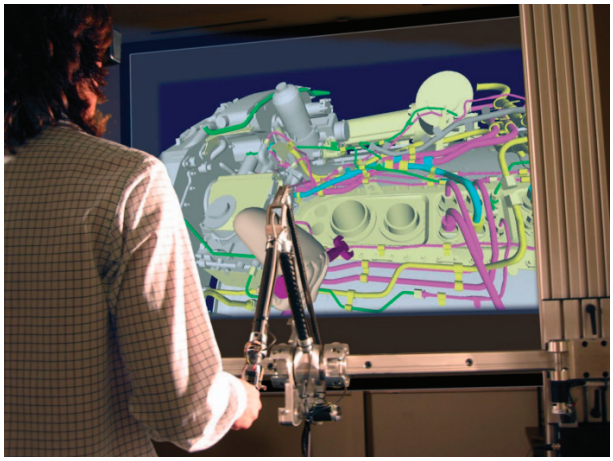

Figure 1.25: *Force feedback simulator setup for mechanical maintenance: a virtual maintainability operation on a CAD aircraft engine model [Bor+04]*

It is about a structure based on the axially compressed buckled beam of bending actuator material. It is a natural bistable and a self-buckled structure (Figure 1.27a).
Indeed, the buckling shape of an IPMC beam is very similar to the bending of three IPMC beams with different boundary conditions [RSM06]. This is why a choice was made: to segment a long IPMC beam (Figure 1.27b) in such a way that the buckling shape is obtained just by controlling the power supply of the segments (Figure 1.27c). Segmentation of a polymer actuator could be done by cutting or etching the electrodes upon one or both of its sides.

The prototype was made on the basis of a gold plated IPMC material with a base of Nafion 117 and dimensions ($4\ mm$, $38\ mm$, $0.175\ mm$). In the initial state, in the absence of an electric field, the beam is clamped at both ends and the mode 1 buckling shape is formed.

The voltage signal V_s in Figure 1.28 is applied to each segment using the connections from Figure 1.27c. The displacement D of the center of the buckled IPMC beam was recorded using a Keyence laser displacement meter. It is shown on Figure 1.28 as well.

The displacement D of the actuator's middle is a near square wave in response to the sine wave input voltage V_s.
The abrupt change from a negative to a positive value of the displacement D and vice versa marks the moment of switching, which is the desired and normal response of the bistable system. This is the response that can be exploited, i.e. snap-through, to feel the force feedback on the finger for a button application for instance (Figure 1.29).

Based on the same IPMC prototype technology, we can imagine a matrix of bistable systems constituting a haptic interface (Figure 1.30).

We propose an interface containing five buttons, with IPMC-based haptic feedback.
As with the single button case discussed earlier, what makes the bistable IPMC in up or down state are the connections to the power source. Bistable IPMCs are also segmented to facilitate this.
Depending on the use, several scenarios of the haptic interface can be imagined.

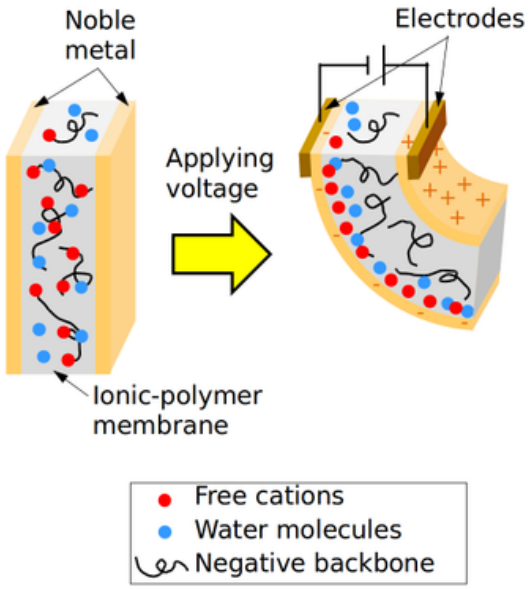

Figure 1.26: *Principle of an IPMC artificial muscle* [3]

A first case is the one where all buttons are off (Figure 1.30a), the case of non-use for example. There is the case where all the buttons are up (Figure 1.30c), and each can have a functionality, or all of them serve the same purpose. There are several intermediate cases, including the case where only the corner buttons are activated (Figure 1.30b). In this later case, a light guide can be added to indicate which button is up.

1.5.2 SMA: bistable SMA and bistable beam activated by SMA

In this paragraph, we will present **alloys** (admixture of metals) with unique properties. These are materials that can change **shape** in response to mechanical stress, electromagnetic fields or temperature.
They are able to **retain information** about the initial shape and reconstitute it after a plastic deformation in response to one of the three previous excitations.
Those are **S**hape **M**emory **A**lloys (**SMA**).

The memory effect was discovered in 1932. It was noticed on an orcadmium alloy. In 1963, it was demonstrated on a nickel-titanium alloy by the Naval Ordnance Laboratory (NiTiNOL).

On a microscopic scale, the shape memory effect is explained by a phase change. Specifically, it is due to reorganisations of the martensite variants [Bel00].

As a return to the original geometry is used, all types of displacements can be obtained, in particular contractions, extensions and also bending and buckling.

It is the last type of deformation that is the subject of the tactile application reported by Vitushinsky *et al.* [VSL09].

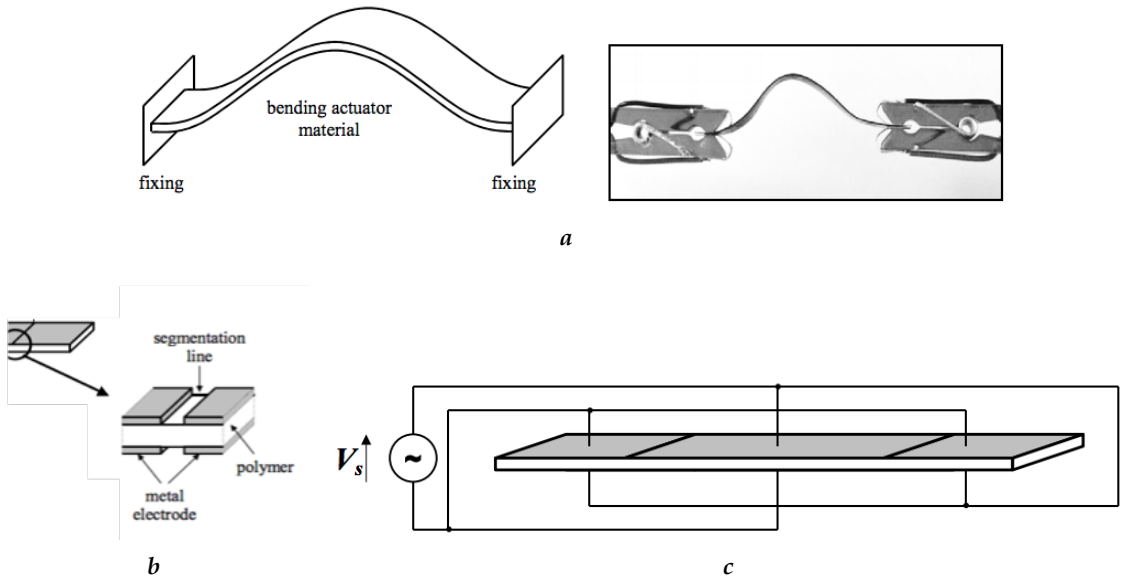

Figure 1.27: *Three-segment test beam: (a) clamped ends, (b) segmentation of the test beam, (c) voltage connections [RSM06]*

It concerns a bistable shape memory actuator for tactile graphic displays.
The actuators are buckled metallic thin-films, having structured Ti–Ni–Cu and Ti–Ni–Hf shape memory alloys on the top and at the bottom, respectively (Figure 1.31a).

The prototype presented good performances. Actuators were switched with actuation voltages in the range of 0.6 to 1.6 V and with currents in the range of 0.6 to 1.8 A. A force feedback of 16 mN with a displacement of 1.2 mm were reached.
The combination of bistable systems on a graphic display offers a promising tactile application for blind people for instance (Figure 1.31b).

Another application of an SMA-based haptic system can be proposed. This is a non-active bistable structure, activated by bonded SMA actuator.
This is the principle of one of Cazottes's tests in his work [Caz09].

The inactive bistable structure in this case is a steel beam, axially compressed to buckling.
We have shown before in this manuscript, and will be presented in detail in Chapter 2, that buckling can lead to two stable states, and we can switch between them (snap-through) by different types of actuation.
The on-surface bonded SMA would allow the switching by creating a distributed moment along the structure.
However, in Cazottes's test bench, the bonding did not hold, due to the high temperature (approaching the glue's vitrification temperature) and especially due to the deformation of the SMA, which contracted by several percent. Another problem with the assembly is due to thermal diffusion. Heat from the SMA will diffuse and may heat neighbouring parts by conduction, including other active areas. Thermal insulation of the actuator from its structure is difficult.

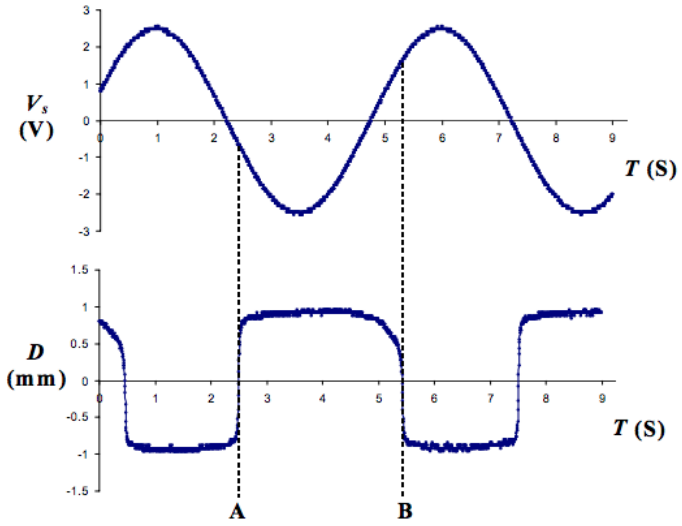

Figure 1.28: *Driving voltage and displacement of the buckled beam center signals [RSM06]*

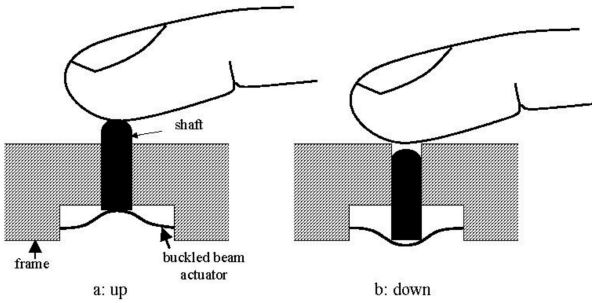

Figure 1.29: *Application of bistability in haptics: a haptic output device [RSM06]*

A final proposal was made: that the SMA be completely separated from its structure. The SMA plate, separated from the structure and trained to press in a specific direction, will press on the structure to switch it (Figure 1.32).

The inactive beam has dimensions (101*20*$0.4\ mm$). It is made of stainless steel with a Young's modulus of $178.5GPa$. The SMA blade is $1\ mm$ thick, it has the same width as the stainless steel beam and its length is 40% of the length of the bistable. It is made of Nickel-Titanium alloy, with a transformation temperature of $60°C$.
This set-up has given satisfaction. It allows the snap-through by heating the SMA. However, as with any SMA actuation, the response time is high (can reach seconds depending on the SMA geometry, material, volume, etc.), as the temperature of the actuator must be raised or decreased by several tens of degrees.

1.5.3 PZ: introduction to the intended application

In the previous paragraph we introduced the possibility of sticking an active element on a bistable structure.
In this part, we will introduce the premise of the thesis work. It is about the exploitation of the bistability and the snap-through of the buckled beam to feel a haptic feedback by

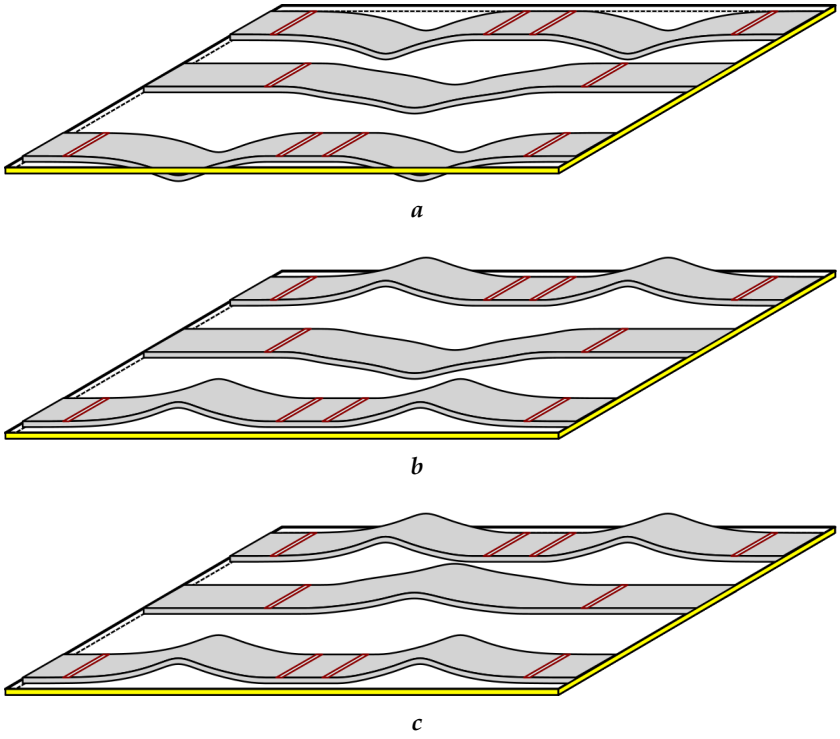

Figure 1.30: *Different states of the buttons in the proposed haptic interface: (a) all buttons are off, (b) centre button is off, others are on, (c) all buttons are on*

actuating through piezoelectric (PZ) materials.
The structure is therefore the buckled beam and the actuator is one or several PZ patches.

To facilitate the design, the PZ actuator is first bonded to a double-clamped steel structure and then the assembly is buckled under axial compression (Figure 1.33).

The characterisation of the complete system will be presented in detail later in Chapter 2 and Chapter 4.
The target application is a button with force feedback or position feedback depending on the performance of the actuator. A matrix of independent buttons on an interface can be imagined based on the single button.
The activation of this system will incorporate both mechanical and electrical aspects: the switching from the up to the down state is done by applying transverse mechanical force (finger pressure) and the activation from the down to the up state is done by electrically energising the PZ actuator.

So here are a number of possibilities for using bistability for haptic feedback, with the use of active materials for actuation.
The bistable system may be the actuator itself, or it may be an inactive structure that is actuated by an external active element.
The study of the last application example represents a large part of the work done in this thesis.

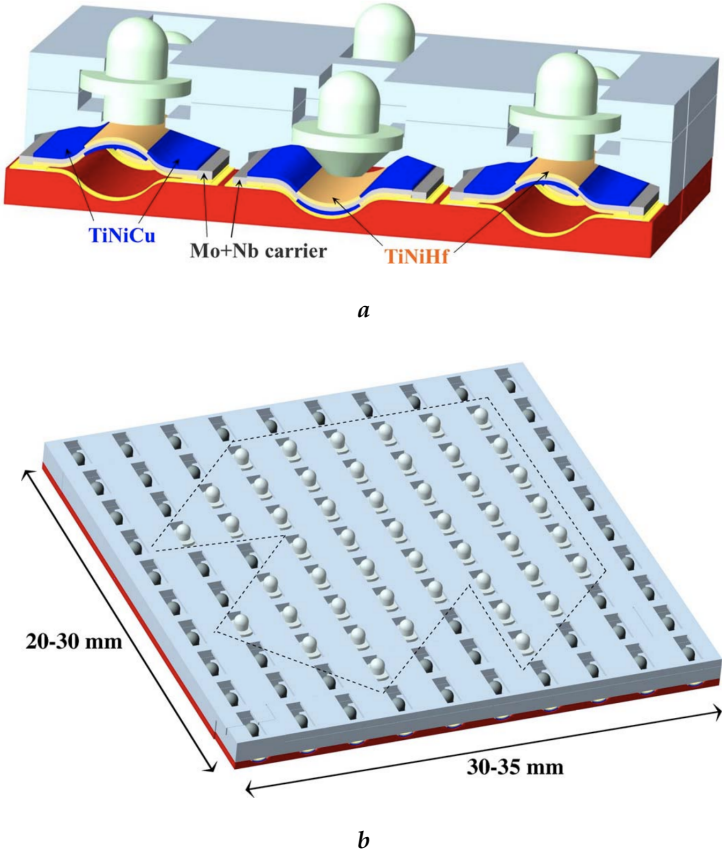

Figure 1.31: *Bistable SMA actuator based on thin-film composite: (a) structured Ti–Ni–Cu and Ti–Ni–Hf shape memory alloys on the top and at the bottom respectively, and intermediate thin-film passive carrier ($M_o + N_b$). Up and down states of SMA actuators are shown. (b)* $10 * 10$ *actuator array forming a tactile graphic application [VSL09]*

1.6 Positioning and contributions of the thesis

Surface activation to make haptic feedback is a major technological stake. Piezoelectric materials are particularly well positioned to meet such a technological challenge. They integrate by nature sensor and actuator functions, allow efficient electrical-mechanical conversion in a small volume and, with optimal sizing, allow to obtain interesting displacement amplitudes.

GeePs laboratory has recognised expertise in the development of devices based on piezoelectric materials [Seg18] [Bra17] [Har12] [CBB08] [CDB08] [Cor+08].
The objective of this thesis is to develop a proof of concept of a haptic feedback system, based on a bistable surface activated by PZ materials.

The thesis incorporates both aspects 'Materials' for understanding the physical mechanisms, and 'systems' aspects for a good understanding of the constraints on the piezoelectric elements.

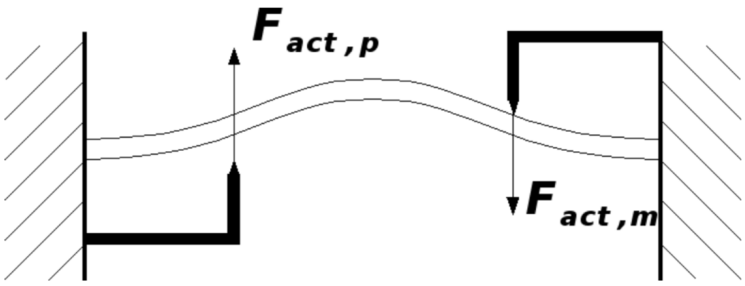

a

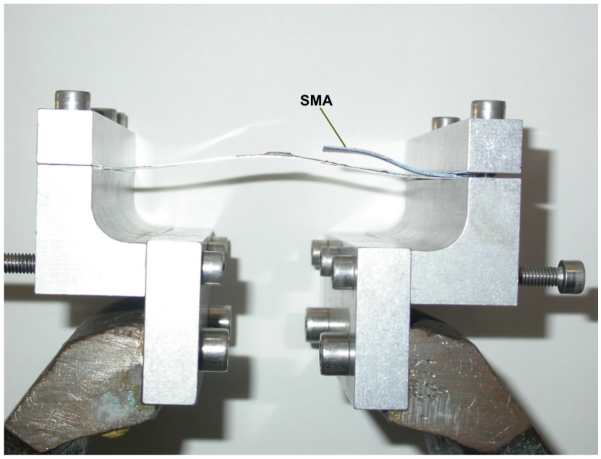

b

Figure 1.32: *Separate SMA actuating a bistable inactive structure: (a) Actuation with two external SMA actuators, each actuator is used to actuate in one direction. (b) Test bench with one SMA actuator to switch from top to bottom [Caz09]*

A benchmark and comparison between PZ actuation models has been performed, with a parametric study to discuss their validity to be applied on different geometry dimensions and different materials. We have tested two equivalent models: force model and moment model on a cantilever actuated by a PZ patch. This result was compared with the result of a study on a finite element design and calculation software. We had therefore the domains of validity of the equivalent actuation models. The study led to a publication in a journal.
The work deals also with two types of bistable surfaces: simple buckled beam (already exists, but with relatively large dimensions compared to ours [Caz+09] [CS15] [Amo20]) and buckled clips (new proposed configuration). In both cases, the bistable surface will be the structure and the actuator will be one or more bonded piezoelectric patches.
Thus, the study consists of characterising bistable systems through modelling and experimentation, and then optimising the external actuation to switch from one stable state to the other.

In the particular case of automotive applications, where driver distraction is a problem, it's important to have touch screens and touch surfaces enriched by haptic feedback.

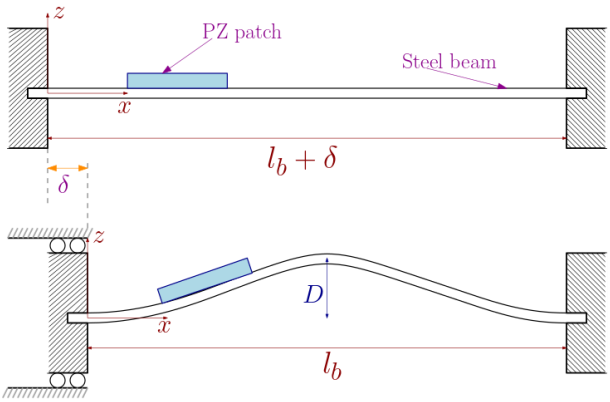

Figure 1.33: *Bistable system with PZ material: PZ actuator bonded on a steel structure, the set is buckled under axial compression*

Haptic interface topologies are proposed so that they can be used on an automotive dashboard. An ongoing patent has been filed for this application.

Chapter 2

Characterisation of bistable systems

Contents

2.1 Introduction

The aim of this chapter is to study in detail two types of bistable structures, with a view to using them later under piezoelectric actuation.
The purpose of this chapter is to demonstrate that first, those chosen systems are bistable and then characterise them mechanically to understand their properties and the levels and location of forces that need to be applied to them to exploit their bistability.
The two systems studied will be axially compressed single beams and laterally pre-stressed 'U' shaped clips. The second system is an alternative solution to duplicate a bistable device in order to have a matrix of independently operated bistable systems.

The entire study is conducted in accordance with the fundamental assumptions of mechanics of materials.
First, the principle of Saint-Venant is considered, with especially its consequence that the results obtained by the calculation of mechanics of materials are valid only at a sufficiently large distance from the region of application of the external mechanical actions.
Second, according to the Navier-Bernoulli hypothesis, the sections normal to the mean line remain flat and normal to the mean line during deformation.

2.2 Simple bistable beam

2.2.1 Introduction

The beam theory, or Euler-Bernoulli theory is used in the field of mechanics of materials. Similarly for the beam hypothesis cited before for piezoelectric materials, the term "beam" refers to an object whose length is large compared to the other dimensions (thin section). Leonardo da Vinci had preceded Galileo, to whom the theory of beams is attributed. Da Vinci, was the first to describe that the deformation varies linearly away from the neutral surface and the coefficient of proportionality being the curvature, without however managing to imagine Hooke's law.
Leonhard Euler and Jacques Bernoulli came up with the first useful theory around 1750, while Daniel Bernoulli, the nephew of the former, wrote the differential equation for vibration analysis.
Beams in general can be subjects to different types of solicitations. Among others, we mention uni-axial tension, shear, pure bending, buckling or a composition of these solicitations.
The type of structure deformation we will deal with in the following is buckling.
The set of parameters used by default for the digital applications in analytical modelling, finite element modelling (FEM) and experiments are summarised in table 3.1.

2.2.2 Buckling of beams

Buckling is an abrupt appearance of a change in shape in a direction different from that of the applied loads.

Beam Parameter	Unit	Value
E_b	GPa	200
t_b	mm	0.3
l_b	mm	50
b	mm	10

Table 2.1: *Dimensions and material parameters used for the FEM of the beam buckling and bistability study*

Buckling often leads to the ruin of structures. However, it can be used to dissipate energy, or create very flexible structures.
It is a design criterion for columns and compressed bars.
This phenomenon is considered an instability because it contains an unstable equilibrium, and is difficult to predict because it is very sensitive to geometric or material imperfections, and to boundary conditions.

Concerning the process to obtain a buckled beam, the basic configuration is a double built-in elastic beam. The beam has one end fixed, the other end can move under the effect of a force.
An axial force P is applied to the movable end. This leads to the displacement δ of this extremity, and consequently the appearance of a transverse displacement D when P exceeds a threshold value (Figure 2.1). Once the desired displacement D_0 is obtained, the supporting device is fixed.

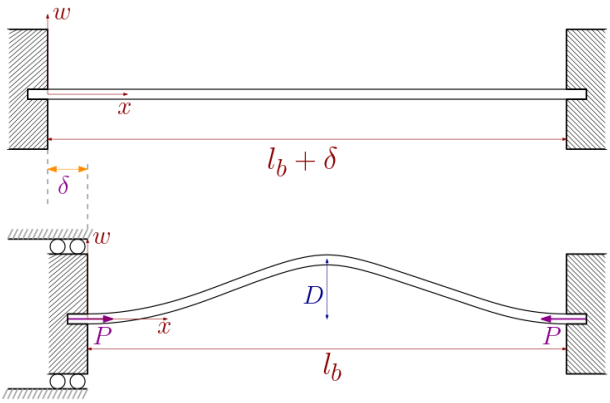

Figure 2.1: *Double clamped beam: process to obtain the buckled structure*

This displacement δ can be decayed into two parts ($\delta = \delta_e + \delta_b$): δ_e related to the elasticity of the beam and δ_b part which generates the central deflection D.
This says that there is a critical axial force, which we note P_{crit}, at which the transverse displacement appears. This is the axial force threshold of the beam, which can be expressed as:

$$P_{crit} = k.\delta_e \simeq \frac{A_b E_b}{l_b}.\delta_e \tag{2.1}$$

where $k \simeq \frac{A_b E_b}{l_b}$ the beam stiffness constant ($N.m^{-1}$), A_b the section (m^2), E_b Young Mod-

ulus (Pa) and l_b the length (m) of the beam.
At this stage of our analysis, P and δ_e are two unknowns. The study in next paragraph will give different expressions and relations between P_{crit}, $\delta = \delta_e + \delta_b$ and D.
We will go a little further, by setting up a second transverse actuating force in the middle of the beam, and look at its influence on the different quantities mentioned before.

2.2.3 Analytical study on buckling variables

We will conduct a mechanical study to determine the relationships between the buckling variables.
We begin by defining the different variables involved (Figure 2.2) and the study hypothesis:

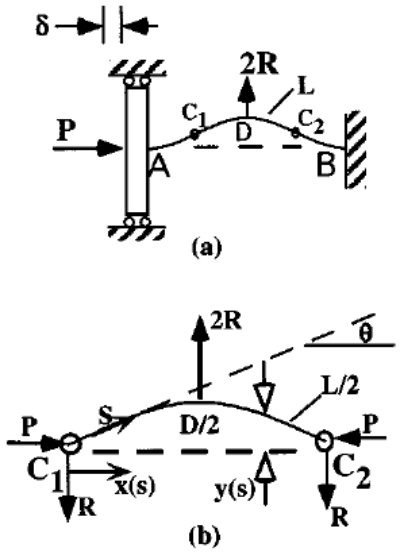

Figure 2.2: *Buckling of a beam and variables involved: (a) 1D complete buckled beam and (b) sinusoidal portion C_1C_2 of the deformed beam [Tah00]*

- Variables : axial force P, central normal force $2R$, axial displacement δ and central displacement D
- Hypothesis :
  - small displacements in relation to the length of the beam $\frac{D}{l_b} << 1$ ($\frac{D}{l_b} < 10\%$)
  - elastic behaviour of materials
  - (C_1C_2) part of the beam after buckling is a sine branch
  - only the first buckling mode appears

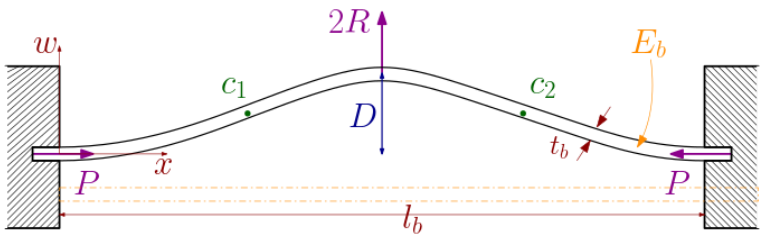

Figure 2.3: *2D buckled structure with different forces involved and beam parameters*

Figure 2.3 presents a 2D view of the buckled system with the addition of the thickness t_b and the material parameter E_b of the beam. The width of the beam will be noted as b.

Let s be the curvilinear abscissa of the beam after deformation. At a small scale of displacement, the curvilinear abscissa is related to x and w by:

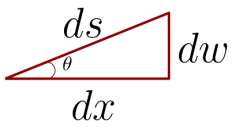

$$\begin{cases} dx = cos(\theta)ds \\ dw = sin(\theta)ds \end{cases} \tag{2.2}$$

For notation, w' and w'' stand for the first and second derivatives of w with respect to s respectively.
We therefore have $w' = sin(\theta)$ with $|w'| << 1$ (small displacement assumption), hence the following relationship:

$$dx = cos(\theta)ds = \sqrt{1 - sin(\theta)^2}ds = \sqrt{1 - w'^2}ds \simeq \left(1 - \frac{w'^2}{2}\right) ds \tag{2.3}$$

we derive w a second time:

$$w'' = cos(\theta)\frac{d\theta}{ds} = \frac{dx}{ds}\frac{d\theta}{ds} \tag{2.4}$$

hence the **curvature** of a deformed beam portion which we define as:

$$\frac{d\theta}{ds} = \frac{w''}{1 - \frac{w'^2}{2}} \tag{2.5}$$

• **Note:** *If the derivation convention is taken with respect to x, i.e. $w' = \frac{dw}{dx}$ and $w'' = \frac{d^2w}{dx^2}$ then the curvature is given in the following known form:*

$$\frac{d\theta}{ds} = \frac{w''}{(1 + w'^2)^{3/2}} \tag{2.6}$$

Under the Euler-Bernoulli hypothesis, which allows the use of the moment-curvature relation [Pop76], we write:

$$\frac{M}{E_b I} = \frac{d\theta}{ds} \tag{2.7}$$

where M is the bending moment $(N.m)$, E_b the Young modulus of the beam (Pa) and I its quadratic moment (m^4) given by: $I = b\frac{t_b^3}{12}$.
For the left hand side half of the portion C_1C_2, the moment-curvature equation could be written as:

$$\frac{-Pw - Rx}{E_b I} = \frac{d\theta}{ds} = \frac{w''}{1 - \frac{w'^2}{2}} \tag{2.8}$$

with the following boundary conditions : $w(0) = 0$ and $w\left(\frac{l_b}{4}\right) = \frac{D}{2}$

With the assumptions of $|w'| << 1$ and based on equation (2.3), equation (2.8) may be approximated by:

$$\frac{-Pw - R\int_0^s \left(1 - \frac{w'^2}{2}\right) \mathrm{d}r}{E_b I} = \frac{w''}{1 - \frac{w'^2}{2}} \simeq w'' \left(1 + \frac{w'^2}{2}\right) \tag{2.9}$$

Assuming that the deformation between C_1 and C_2 is a sine branch, we write:

$$w(x) = \frac{D}{2} sin\left(\frac{2\pi}{l_b} x\right) \tag{2.10}$$

To solve the differential equation (2.9), we use the approximation solution for w in (2.10). We then carry out the necessary integral and derivatives:

$$\begin{aligned} -P\frac{D}{2} sin\left(\frac{2\pi}{l_b} x\right) - R\left[x\left(1 - \frac{\pi^2 \left(\frac{D}{2}\right)^2}{l_b^2}\right) - \frac{\pi \left(\frac{D}{2}\right)^2}{4l_b} sin\left(2\frac{2\pi}{l_b} x\right)\right] = \\ -E_b I \frac{D}{2}\left(\frac{2\pi}{l_b}\right)^2 sin\left(\frac{2\pi}{l_b} x\right)\left[1 + \frac{1}{2}\left(\frac{2\pi}{l_b}\frac{D}{2}\right)^2 cos^2\left(\frac{2\pi}{l_b} x\right)\right] + Res\,(D, x) \end{aligned} \tag{2.11}$$

where $Res(D, x)$ is the residual error, due to the replacement by an approximate solution in the differential equation.
To find mainly the value of the unknown displacement D, as a function of the applied forces and the beam parameters, we apply the weighted residual method, more specifically the Galerkin method [Fin13]:

$$\int_0^{\frac{l_b}{4}} sin\left(\frac{2\pi}{l_b} x\right) Res\,(D, x)\ \mathrm{d}x = 0 \tag{2.12}$$

where the test function $sin\left(\frac{2\pi}{l_b} x\right)$ respects the two conditions of use: same boundary conditions and same or approximately the same shape as the proposed solution.

We obtain after calculation an algebraic equation from which we express the transverse displacement D as a function of the applied efforts and parameters of the beam:

$$\frac{P}{P_{crit}}\frac{D}{2l_b} + \frac{2R}{P_{crit}}\left[\frac{1}{\pi^2} - \frac{4}{3}\left(\frac{D}{2l_b}\right)^2\right] = \frac{D}{2l_b}\left[1 + \frac{\pi^2}{2}\left(\frac{D}{2l_b}\right)^2\right] \tag{2.13}$$

where we define P_{crit}, the axial force at which the beam starts to buckle ($P > P_{crit} \Rightarrow D \neq 0$). It's given by equation (2.1).
The expression with which P_{crit} has been replaced in the equation (2.13) is demonstrated by Timoshenko [Tim36]:

$$P_{crit} = 4\pi^2 \frac{E_b I}{l_b^2} \tag{2.14}$$

- **Particular cases:**

1. Only the transverse force acts on the beam: $P = 0$
   The relationship between the transverse force $2R$ and the displacement D in this case is written as:
   $$2R = P_{crit}\frac{D}{l_b}\left[\frac{1+\frac{\pi^2}{2}\frac{D^2}{4l_b^2}}{\frac{2}{\pi^2}-\frac{8}{3}\frac{D^2}{4l_b^2}}\right] \tag{2.15}$$

2. Only the axial force is involved: $2R = 0$
   The relationship between the axial force P and the displacement D in this case is written as:
   $$P = P_{crit}\left[1+\frac{\pi^2 D^2}{8l_b^2}\right] = P_{crit}\left[1+\frac{1}{2l_b}\frac{\pi^2 D^2}{4l_b}\right] \tag{2.16}$$
   Equation (2.16) can also be written as:
   $$P = P_{crit} + \frac{P_{crit}}{2l_b}\frac{\pi^2 D^2}{4l_b} = P_{crit} + K_b\delta_b \tag{2.17}$$
   with $K_b = \frac{P_{crit}}{2l_b}$ expressing the stiffness of the beam when the buckling threshold is crossed: it is a post-buckling stiffness, and
   $$\delta_b = \frac{\pi^2 D^2}{4l_b} \tag{2.18}$$
   the post-buckling axial displacement, which is responsible for the appearance of the transverse displacement D.

Combining the two equations (2.1) and (2.18) which give δ_e for the limit before buckling, and δ_b which causes the transverse displacement, we can plot the curve in Figure 2.4. It concerns the transverse displacement D as a function of the axial displacement with its two components $\delta = \delta_e + \delta_b$.

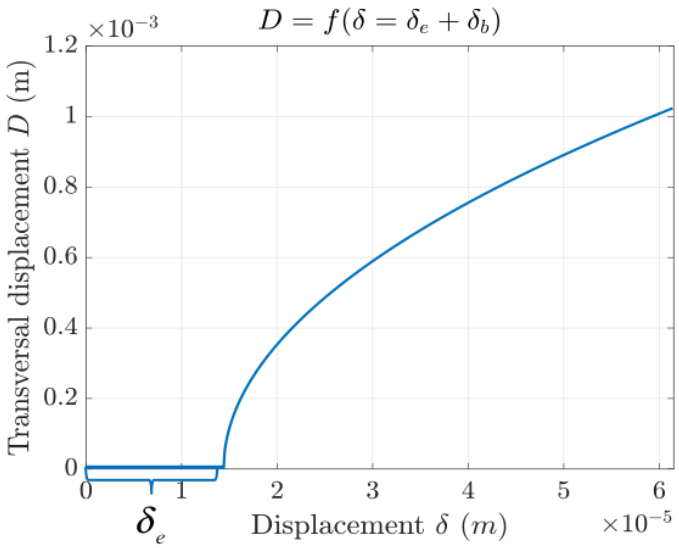

Figure 2.4: *Double clamped beam: transverse displacement D as a function of axial displacement δ*

It is normal that for the first part, i.e. $\delta<\delta_e$, the transverse displacement is zero. There is no buckling yet. This is the linear behaviour of the beam, which is characterised by its stiffness and P_{crit}.
We continue to push axially the moving end until we get the desired transverse displacement. The specification envisages a stop at around $D = 1\ mm$.
This is a deformation value that is easily felt with a finger, and the force levels to be applied are relatively small.

- **Comparison with finite element calculation:**

To validate the analytical result, we will conduct a buckling study with the numerical modelling code Comsol under the plane stress assumption.
Indeed, this software contains by default a buckling module that we can use.
However, the results of the displacements obtained, in particular the transverse displacement, are not consistent with the dimensions of the system: transverse displacement of the order of metres is found for our beam of centimetric dimensions.
The explanation for this is that once buckling is initiated with a P_{crit} in the numerical modelling, there is no longer an axial reaction force to establish equilibrium. The numerical result of the transverse displacement keeps increasing, so it gives an insignificant (too high) value.
The Comsol buckling modulus is not then used to determine what happens after buckling.
Its role is mainly to determine the critical values of the axial force $P_{crit,i}$ for which the buckling modes $i \in \{1, 2, 3...\}$, under different boundary conditions, appear.

The solution is to conduct a post-buckling study. Its principle is as follows.
We take a simple beam with one end clamped. The beam is axially compressed by moving the end that is free to move. We have the choice to compress the beam by applying an axial force or an axial displacement. Both approaches lead to the same result.
Because we are using an elasticity package this time, and not a buckling package, the beam has a linear and elastic behaviour. This means that we can compress it as much as we want without any transverse deformation appearing. This is due to the symmetry of the stresses in the beam section after compression.
We need to break the stress symmetry so that the transverse displacement occurs, i.e. so that the beam buckles.
One method of breaking stress symmetry is to apply a very small transverse force (of the order of $0.1\ N$) at the middle of the beam, so that it breaks the stress symmetry and at the same time, not influence the final result, i.e. the force, displacement and strain levels.
This small force induces an asymmetry in beam stresses, which is responsible for structures buckling under axial force in the experiment.
The structure therefore buckles and we stop at the same displacement level as in the analytical model $D = 1\ mm$ (Figure 2.5). This is called **post-buckling** study.

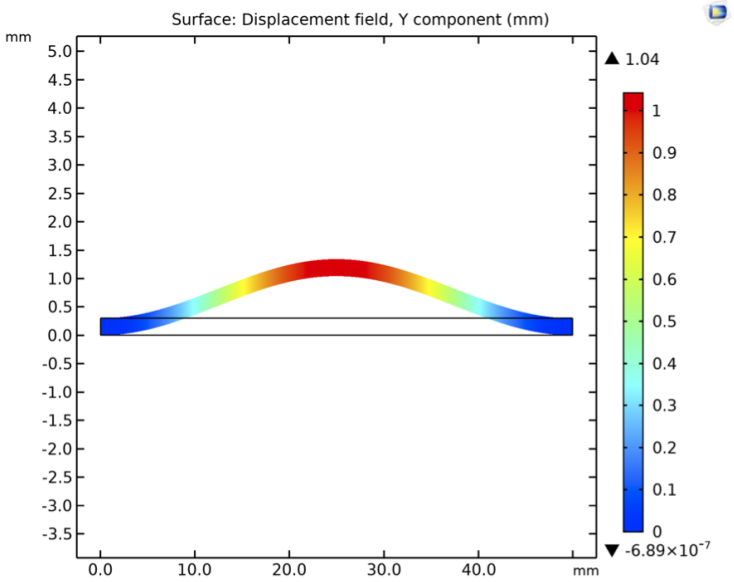

Figure 2.5: *Numerical modelling of buckling under axially applied force or displacement*

Technically, the axial force or axial displacement on the free moving end is applied with a sweep. This allows all intermediate states to be passed through before the desired transverse displacement D is reached. It then allows the transverse displacement D to be plotted against the axial displacement δ.
Based on this, we plot the curve ($D = f(\delta)$) of the analytical and the numerical model, and make the comparison to test the consistency of the analytical one.
Figure 2.6 shows the plot of the two analytical and numerical curves of $D = f(\delta)$.

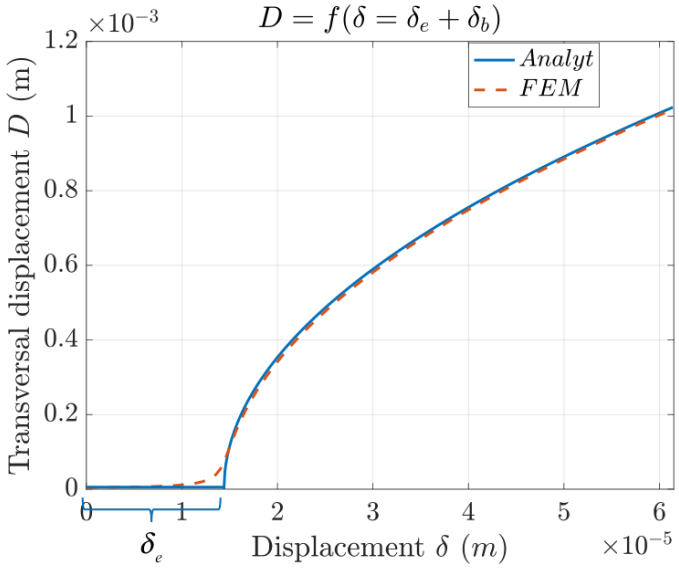

Figure 2.6: *Analytical and FEM of buckling process of a double clamped beam: transverse displacement D as a function of axial displacement δ*

It can be seen that both curves have the same shape. The numerical curve starts to have transverse displacement a little in advance. This is mainly due to the small trans-

verse force which breaks the symmetry and favours buckling in one direction (upwards here) rather than the other depending on its sign.
Now that we have the buckled structure, we fix all the ends and maintain the resulting displacement $D \simeq 1\ mm$. We will then model the effect of the transverse force $2R$ on the beam displacement D.

- **Bistability:**

Analytical model (Equation (2.13)), which describes the case where the beam is buckled and can be actuated with a transverse force, can be rewritten as:

$$2R = \frac{P_{crit}}{\frac{1}{\pi^2} - \frac{4}{3}\left(\frac{D}{2l_b}\right)^2}\left[\frac{D}{2l_b}\left[1 + \frac{\pi^2}{2}\left(\frac{D}{2l_b}\right)^2\right] - \frac{P}{P_{crit}}\frac{D}{2l_b}\right] \tag{2.19}$$

For a fixed $P > P_{crit}$, which in turn fixes the initial transverse displacement due to buckling and that we note $D_0 \simeq 1\ mm$, we can plot the curve ($2R = f(D)$) and analyse its shape (Figure 2.7).

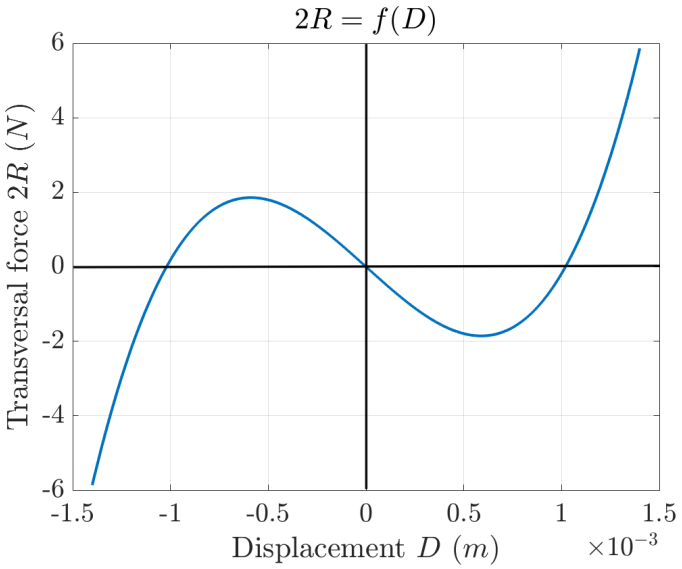

Figure 2.7: *Transverse force $2R$ versus transverse displacement D for a buckled beam with a fixed axial force $P > P_{crit}$*

First of all, the plot has the appearance of the classical curve of bistable systems mentioned in chapter 1. It is a system that switches from one equilibrium state to another equilibrium state, during the negative stiffness phase (downward slope on the graph).
To validate this conclusion, we plot the potential energy related to the transverse force and the displacement it induces as a function of this displacement itself (Figure 2.8).

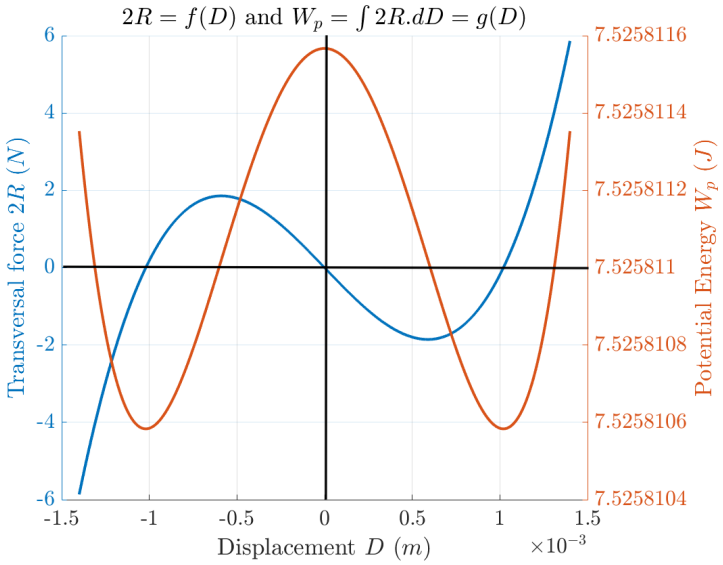

Figure 2.8: *Potential energy related to the transverse force $2R$ versus transverse displacement D for a buckled beam together with $2R = f(D)$ plot*

Based on this Figure 2.8, the potential energy $W_p = \int 2R.dD$ in red has three local optima, two minimum and one maximum. This means that the system has two stable equilibrium states. The maximum energy corresponds to the unstable equilibrium position.
It is therefore a bistable system.

2.2.4 Numerical modelling of bistability

On FEM software, the process for testing bistability is relatively the same as in analytical modelling. We fix the edges to maintain the initial displacement D_0, and it is this configuration that we subsequently use as the basic structure.
On this structure, we apply a transverse force in the middle and plot the transverse force versus transverse displacement curve.
We notice in this case that the FEM diverges as the transverse displacement approaches zero (flat beam).
This is due to the fact that this position is an unstable position, and the FEM code is not able to handle either instabilities or branch jumps corresponding to the beam snap-through.
There are two equivalent methods for the FEM code to converge even around the unstable point: displacement control or force control, and their results are similar.
To be precise, both methods are equivalent to controlling in displacement since the displacement is the size that undergoes the discontinuity in modelling and at the same time it indicates the point of instability.
The displacement control consists in imposing on the middle point of the beam, already at $D_0 = 1\ mm$, a transverse displacement which goes for instance from 0 to $2\ mm$ downwards in our Figures convention. Controlling the displacement no longer poses the prob-

lem of sudden switching or instability. The transverse force versus transverse displacement curve is therefore plotted by retrieving the reactive force in Comsol along the path, from top to bottom.
Force control uses the same trick except that the $2R$ force itself is applied to the middle of the buckling beam. To avoid branch jumping and the problem of instability, it is imposed on this force to be applied in such a way that the induced displacement follows precise sweep values.
This force $2R$ (equivalent to RR in Comsol figures) is defined as shown in the figure 2.9.

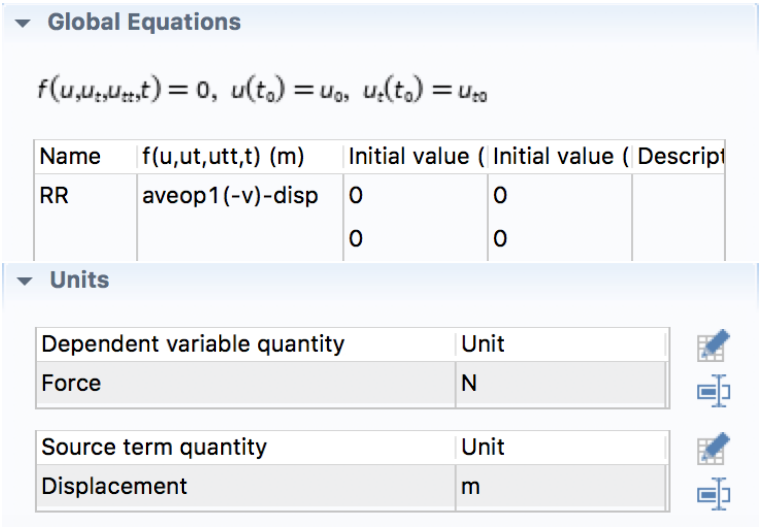

Figure 2.9: *Transverse force definition on numerical software to avoid the problem of divergence of the calculation during snap-through and especially the instable equilibrium*

The $2R$ equation then dictates that the value followed by the induced transverse displacement v (defined with an average $aveop1$ for use in a global equation) must follow the values imposed by the user (noted $disp$).
Figure 2.10 shows three main steps of the snap-through, going from the upper equilibrium state to the lower one.
Thus, we can plot the curve $2R$ as a function of the transverse displacement ($disp$ or v) of the beam midpoint.
The shape of the curve $2R = f(D)$ under FEM is given in Figure 2.11. The result is the same whether for displacement control or force control.

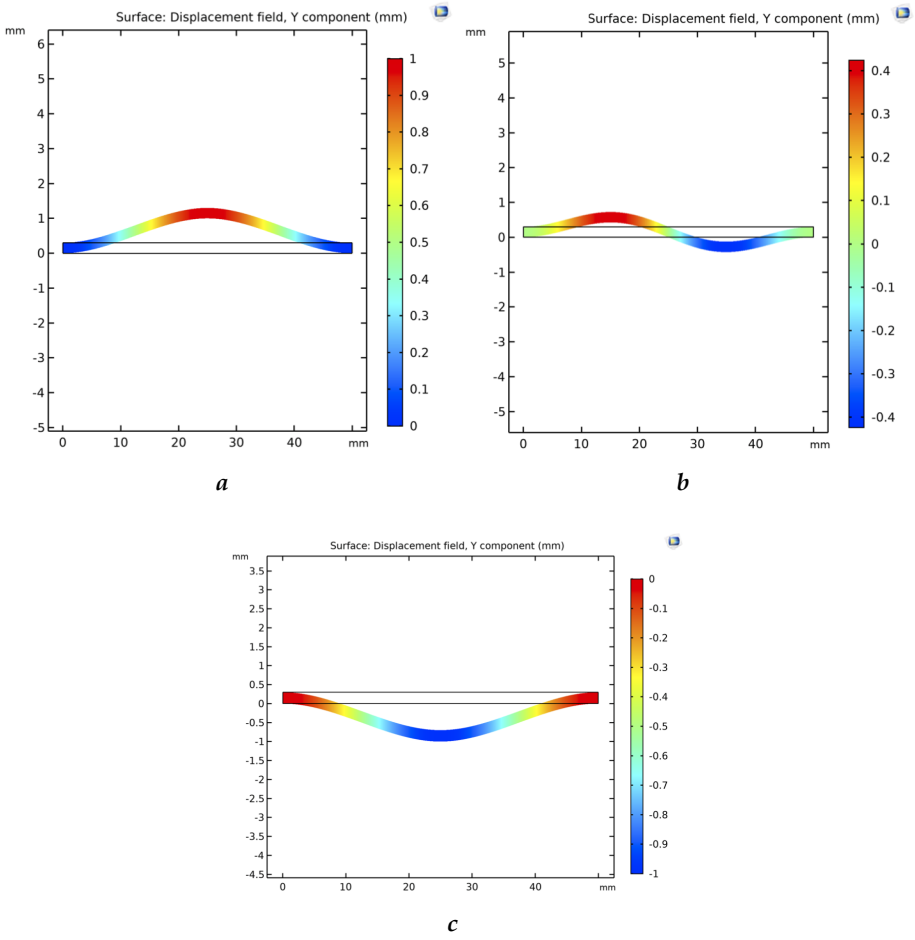

Figure 2.10: *Three different stages of switching from the upper to the lower equilibrium state: (a) first stable upward state of equilibrium, (b) unstable state of equilibrium with onset of mode 2 buckling and (c) second stable downward equilibrium state*

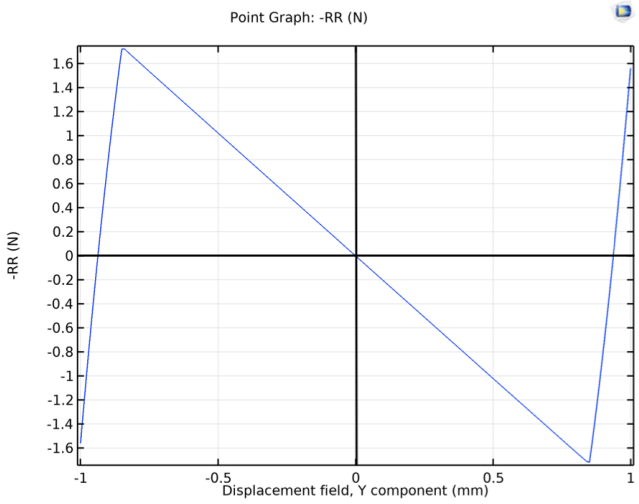

Figure 2.11: *FEM of a force displacement bistable curve with a second mode snap-through*

Compared to the analytical model, the FEM gives approximately the same switching force levels, corresponding to the local optimum points of the curve $2R \sim RR = f(D)$. The force levels are in general theoretically lower when the beam goes through a mode 2 instead of mode 1 in snap-through.
The passage through mode 2 can be deduced from the shape of the curve over the negative stiffness range (the values of the displacement between the two optima). If the curve is a straight line, it is a mode 2 transition. If the curve is polynomial of degree strictly greater than 1, it is a mode 1 transition since these two modes are sufficient to describe the snap-through phenomenon [Caz09].

2.2.5 Experiment

An experimental study of buckling and mechanical actuation of the bistable system by a transverse force is conducted.
The aim is to experimentally validate the bistability curve of the buckled steel beam.
The idea is to compress the beam with the dimensions given in the introduction, between two jaws that can slide or be fixed.
The beam is therefore axially compressed to buckling with an initial midpoint deflection of $D_0 \simeq 1\ mm$. The deflection is measured with a Keyence laser sensor.
From this basic configuration, we apply an incremental transverse force, in the form of weights suspended in the middle of the beam, and we measure the displacement generated downwards by this mechanical load using the laser sensor (see Figure 2.12).
By multiplying the mechanical load by the value of gravity and taking the corresponding displacement, we can plot the curve $2R = f(D)$.

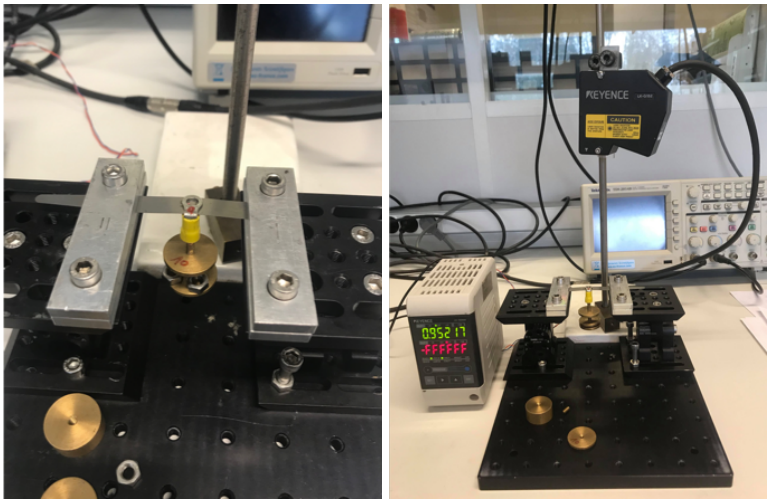

Figure 2.12: *Test bench for plotting transverse force $2R$ versus transverse displacement D: force is applied by suspended masses and displacement is measured with a Keyence laser sensor*

The experimental test is repeated on a multitude of beams with different thicknesses. We stop at $t_b = 0.3\ mm$ because it is hard, above this value, to obtain experimentally the

bistability at the initial displacement of around $1\ mm$. We actually need more deflection to have a bistable beam with the material we have (steel).
Figure 2.13 shows good consistency between the predictions of the analytical model $2R = f(D)$ for a P_{crit} that fixes the initial displacement D_0, and experiment. Some differences can be noticed, and this is mainly due to measurement errors.

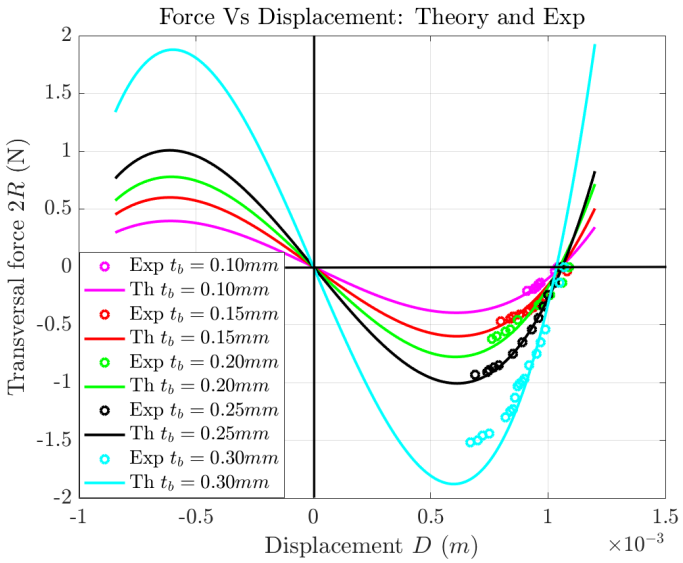

Figure 2.13: *Transverse force $2R$ versus transverse displacement D for a buckled beam: theory and experiment for different values of beam thickness*

The stop point of the measurements is the point of switching from the high state to the low state. This is done instantaneously and the midpoint shift goes directly from a positive to a negative value.
Holding the beam along its path during the switchover and measuring the reactive force it needs to stay in equilibrium is what will allow the whole curve $2R = f(D)$ to be reproduced experimentally. However, this is a difficult task.
What interested us in this characterisation study is mainly the snap-through limit point.

2.2.6 Conclusion

This part was dedicated to the characterisation of the buckled beam.
First, a beam undergoes axial compression and buckles. We have modelled the buckling analytically and numerically and compared the two approaches. This shows good coherence.
Then, from this deformed configuration, the impact of a transverse force was modelled and experimentally tested to ensure the results validity of the beam's response to transverse mechanical force, in particular the snap-through phenomenon.
We therefore have an idea of the level of force that needs to be applied, in particular to the bistable beam of thickness $t_b = 0.3\ mm$, to make it switch from one stable state to the other.

2.2.7 Matrix of bistable systems: experimental prototype

So far we have worked with simple beams.
Our application, which will be discussed in detail in Chapter 4, is to have not only a bistable beam, but rather a matrix of bistable systems that can be operated independently.
It remains technically complicated to axially actuate a plate with holes, and force the buckling of the filled parts only.
One idea is to deform the parts that form beams on the plate, by forcing with a transverse force and with plasticising to maintain a deflection.
Figure 2.14 shows the concept of the perforated plate to be prototyped, to have deflections on each beam.
The plastic deformation method proposed by the CLABAUT supplier is the folding method.

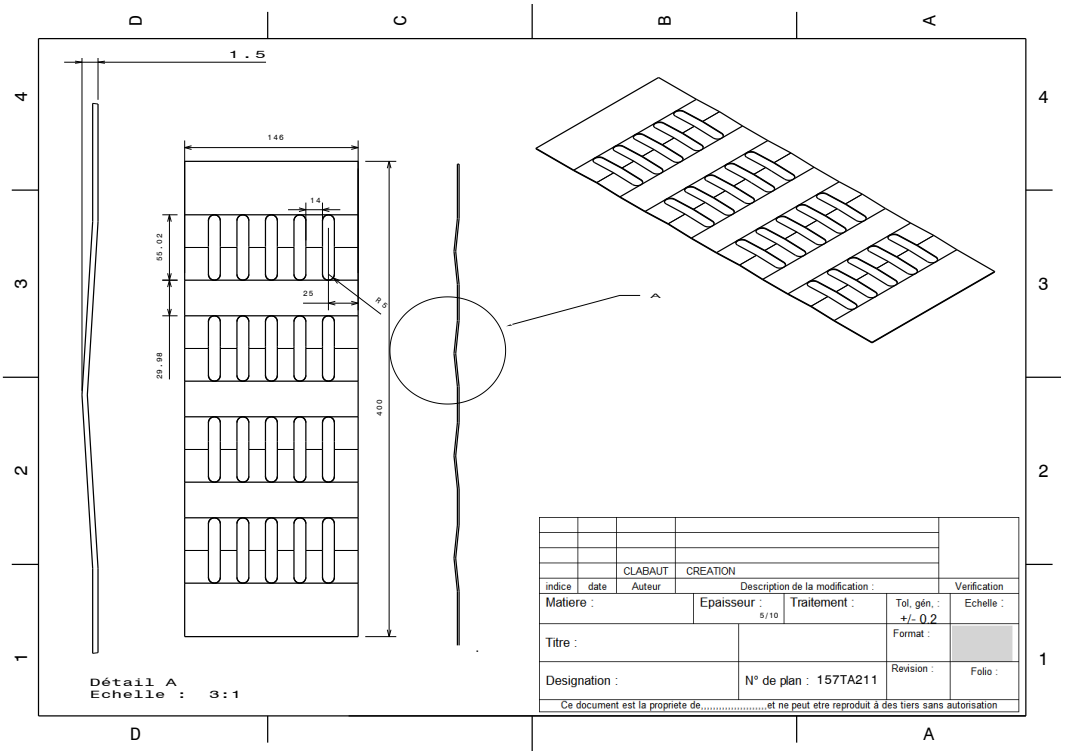

Figure 2.14: *Architecture of bistable systems array to be prototyped. Beams are plastically deformed using the folding method; CLABAUT offer*

To make a matrix of bistable systems, we could have taken single beams between the jaws and compressed them axially.
The problem with this method is that we are not sure that we are pressing in the same way on all the simple beams (boundary conditions), hence the different deflections, and we are also limited in terms of beam rows. We are only allowed one.

We first clamped the whole plate (in Figure 2.15a) between two jaws and tested the bistability of its constituent beams by pressing from top to bottom and vice versa. The beams did not exhibit bistable behaviour.

We moved to a lower level, testing the bistability for only one row of deformed beams, which is cut from the plate and clamped at its ends (see Figures 2.15c and 2.15d). The beams are worked downwards and upwards, trying to achieve symmetry of the two stable positions. However, there is no bistability that appears, and all intermediate positions between top and bottom are equilibrium positions.
Eventually, only a simple deformed beam with plastification is taken from this set. It is clamped from both ends and worked up and down (see Figure 2.15b). The bistability does not appear on a single beam either.

The conclusion we finally came to is that these beams undergoing plastic deformation do not exhibit bistable behaviour.

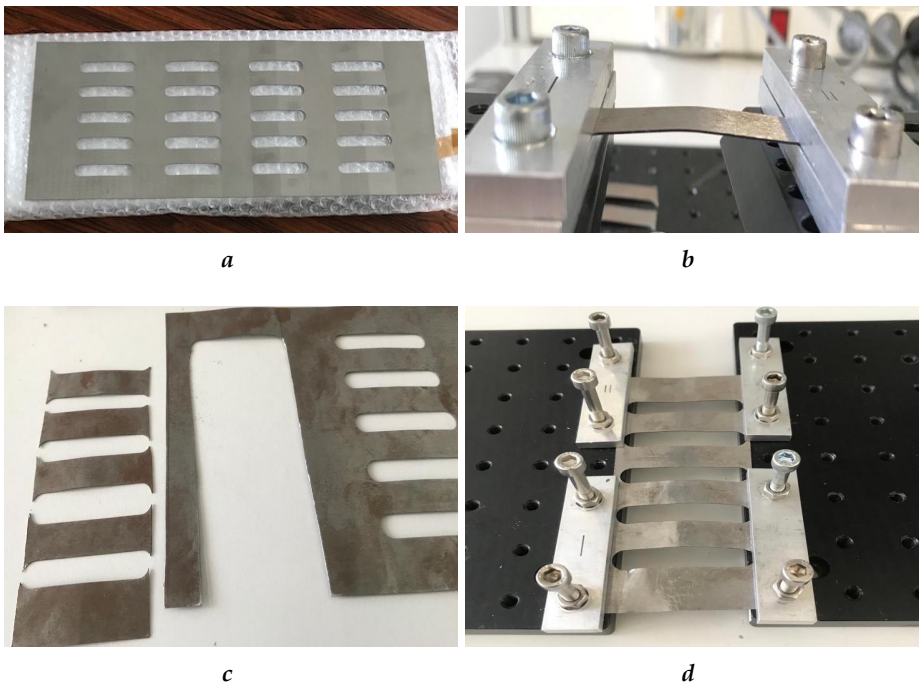

a *b*

c *d*

Figure 2.15: *Prototype of the bistable systems matrix: (a) the whole plate, (b) single beam cut from the prototype and double-clamped, (c) prototype cut into single beams, (d) prototype cut into beam rows*

One explanation we can give for this finding is that plastic deformation induces residual stress. This is a concentration of stress in one area of the beam, in the example of the prototype, more than in other areas.
The application of a transverse force does not significantly change the stress distribution. When changing the state of the beam from top to bottom, the residual stresses remain approximately the same.
The flat state of the beam, for example, is not a purely compressed state with stresses only axial and symmetrical to the x axis. This means that this state cannot be an equilibrium state, nor can the two states at the top and bottom.

The plasticising solution has therefore not been proven to solve the problem of a matrix of bistable systems.
We had to think of another solution, which is necessarily based on elasticity in order to recover the energy stored in the system elastically.
Hair clips present a good bistable alternative that explores elasticity, and they are easily duplicated to make an array of independent bistable systems.
We will base our new bistable system on the principle of hair clips.

2.3 Clips modelling and experiment

2.3.1 Introduction: operating a new solution, elasticity instead of plasticity

Recovering energy stored by plastic deformation is not easy in our application. We proposed an alternative solution: elasticity instead of plasticity.
Hairbars exploit the buckling due to lateral bending of the two bars when they are brought together. These are pre-stressed bistable systems.
The same principle will be used to make bistable two beams connected on one side and separated with a slot in the middle, forming a 'U' shape.
Initial design and numerical modelling work were carried out to ensure the buckling of the 'U' shaped bars. We then ensured that these systems are bistable. Based on this, prototypes of single bars (for re-measurement and actuation by PZs in Chapter 4) and 'U' shaped bars were manufactured.

2.3.2 Characterisation: FEM

The new system, based on the principle of hairpins which are bistable, will be characterised with respect to its buckling first and then its bistability.
Several configurations were tested. The systems selected were a 'U' shaped clip, formed by two bars of dimensions (70,10,0.3 mm) and another clip whose bars are of dimensions (70,14,0.3 mm) (see Figures 2.16a and 2.16b).

There is a gap between the two bars of the clip. The width of this slot determines the transverse displacement when the system buckles.
We set a gap of $1\ mm$. This induces a transverse displacement in the middle of the system around $1\ mm$, which changes when we are far or near the edges of the bistable system.
We start with a buckling test. This is to get a transverse displacement when both bars are pre-stressed.
In modelling, because of the symmetry of the stresses, buckling does not occur. This is similar to the case of a purely compressed simple beam. The solution in this case is to break the symmetry of the stresses by applying a small force ($0.1\ N$ for instance), either upwards or downwards depending on the direction in which buckling is desired.
The two free ends of the clip are gradually brought together until they meet in the middle.
The impact of this imposed lateral displacement on the transverse one of the system is

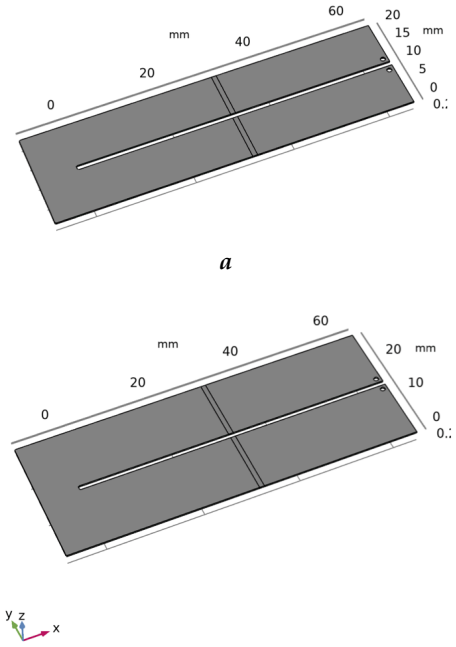

Figure 2.16: *Two examples of 'U' shaped systems chosen for modelling and prototyping: (a) two bars of dimensions* (70,10,0.3 mm) *and (b) two bars of dimensions* (70,14,0.3 mm)

plotted. This is given in the Figures 2.17a and 2.17b for the two types of 'U' shaped system.

As in the case of a simple beam buckling, we notice that from a critical value of imposed lateral displacement, the system starts to buckle. This value depends on the dimensions of the buckling system as the gap between the two bars is fixed (1 mm).
When the two extremities are brought together in the middle of the gap, the middle displacement on one bar is a little more than 1 mm, a value we have set for deflection during this work.
Once the two ends meet in the middle of the gap and the system buckles, we consider these boundary conditions of the system as the new starting configuration. Now, we have a buckled 'U' shaped system.
From this configuration, the bistability of the pre-stressed system will be tested.
The two techniques used for the case of a simple beam can also be used here. We can drive the system in force as well as we can drive it in displacement. Both methods are equivalent as explained above. The displacement control is chosen for the FEM analysis of our system.
However, it must be highlighted that for such a case of study, i.e. the switching of a pre-stressed 'U' shaped system from one state to another, the control of the system is not sufficient for the calculation to converge.
There is a small and very sensitive region on the surface of the 'U' system that allows the calculation to converge, and gives therefore the entire transverse force versus transverse displacement curve. Otherwise, the numerical calculation diverges when arriving at the middle equilibrium position, and we obtain only half of the curve.

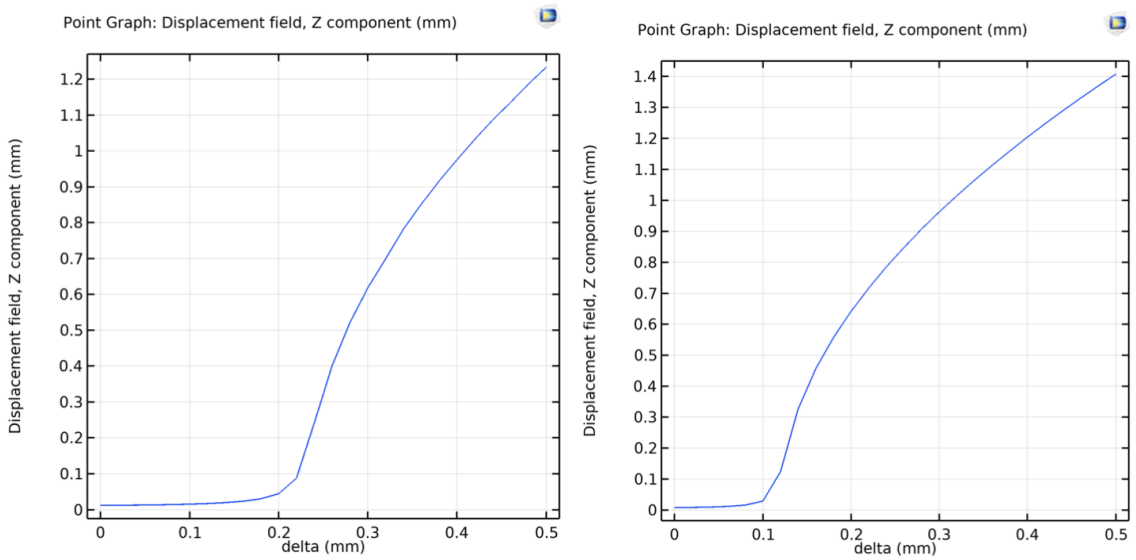

Figure 2.17: *Buckling of clips due to pre-stressing of bars: curve of the transverse displacement in the middle of the bar as a function of the displacement imposed on the ends along 'y' axis: (a) two bars of dimensions* (70,10,0.3 mm) *and (b) two bars of dimensions* (70,14,0.3 mm)

In this sensitive area, the effort is a continuous function of the displacement. This area is given around the lateral line in Figures 2.18a and 2.18b, on the left side of the buckled clips. It is located, for the system dimensions we have, approximately $11\ mm$ from the middle of the clips.

The resulting transverse force vs transverse displacement curves are given, for each dimension of the system in Figures 2.19a and 2.19b.

The curves are continuous at the point (0,0), and closely resemble the classical curve of bistable systems with two stable and one unstable equilibrium states.
The switching points correspond to the local optimums: the local minimum for switching from top to bottom and the local maximum for the other switching.
The $21\ mm$ total width system is easier to switch, with a snap-through effort of about $2\ N$ compared to the $29\ mm$ total width system (switching at $4.5\ N$).

If we drive in displacement the middle of the buckled system (or a line close to it), the force-displacement curve is discontinuous at the zero force unstable equilibrium position. This discontinuity can be noticed if we plot the curve for a model of the snap-through from top to bottom until the calculation stops in the unstable position, then from bottom to top until the calculation stops, then we concatenate the two curves on the same graph (see Figures 2.20a and 2.20b).

These figures bring together the two studies done on one type of clips to give the full bistability curve. The curve contains a discontinuity at the point of unstable equilibrium. This is the same type of discontinuity that we find when actuating a simple beam with

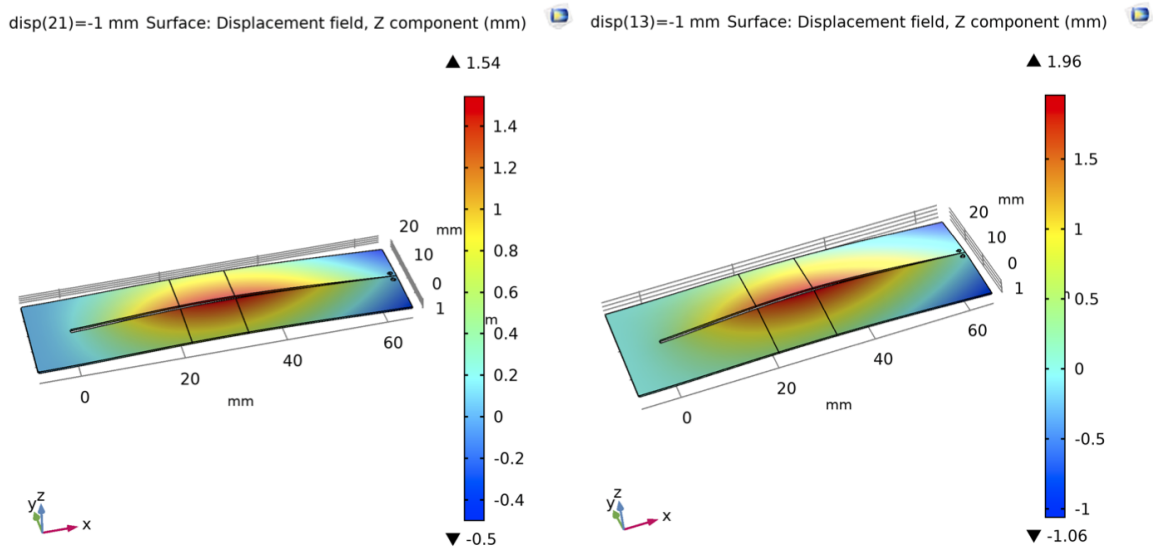

Figure 2.18: *Displacement control of a specific 'U' shaped system area (11 mm away from the middle to the left side) for convergence of the numerical calculation and obtaining the full bistability curve: (a) dimensions of (70,10,0.3 mm) and (b) dimensions of (70,14,0.3 mm)*

an effort (force or moment) offset from the middle (see Figure 2.21).

The characteristic points in Figure 2.21, as in Figures 2.20a and 2.20b, correspond to particular situations: A and C for stable equilibrium, B and D for unstable equilibrium (stoppage of numerical calculation), and local optimums E and F for snap-through points.

2.3.3 Characterisation: experiment

Now that we have numerically characterised the 'U' shaped device, an experimental study will be conducted for validation.
Clips identical to those used in the numerical model have been manufactured. The supplier, AMH, cut the single beams and 'U' clips using an electro-erosion machine to avoid as much as possible material damage at the edges.
First, we pre-stress the system by approaching the two free ends of the 'U'. Due to the imperfections of the material constituting the system, the 'U' buckles and a transverse displacement of the same order as in the FEM calculation appears.
We use the two small holes at the end of the 'U' to slide a metal wire in and tighten it to keep the lateral pre-stress.
We can notice at this point that the system we have is bistable, like a hair clip. It is put between clamping bars for attachment purpose only (see Figure 2.22).

To characterise the snap-through of the system, i.e. to know the effort needed to go from one stable state to the other, we propose a test bench.
The aim is to progressively apply a transverse force, starting from the top state of the buckled 'U' shaped system, and to measure the transverse displacement induced by this

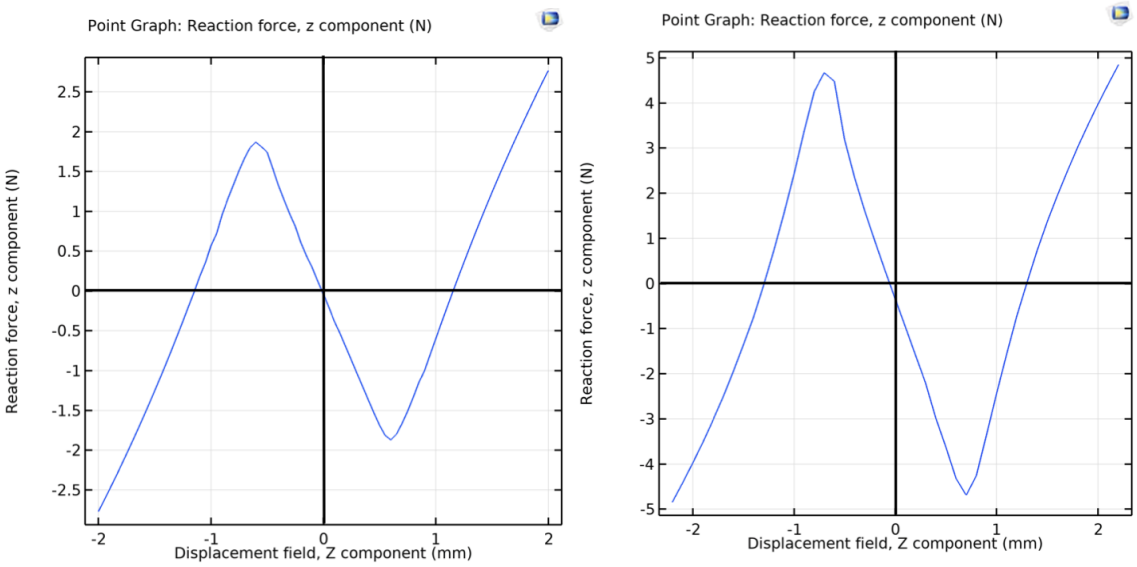

Figure 2.19: *Bistability curves: transverse force versus induced transverse displacement, (a) 'U' shaped system of dimensions* (70,10,0.3 mm) *and (b) 'U' shaped system of dimensions* (70,14,0.3 mm)

force up to the switching moment. This will be compared to the numerical study, in particular the snap-through needed forces.
The test bench for this characterisation contains the bistable system clamped between two jaws, calibrated weights hung to apply the transverse force and a laser sensor to measure the displacement induced by the force application (see Figure 2.23).

We can then take the level of force applied and the displacement induced, and plot the force-displacement characteristic. The measurements are repeated to analyse the repeatability and error bars are plotted. The comparison of the experiment with the FEM, and the error bars for both dimensions of the 'U' are shown in Figure 2.24.

To avoid measurement aliases at the beginning, we start by putting a relatively high weight at the beginning, and then we add a few grams each time (10 g in general).
We note a correspondence between FEM and experiment. Through the experiments carried out, the repeatability seems good. The experiment gives a switching moment which is close to the local optimum of the curve (snap-through moment given by the model).
The differences noted are mainly due to measurement errors as well as to the difficulty of adjusting the system: bringing the ends of the 'U' closer together, metal wire used for buckling, etc.

2.3.4 Conclusion

This section was dedicated to the characterisation of 'U' shaped clips.
First we start by buckling this 'U' shaped system using lateral pre-compression. FEM showed that buckling occurs and that the resulting system is indeed bistable. From this

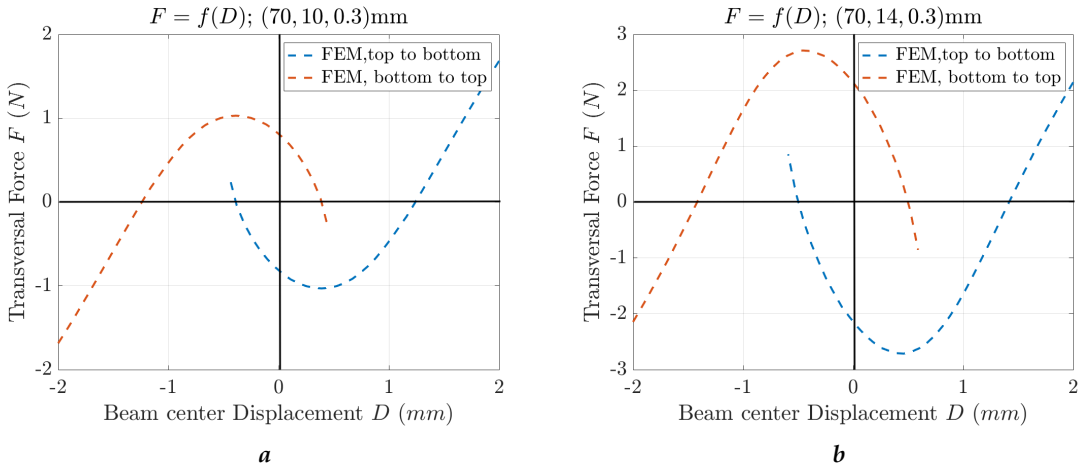

Figure 2.20: *FEM of bistability: transverse force versus induced transverse displacement with a discontinuity at the point of unstable equilibrium, (a) 'U' shaped system of dimensions* (70,10,0.3 mm) *and (b) 'U' shaped system of dimensions* (70,14,0.3 mm)

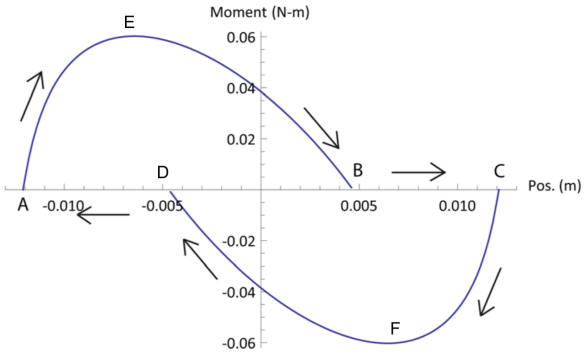

Figure 2.21: *Displacement vs moment curve for offset actuation from the middle position: actuation at 23.33% along the length of the beam [CS15]*

pre-stressed configuration, we characterised the system by its bistability curve and validated it by experiment. There was a coherence between the model and the experiment. For the dimensions of the 'U' systems we have prototyped, the force levels to switch from one stable state to the other are respectively of the order of 1 N for the smallest and 3 N for the largest.
The bistability curve for actuation in the middle of the 'U' clips looks like that of an offset actuation of a single beam, initially buckled and actuated transversely.

2.4 Conclusion

In this chapter we have proposed a first example of a bistable system: simple beam compressed to buckling. We have characterised this system analytically and numerically and validated the results obtained by experiment. For our type of dashboard application, we had to think about duplicating this system to end up with a matrix of bistable systems. It

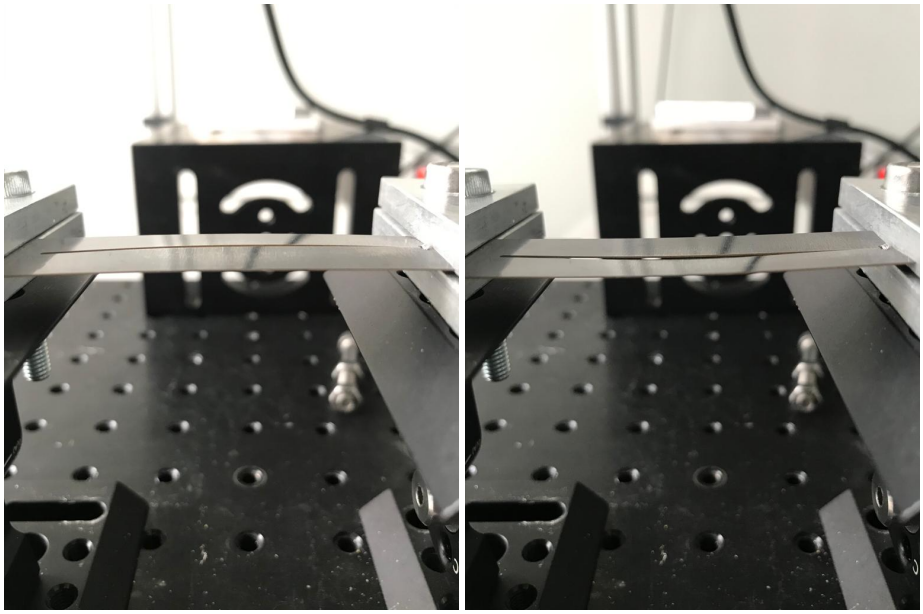

a *b*

Figure 2.22: *Bistable clips (70,10,0.3 mm) between clamping bars: (a) 'U' shaped system in the top stable state and (b) 'U' shaped system in the bottom stable state*

is difficult to make a bistable system matrix just by plate compression, as is the case with a simple beam.
We thought of a solution based on plasticising, but the system obtained after prototyping was not bistable.
It is then necessary to think of a solution which is based on elasticity and which allows the recovery, if necessary, of the energy stored in the bistable system, during the passage from one stable state to the other. So we proposed a system based on the same principle as the bistable hair clips.
Since the system obtained after buckling is bistable, we can make as much of it as we want and attach it between clamping bars to obtain a matrix of bistable systems. The problem of having a single beam that has to be compressed to be bistable no longer exists. The jaws are no longer used for compression, but only for support.
This paragraph marks the end of a purely mechanical part of the analysis. In the next Chapter 3 we will carry out an electrical study to model the equivalent effort of piezoelectric materials actuation on structures.

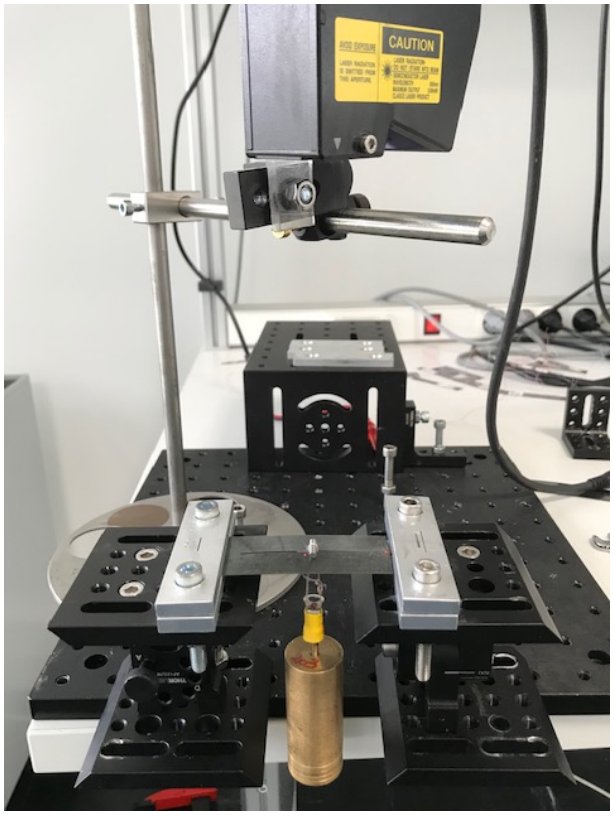

Figure 2.23: *Bistable characterisation test bench: hanging weights for transverse force application and Keyence laser sensor for measuring the induced displacement*

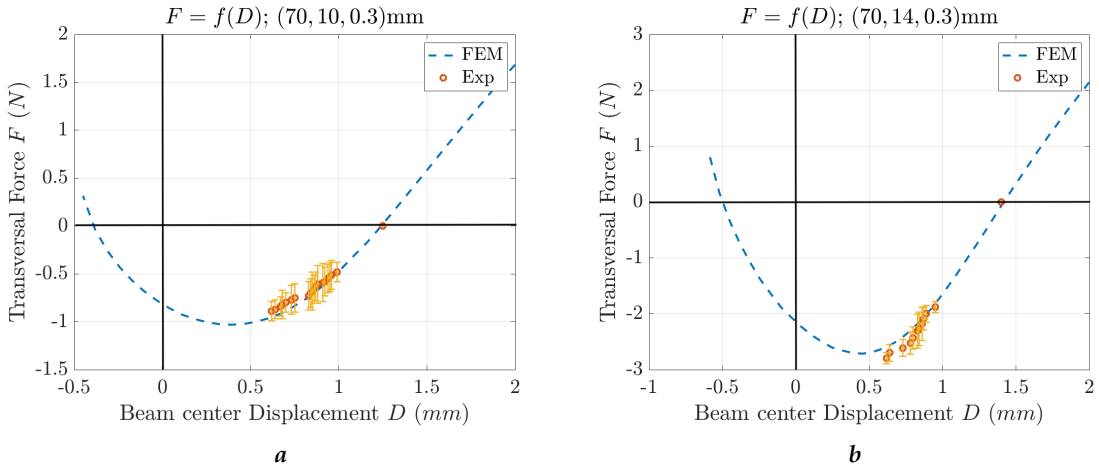

Figure 2.24: *FEM and experiment to characterise the system response to a transverse force until snap-through: (a) 'U' shaped system of dimensions* (70,10,0.3 mm) *and (b) 'U' shaped system of dimensions* (70,14,0.3 mm)

Chapter 3

Modelling of piezoelectric actuation

Contents

3.1 Introduction

The aim of this chapter is to assess the range of validity of two main analytical approaches to model the static effect of a piezoelectric (PZ) patch on an elastic beam.
The purpose of this chapter is to demonstrate that PZ actuation can be replaced by any pure equivalent mechanical effort if some geometric and material conditions are respected. This allows us, in the following, to replace the action of the PZ materials on our bistable surface by equivalent efforts. Such an analytical model makes it easier to understand and anticipate the snap-through phenomenon on bistable systems.
The first approach replaces the PZ patch by two equivalent opposite forces and the second by two equivalent opposite moments. A parametric evaluation is performed on a case study consisting of a PZ patch bonded to a cantilever beam structure. The corresponding Finite Element Analysis (FEA or FEM) is performed using COMSOL Multiphysics to serve as a reference solution for the problem.
In a first part, the study case is presented. The two analytical approaches are then presented and followed by the FEA implementation. A parametric study is then performed for different material and geometrical parameters. This allows defining the range of validity of the analytical models by comparison to FEA results.

3.2 From a double clamped to a clamped-free beam: PZ modelling

3.2.1 Introduction

The final aim of this study is to finally analyse the snap-through of a bistable system by PZ actuation. The model of the PZ actuation should allow to replace the PZ elements by equivalent forces. In the literature, several models exist. Among others we find force models and moment models, whose replacement principle is shown in Figure 3.1a. The particularity of this case study, i.e. the bistable system actuated by PZ patches, is its complexity. It takes into account the compression forces which in turn cause bistability. However, the PZ actuation is independent of the type of system studied.
For these reasons, a choice was made. The modelling of the effect of PZ materials on a structure will be done for a simple cantilever, where just the actuation of the PZ is involved, in the absence of compression or other external forces. Then this model can be used on any other structure (see the transition from Figure 3.1a to Figure 3.1b).

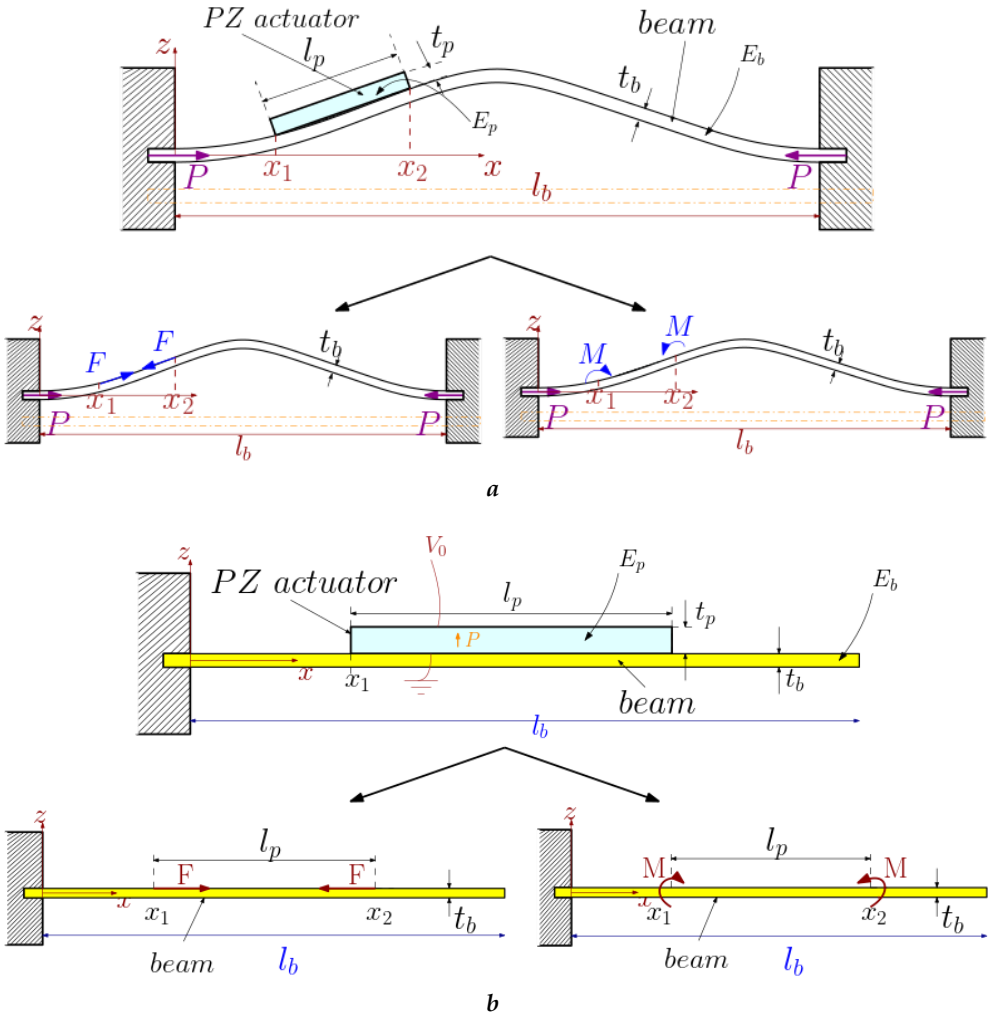

Figure 3.1: *Equivalent models of the PZ actuation. Forces (to the left) and moments (to the right) models: (a) compressed bistable beam actuated by a PZ patch and (b) a cantilever beam actuated by a PZ patch*

In many applications, the PZ material is a patch bonded on a structure. The working principle of the device then relies on the interaction between the PZ patch and the structure (actuation, sensing or both).
In order to model the action of a PZ patch bonded on an elastic structure, several approaches are available. A variational formulation, combined to the coupled constitutive relations of PZ materials, can be used [Cor+08]. The problem cannot usually be solved analytically, and the implementation of a numerical model is required.
With the objective of establishing analytical relationships, Crawley *et al.* [CL87] modelled the action of symmetrical bonded patches on an elastic structure, by using two equivalent pin-force, tangent to the surface of the structure. Alternately, Piefort [Pie01] or Salaün *et al.* [Sal+08] modelled the action of a PZ patch by two opposite moments, applied at the location of the patch extremities on the elastic structure.
There are also other models for predicting the system (substrate + actuator) response for thin and thick structures. We mention three of them in the following. First, the consis-

tent plate model [CL89] that formulates the strain energy relations for a laminated plate, under the assumptions of thin and classical laminated plate theory. Second, the strain energy model [WR91] that models laminate beams and plates with attached or embedded finite length spatially-distributed induced strain actuators. Third, modes selective excitation [DFR91] that predicts the behaviour of two dimensional patches of PZ material bonded to the surface of an elastic structure and used as vibration actuators.

With regard to this part of the study, we will focus more on the use of an analytical approach. This allows us to have exact and explicit formulas for the pin-force and pin-moment equivalent to the action of the PZ actuator. This also allows the use of equivalent efforts to carry out a mechanical study, where the differential equations have ordinary solutions, unlike the energy approach, which in many cases results in equations that require numerical tools to solve.

3.2.2 Study case

The considered problem (Figure 3.2) consists in an elastic beam (e.g. steel), with length l_b and thickness t_b, blocked on its left side. The longitudinal linear elastic behaviour of the beam (along direction x) is characterised by the Young modulus E_b. A PZ patch (e.g. PZT), with length l_p and thickness t_p is bonded on the upper side of this cantilever beam. The PZ patch and the cantilever beam have the same width b. x_1 is the x-coordinate such that the patch is bonded to the beam on the zone $[x_1 \;\; x_1 + l_p]$. The Young modulus of the PZ patch along direction x is noted E_p. The PZ patch is equipped with electrodes on its upper and lower sides. V_0 is the voltage applied between these electrodes, the polarisation of the PZ patch being upward as shown in Figure 3.2. The transverse PZ coefficient of the PZ patch is denoted by d_{31}.

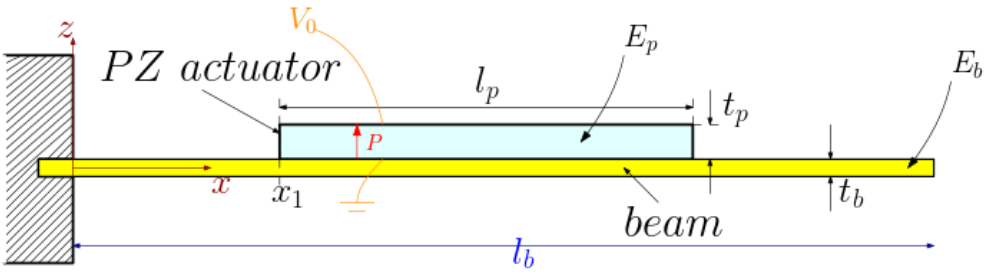

Figure 3.2: *Case study of a PZ patch bonded to an elastic cantilever beam: geometric and material parameters*

The different models (analytical and FEA) for this study case problem will be compared using the vertical displacement δ at the free (right) end of the cantilever beam. The longitudinal strain in the beam and in the PZ patch will be noted ϵ_b and ϵ_p, respectively. This analytical study is carried out under the assumption of plane stress.

3.3 Equivalent models of piezoelectric actuation

3.3.1 Equivalent pin-force model

The pin-force model [BU85; CA90] describes the action of the PZ patch on the beam by two opposite forces with module F, placed at the extremities of the PZ patch (Figure 3.3).

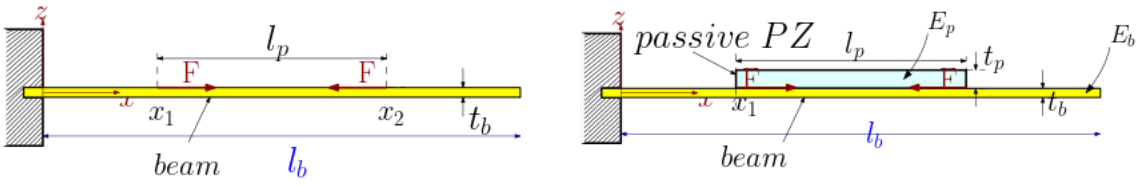

Figure 3.3: *Simplification of the action of a PZ patch on an elastic structure using the pin-force model, cases where PZ stiffness is not considered (on the left) and is considered (on the right)*

Several variants of the pin-force model can be obtained by following different assumptions. A first pin-force model can be developed assuming that the strain remains uniform throughout the section of the structure (Figure 3.4). This assumption can be used when the structure is made of symmetrically bonded patches on each side of the beam.

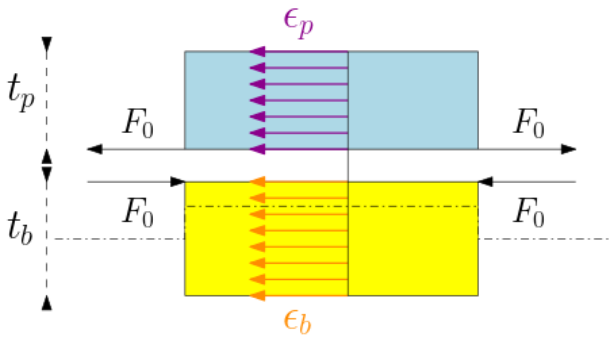

Figure 3.4: *A first pin-force representation assuming uniform strain along the cross section of the beam and PZ patch ($\epsilon_b = \epsilon_p$)*

Although this assumption is obviously not relevant to describe the study case of Figure 3.2 subjected to bending, the corresponding result is given below because it serves as a basis for more general configurations. In the absence of any external longitudinal force, the pin-force F_0 under uniform strain assumption, is given by (see Appendix A.1):

$$F_0 = -\frac{bE_b t_b}{1+\psi}\Lambda \tag{3.1}$$

with

$$\psi = \frac{E_b t_b}{E_p t_p} \tag{3.2}$$

and Λ the stress-free PZ strain of the PZ patch along the x-direction:

$$\Lambda = \frac{d_{31} V_0}{t_p} \tag{3.3}$$

Such model cannot describe bending, so that the obtained deflection δ is zero whatever the applied voltage.

A more refined pin-force model can be developed by maintaining the strain constant across the section of the PZ patch but assuming a linear variation of the strain across the section of the elastic beam (Figure 3.5). In that case, the application of a voltage V_0 will result in a deflection δ.

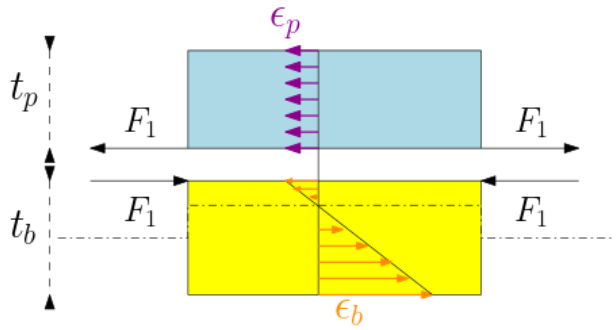

Figure 3.5: *A pin-force representation assuming uniform strain along the cross section of the PZ patch and a linear variation of the strain along the cross section of the elastic beam*

The pin-force F_1 in that case is given by (see Appendix A.2.1):

$$F_1 = -\frac{bE_b t_b}{3+\psi}\Lambda \tag{3.4}$$

In the construction of this model F_1, it should be mentioned that the stiffness added by the presence of the PZT patch is not taken into consideration.

A more precise pin-force model [CR94] can be obtained by adding the stiffness of the PZ patch to the stiffness of the structure, the resulting model is F_2 (Figure 3.6).

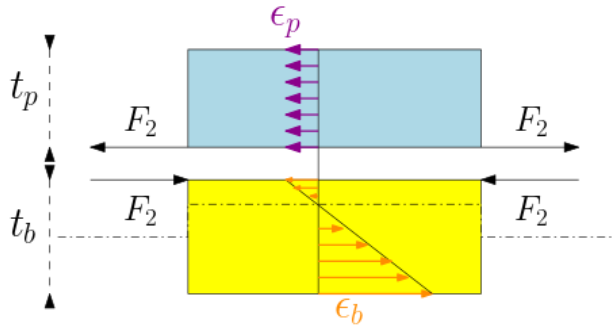

Figure 3.6: *A pin-force representation assuming uniform strain along the cross section of the PZ patch and a linear variation of the strain along the cross section of the elastic beam. Actuator flexural stiffness is added to the model*

The pin-force model F_2 in that case is given by (see Appendix A.2.2):

$$F_2 = -\frac{bE_b t_b}{3+\psi+\frac{t_p^2}{3t_b^2}}\Lambda \tag{3.5}$$

As mentioned by Chaudhry *et al.* in their paper [CR94], the F_2 pin-force model contains some contradiction in it from a theoretical standpoint. By assuming a constant strain distribution in the actuator, we are in fact specifying that the actuator does not bend. However, the assumption of constant strain in the actuator seems acceptable, but neglecting the actuator flexural stiffness is what really leads to the discrepancy in the pin-force model for thin structures.

3.3.2 Equivalent two-moment model

The two-moment model [GF98] describes the action of the PZ patch on the beam by two opposite moments with module M, placed at the extremities of the PZ patch (Figure 3.7). In this model case, the strain is assumed to vary linearly across the sections of both the elastic beam and the patch.

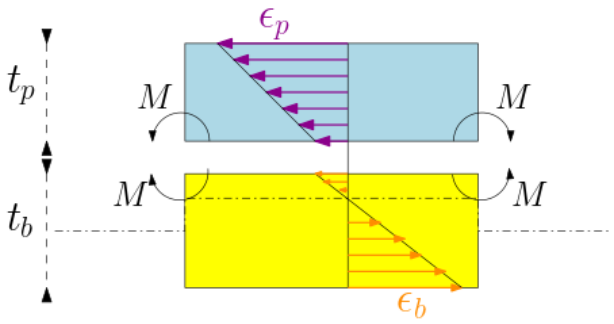

Figure 3.7: *A two-moment representation assuming a linear variation of the strain along both the cross section of the elastic beam and PZ patch. Actuator flexural stiffness is included in the model*

The extension and bending of the elastic beam is described by the strain field ϵ_b. This strain field can be written as the sum of a uniform strain (extension part) and a linearly varying strain (bending part). This strain can be seen as the result of the application of the two opposite moments. The moment M in that case is given by (see Appendix A.3):

$$\frac{M}{bE_p} = g(t_b, t_p, E_b, E_p, z_n).\Lambda \tag{3.6}$$

with g a function of different parameters t_b, t_p, E_b, E_p, z_n, where z_n defines the neutral axis of the beam (z position for which the strain ϵ_b is zero):

$$z_n = \frac{E_p\left(t_p^2 + t_p t_b\right)}{2\left(E_b t_b + E_p t_p\right)} \tag{3.7}$$

3.4 Expression of the deflection in the study case

Equations (3.4) and (3.5) give the expressions for a pin-force model without considering the stiffness of the PZ patch ($F = F_1$) and with considering it ($F = F_2$), respectively. Equation (3.6) defines a two-moment model with the moments applied at the patch extremities. The modelling options for the modelling of a cantilever beam, taken as the

reference study case, are illustrated in Figure 3.8.

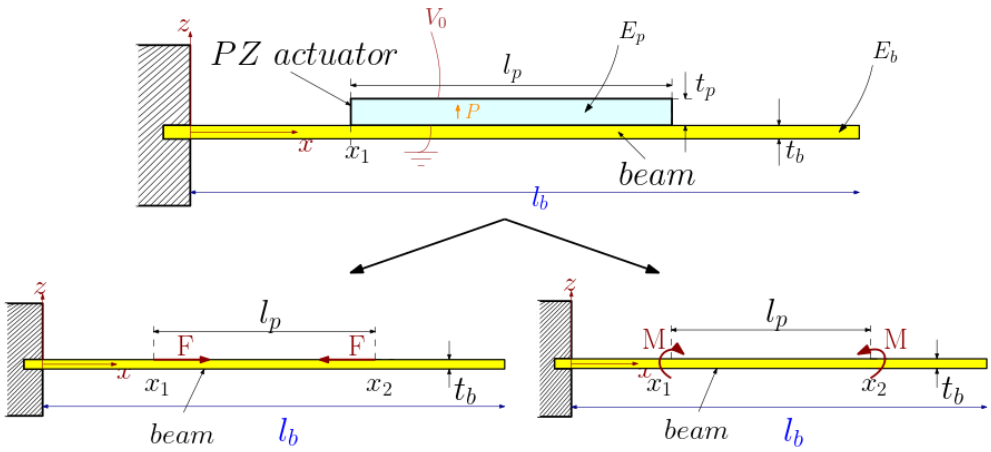

Figure 3.8: *Two modelling options for a cantilever beam actuated by a PZ patch: pin-force (left) and two-moment (right) models*

Using the standard Euler-Bernoulli theory, the expression of the transverse displacement $w(x)$ of the beam neutral axis (along z-direction) can be directly derived form the expressions of F_1, F_2 or M. The deflection δ at the free (right) end of the cantilever beam is then simply given by:

$$\delta = w(x = l_b) \tag{3.8}$$

This value δ will be used in the following as the comparison indicator between the different modelling approaches.

According to Euler-Bernoulli theory, the transverse displacement $w(x)$ must obey the following equation:

$$w'' = \frac{d^2w}{dx^2} = -\frac{M_{fz}}{(EI)} \tag{3.9}$$

M_{fz} is the bending moment of the beam and (EI) is the bending stiffness of the beam. It is defined as:

$$(EI) = E_b I_b \tag{3.10}$$

for the F_1 model, and as:

$$(EI) = E_b I_b + E_p I_p \tag{3.11}$$

for the F_2 and M models. The difference between these definitions comes from the fact that the bending stiffness of the PZ patch is not neglected in the two latter models. The definition of the bending moment M_{fz} naturally leads to consider three distinct areas on which the transverse displacement is defined. The expression of the transverse displacement $w(x)$ is given below according to the three considered approaches. It is noted $w_{F1}(x)$, $w_{F2}(x)$ and $w_M(x)$ for the F_1, F_2 and M models, respectively.

For $0 \leq x < x_1$:

$$w_{F1}(x) = w_{F2}(x) = w_M(x) = 0 \tag{3.12}$$

For $x_1 \leq x < x_2$:

$$\begin{cases} w_{F1}(x) = -\dfrac{F_1 t_b}{4E_b I_b}.(x-x_1)^2 \\ w_{F2}(x) = -\dfrac{F_2 t_b}{4\left(E_b I_b + E_p I_p\right)}.(x-x_1)^2 \\ w_M(x) = -\dfrac{M}{2\left(E_b I_b + E_p I_p\right)}.(x-x_1)^2 \end{cases} \tag{3.13}$$

For $x_2 \leq x \leq l_b$:

$$\begin{cases} w_{F1}(x) = -\dfrac{F_1 t_b}{2E_b I_b}.(x_2-x_1).x \\ \qquad\qquad + \dfrac{F_1 t_b}{4E_b I_b}.(x_2^2-x_1^2) \\ w_{F2}(x) = -\dfrac{F_2 t_b}{2\left(E_b I_b + E_p I_p\right)}.(x_2-x_1).x \\ \qquad\qquad + \dfrac{F_2 t_b}{4\left(E_b I_b + E_p I_p\right)}.(x_2^2-x_1^2) \\ w_M(x) = -\dfrac{M}{E_b I_b + E_p I_p}.(x_2-x_1).x \\ \qquad\qquad + \dfrac{M}{2\left(E_b I_b + E_p I_p\right)}.(x_2^2-x_1^2) \end{cases} \tag{3.14}$$

The deflection δ_{F1}, δ_{F2} and δ_M for the F_1, F_2 and M models, respectively, can then be easily obtained at the position $x = l_b$:

$$\begin{cases} \delta_{F1} = w_{F1}(l_b) = -\dfrac{F_1 t_b}{2E_b I_b}.(x_2-x_1).l_b \\ \qquad\qquad + \dfrac{F_1 t_b}{4E_b I_b}.(x_2^2-x_1^2) \\ \delta_{F2} = w_{F2}(l_b) = -\dfrac{F_2 t_b}{2\left(E_b I_b + E_p I_p\right)}.(x_2-x_1).l_b \\ \qquad\qquad + \dfrac{F_2 t_b}{4\left(E_b I_b + E_p I_p\right)}.(x_2^2-x_1^2) \\ \delta_M = w_M(l_b) = -\dfrac{M}{E_b I_b + E_p I_p}.(x_2-x_1).l_b \\ \qquad\qquad + \dfrac{M}{2\left(E_b I_b + E_p I_p\right)}.(x_2^2-x_1^2) \end{cases} \tag{3.15}$$

It can be noticed that all models give a similar form for the expression of the deflection δ so that equation (3.15) can be re-written as follows:

$$\begin{cases} \delta_{F1} = K.\dfrac{1}{3+\widetilde{E}.\widetilde{T}} \\ \delta_{F1} = K.\dfrac{1}{3+\widetilde{E}.\widetilde{T}+\frac{1}{3\widetilde{T}^2}} \\ \delta_M = K.\dfrac{\widetilde{T}(1+\widetilde{T})}{\widetilde{E}.\widetilde{T}^3+4\widetilde{T}^2+6\widetilde{T}+4+\widetilde{E}} \end{cases} \tag{3.16}$$

where

$$K = \frac{6d_{31}V_0}{t_b t_p} l_b l_p \left(1 - \frac{l_p}{2l_b} - \frac{x_1}{l_b}\right) \tag{3.17}$$

and $\widetilde{T} = \frac{t_b}{t_p}$ and $\widetilde{E} = \frac{E_b}{E_p}$ are dimensionless parameters characteristic of the structure geometry and material choice, respectively.

Comparing the three analytical models then reduces to comparing the dimensionless functions f_{F1}, f_{F2}, f_M, defined by equation (3.18):

$$\begin{cases} f_{F1}(\widetilde{T}, \widetilde{E}) = \dfrac{1}{3 + \widetilde{E}.\widetilde{T}} \\ f_{F2}(\widetilde{T}, \widetilde{E}) = \dfrac{1}{3 + \widetilde{E}.\widetilde{T} + \frac{1}{3\widetilde{T}^2}} \\ f_M(\widetilde{T}, \widetilde{E}) = \dfrac{\widetilde{T}(1+\widetilde{T})}{\widetilde{E}.\widetilde{T}^3 + 4\widetilde{T}^2 + 6\widetilde{T} + 4 + \widetilde{E}} \end{cases} \tag{3.18}$$

It is then evident that, if the deflection δ in the cantilever beam problem is taken as the comparison indicator, the difference between the three approaches only depends on the dimensionless parameters $\widetilde{T}$ and $\widetilde{E}$, namely the ratio of the thicknesses and the ratio of the Young modulus of the elastic beam and PZ patch. The functions $f(\widetilde{T}, \widetilde{E})$ will be named "normalised deflections" in the following.

3.5 Parametric study

The normalised deflections f have been calculated for the three analytical models of interest for different thickness ratios $\widetilde{T}$ varying from 0.1 to 10, and for different Young modulus ratios $\widetilde{E}$ varying from 0.1 to 5.
The results obtained with the three models for the normalised deflections f are presented in Figure 3.9.

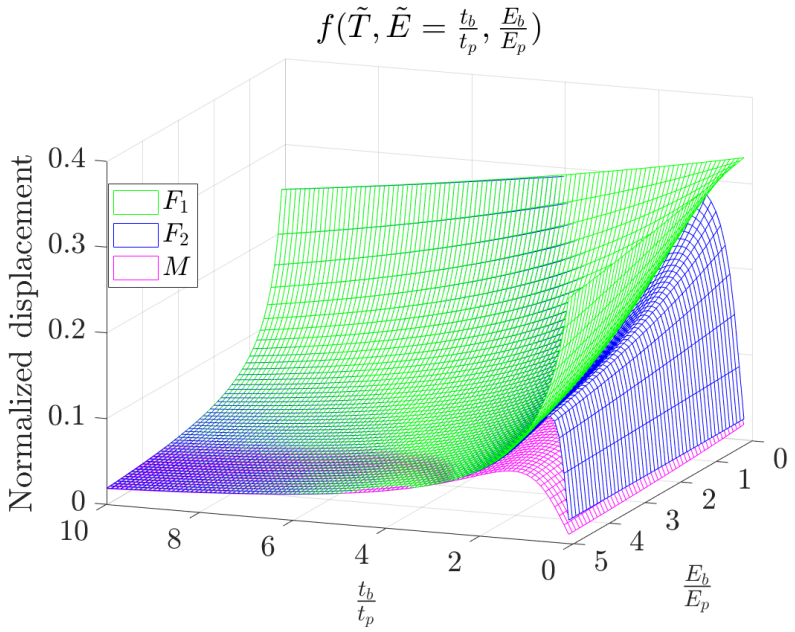

Figure 3.9: *Comparison of the pin-force (F_1 and F_2) and two-moment (M) models for the normalised deflection f in the cantilever beam reference problem*

For thickness ratios $\widetilde{T} \leq 2$, the responses are significantly different between the three models, with relative differences of more than 30% on average, regardless of Young modulus ratio $\widetilde{E}$. For $\widetilde{T} \geq 2$, F_1 and F_2 models are close but remain different from the results of the two-moment model. Finally, on the area defined by $\widetilde{T} \geq 4$ and $\widetilde{E} \geq 2$, the three analytical approaches provide very similar results, with relative differences of less than 6%, so that they could be indifferently used in that range of parameters.

3.6 Validation using FEA

The analytical approaches state that the normalised displacement only depends on $\widetilde{T}$ and $\widetilde{E}$, the thickness and Young modulus ratios of the beam and the PZ patch. This result is tested using a FEA simulation that will provide a reference solution. In agreement with the analytical models, the FEA study is implemented under the assumption of plane stress.

Regarding the FEA simulations, the dimensions and material parameters have been set as follows. The PZ material under consideration is PZT so that the transverse PZ coefficient d_{31} is 62.10^{-12} m/V and the Young modulus E_p is 81 GPa, which are typical values for PZT [1]. The range of exploration for the dimensionless parameter $\widetilde{E}$ has been set to $\{0.1$ to $5\}$. The beam Young modulus is defined by $E_p.\widetilde{E}$ and ranges from 8 GPa to 405 GPa. This wide range includes typical values for steel or aluminium. For the thickness of the PZ patch, it has been considered in the range $\{0.1$ mm to 3.1 $mm\}$, which corresponds to typical commercial available thicknesses for PZT patches. The range of exploration for

[1] http://www.noliac.com/

the dimensionless parameter $\widetilde{T}$ has been set to $\{0.1$ to $10\}$. This choice covers thicknesses for the beam from $0.01\ mm$ to $30\ mm$. All other parameters have been given fixed values. The set of parameters used for the FEA simulations are summarised in table 3.1.

For each FEA simulation, the normalised deflection f_{FEA} is obtained by dividing the deflection δ by the parameter K defined by equation (3.17). Then, for each value of t_p, the normalised deflection is plotted against $\widetilde{T}$ and $\widetilde{E}$.

Parameter	Unit	Value
PZ		
E_p	GPa	81
t_p	mm	$[0.1 : 0.3 : 3.1]$
l_p	mm	10
b	mm	10
d_{31}	m/V	62.10^{-12}
Voltage V_0	V	100
Position x_1	mm	10
Beam		
E_b	GPa	$E_p.\widetilde{E}$
t_b	mm	$t_p.\widetilde{T}$
l_b	mm	40
b	mm	10
Parameter ratios		
$\widetilde{E}$	-	$[0.1 : 0.5 : 5]$
$\widetilde{T}$	-	$[0.1 : 0.5 : 10]$

Table 3.1: *Dimensions and material parameters used for the FEA simulation of the cantilever beam case study.*

Figure 3.10 shows the ($\widetilde{T}$,$\widetilde{E}$,f_{FEA}) plot for the two extreme values of t_p. All intermediate calculations are positioned evenly between the two extreme curves. A third curve of the average between the two is then plotted. We first notice that the obtained trends are consistent with Figure 3.9.

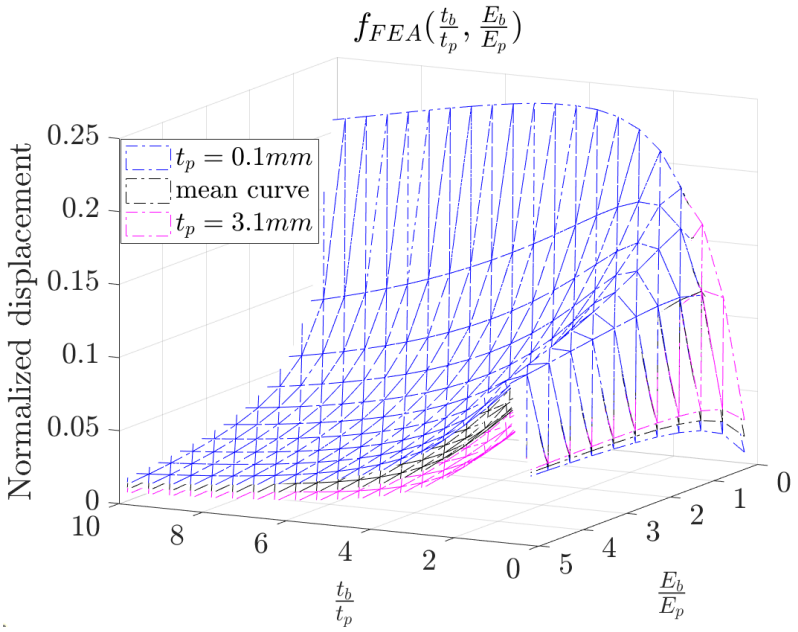

Figure 3.10: *3D FEA results of the normalised deflection f_{FEA} for different PZT thicknesses t_p*

From Figure 3.10, it is clear that the normalised deflection is not only a function of the dimensionless ratios $\widetilde{T}$ and $\widetilde{E}$, as stated by the analytical approaches, but is also affected by the thickness of the patch.

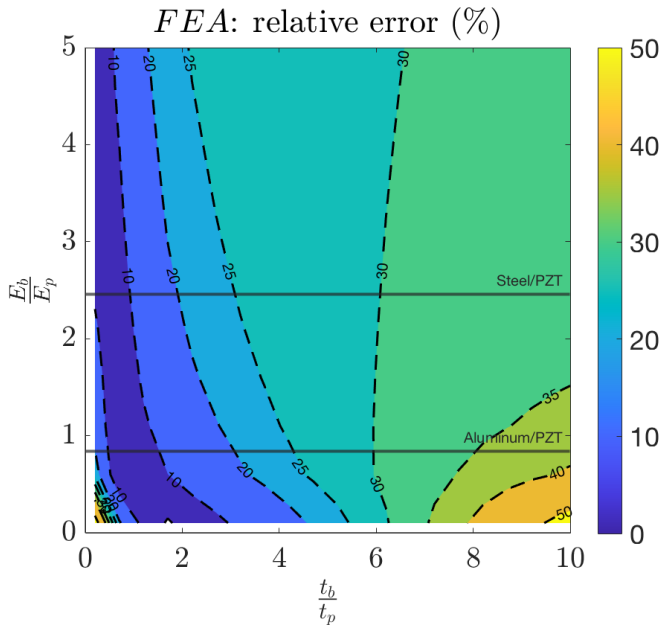

Figure 3.11: *Relative error between ($\frac{t_b}{t_p}$,$\frac{E_b}{E_p}$,f_{FEA}) two extreme curves, isobase map. Light yellow denotes values greater than or equal to 50%. The two horizontal lines are corresponding to $\widetilde{E}$ of the steel and aluminium association with PZT*

Figure 3.11 shows the relative error (defined as $|f_{(FEA,0.1)} - f_{(FEA,3.1)}|/f_{(FEA,3.1)}$ between the two extreme curves ($tp = 0.1\ mm$ and $tp = 3.1\ mm$). This leads to define an error threshold, below which this assumption $f = f(\widetilde{T}, \widetilde{E})$ is considered valid. We pro-

pose, according to the error map and isovalues, that for a relative error below 20% (blue region in Figure 3.11), the normalised deflection will be considered as correctly defined by the parameter ratios. The comparison between the analytical models and the FEA model will only be investigated in this range of parameter variation. Outside this range, even in the case where the error between the analytical models and the FEA model is relatively small, nothing can be concluded.
The statement of dependence only on parameter ratios ($\widetilde{T}, \widetilde{E}$) is not restricted to a specific area in the analytical case, unlike the FEA model. The reason behind this lies in the simplifying assumptions of the analytical model: bringing the action of the patch to a point of application, simplifying the behaviour law of the PZ material to only isotropic and x-axis behaviour, while the FEA model takes into account all components of the coupling and compliance matrices of the PZT...

The 2D FEA simulations are now compared to analytical results. The reference result f_{FEA} is chosen to be the mean curve from Figure 3.10. Error maps of the three analytical models (f_{F1}, f_{F2}, f_M) with respect to that reference result f_{FEA} are presented in the following figures.
It is reminded that the analytical model validity is investigated only in the region where the definition of the normalised deflection f as a function of only ratios $\widetilde{T}$ and $\widetilde{E}$ is considered valid. This range has been reported from Figure 3.11 on all figures with dashed red isovalues.

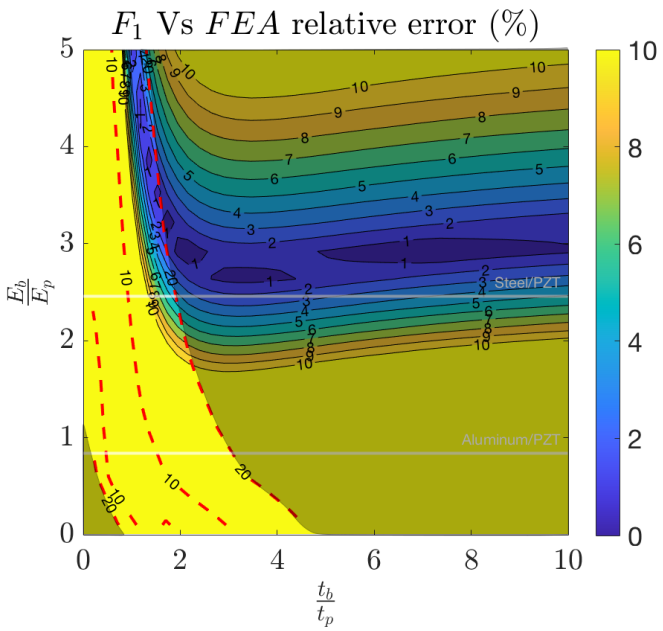

Figure 3.12: *Relative error between the F_1 pin-force model and the FEA solution taken as reference. Range delimited by dotted red lines: all models assume the same statement (dependence only on $\frac{t_b}{t_p}$ and $\frac{E_b}{E_p}$). A mask is added outside the domain validated by FEA. The two horizontal lines are corresponding to $\widetilde{E}$ for steel and aluminium association with PZT*

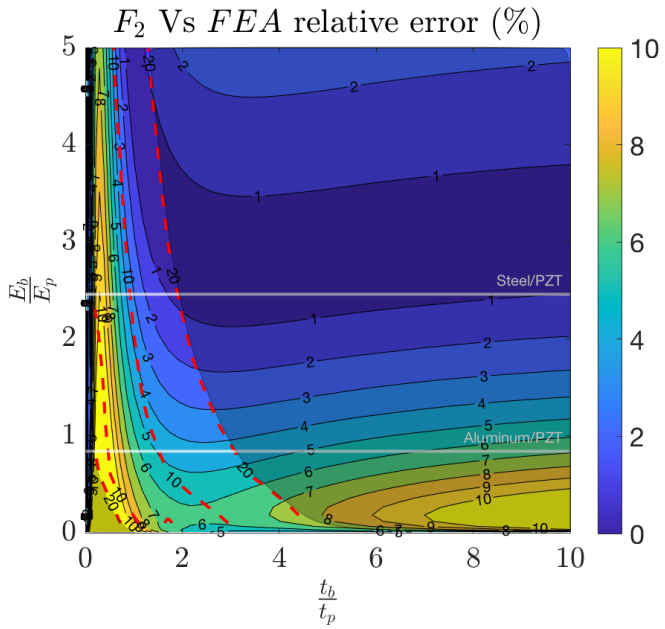

Figure 3.13: *Relative error between the F_2 pin-force model and the FEA solution taken as reference. Range delimited by dotted red lines: all models assume the same statement (dependence only on $\frac{t_b}{t_p}$ and $\frac{E_b}{E_p}$). A mask is added outside the domain validated by FEA*

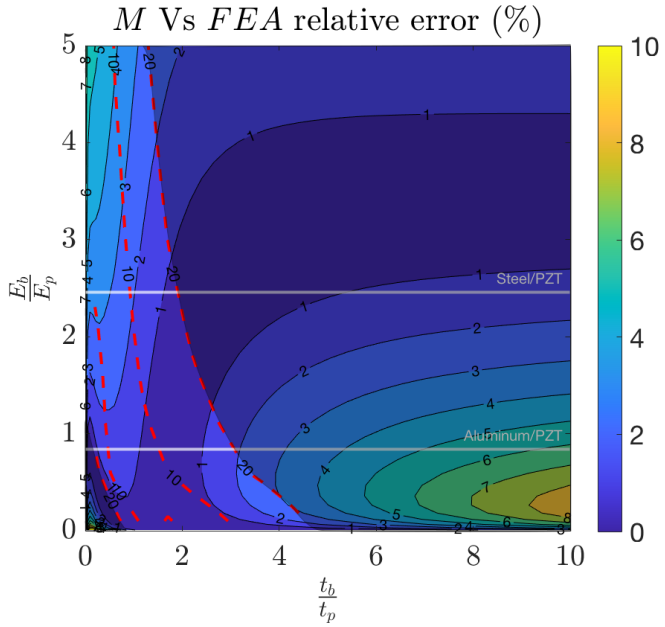

Figure 3.14: *Relative error between the two-moment model and the FEA solution taken as reference. Range delimited by dotted red lines: all models assume the same statement (dependence only on $\frac{t_b}{t_p}$ and $\frac{E_b}{E_p}$). A mask is added outside the domain validated by FEA*

In order to allow a clearer comparison between the three analytical models, all colour maps have been saturated above error values of 10%. A value of 10% (yellow) designates an error equal or higher than 10%.

The inaccuracy of the F_1 model can be very high as shown in Figure 3.12, especially

when $\widetilde{E} = \frac{E_b}{E_p} \leq 2$. However, the study shows that the F_1 model, despite its simplicity, can describe the behaviour of the system when $\widetilde{T} = \frac{t_b}{t_p}$ is around 1.5 and $\widetilde{E} \geq 2$, with errors lower than 6%.
The F_2 model is slightly better as shown in Figure 3.13. For $\widetilde{T} \geq 1$ in the investigation zone, the relative error generally remains less than 6%.
The two-moment model, associated to less drastic assumptions, logically shows the best results (see Figure 3.14). In the full range tested for the two dimensionless parameters $\widetilde{T}$ and $\widetilde{E}$, in the investigation zone, the relative error does not exceed 3% in a large part of the investigation zone, and stays below 6% almost everywhere.

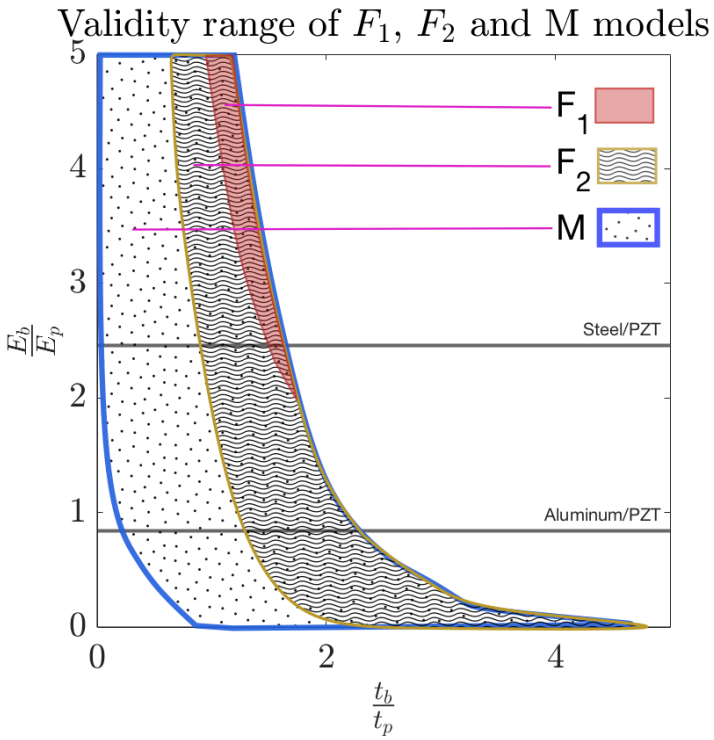

Figure 3.15: *Conclusion on the validity domains of the three analytical models, with respect to the FEM calculation*

To summarise the analysis, Figure 3.15 shows the areas of validity of the analytical models F_1, F_2 and M, based on the FEA results.
Taking into account classical beam materials: steel and aluminium, we can highlight the following findings.
F_1 model is not applicable for either the Steel-PZT or Aluminium-PZT combination. It can be used for other types of materials in a very narrow range of thickness ratios (around $\widetilde{T} = 1.5$).
F_2 model can be used for a Steel-PZT combination, where the thickness ratio meets the $1 \leq \widetilde{T} \leq 2$ condition. It can be used for Aluminium-PZT too. The condition on thickness ratio is approximately $1.5 \leq \widetilde{T} \leq 3$.
M model can be applied to both steel and aluminium cases. The only requirement is that the condition on the investigation zone, validated by FEA, is respected. This concerns

ratios $0.1 \leq \widetilde{T} \leq 2$ for steel beam and $0.5 \leq \widetilde{T} \leq 2.5$ for aluminium beam.

3.7 Conclusions

After the analysis carried out in this chapter, the following conclusions can be drawn:

- There are at least two approaches to model the action of a PZ patch on a beam: pin-force model and moment model.
- The comparison between these models can be summarised to a function of dimensionless parameters: thicknesses and Young modulus ratios.
  However, FEA results showed that the action of PZT can be accurately modelled by such a function only in a given range of dimensionless parameters.
- Three dimension plots and error maps of analytical and numeric models show that they are roughly equivalent for the following range of dimensionless parameters: $\widetilde{T}$ around 1.5 and $\widetilde{E} \geq 2$. Pin-force model with uniform strain distribution on the active element could be used over the above ranges. This model is very simple to implement and in this case, it gives similar results as the two other models.
- Pin-force model with uniform strain distribution on only the active element gives relevant results and could be used, especially when the thickness of the beam is 1 to 4 times larger than the PZ, and for many types of materials in the case where the flexural stiffness of the actuator is added.
- Moment model, which models the action of a PZ patch by two moments applied at its ends, is the best model. Its results are validated by comparing its prediction on deflection with the results obtained from the the commercial finite element 2D code.

The study carried out dealt with the case of static excitation of the actuator. The dynamic case where the actuator is supplied with frequency voltage is a prospect for future work.

It resulted in a conclusion about the validity ranges of each equivalent model of PZ actuation.
We have highlighted some conclusions regarding the use of conventional beam materials (steel and aluminium) combined with PZT: we have given a user who wants to apply the equivalent actuation models for a Steel-PZT combination, an Aluminium-PZT combination or others, the validity ranges (thickness ratios and Young's modulus ratios) for which the use of the F_1, F_2 or M models is possible.
We can imagine an application in which one or more PZ actuators actuate a disc to achieve a certain shape. A shape that is needed to mix an aqueous solution or liquids

in a certain way, or to reduce vibrations in a rotating machine if PZ actuator are connected to one of its parts.
Another application, and the one we are aiming at for the continuation of our project, is the actuation of a bistable buckled beam from one stable equilibrium state to another. We plan to integrate such a system into the car's dashboard to generate haptic feedback to the finger upon touch (see Figure 3.16).
The particularity of this case study, i.e. the bistable system actuated by PZ patches, is its

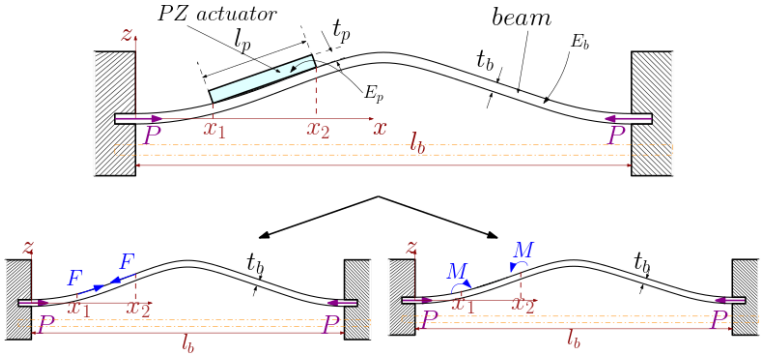

Figure 3.16: *Forces and moments equivalent models in the case of a P-compressed bistable beam actuated by a PZ patch*

complexity compared to cantilever case. It takes into account the compression forces P which in turn cause bistability [Van98]. However, the PZ actuation is independent of the type of system studied.
For these reasons, the modelling of the effect of PZ materials on a structure is done for a simple cantilever, where just the actuation of the PZ is involved. Then this model can be used on other structures.

Chapter 4

Piezoelectric activation of bistable systems

Contents

4.1 Introduction

The aim of this chapter is to study analytically, by Finite Element Modelling (FEM) and experimentally the feasibility of switching a bistable system from one state to another using only piezoelectric (PZ) actuation.
The purpose of this chapter is to demonstrate that the equivalent moment models developed in the previous chapter are valid to replace the PZ actuation in the case of a buckled system by axial compression. We will conduct an optimisation study to minimise the tension required to switch the structure from one stable state to the other, by adjusting the position of the PZ patch. This will be done analytically and by FEM. The comparison between the two results will serve to validate the use of equivalent actuation models (especially of moments) in this compression case, to understand and anticipate the snap-through of a bistable system.
The interesting positions of the PZ patches on a bistable structure will be exploited to make an experimental prototype which will serve for validation.
We will deal with the case of the two selected bistables: axially compressed single beam and laterally compressed 'U' shaped clips.

4.2 Analytical and FE modelling

The study is conducted in accordance with the fundamental assumptions of mechanics of materials.
The principle of Saint-Venant is considered.
According to the Navier-Bernoulli hypothesis, the sections normal to the mean line remain flat and normal to the mean line during deformation.
$|w'| << 1$ for very small displacement is an assumption that will allow us to neglect the rotation angle after deformation in the expression of the curvature.

4.2.1 Simple beam actuated by PZ actuators

In this section we will present the first case of the simple beam. This is a steel beam on which a PZ patch is perfectly bonded.
When the system buckles, the ends are fixed when the desired travel is reached.
By supplying voltage to the PZ patch, it actuates the structure to allow switching from one stable equilibrium state to another.
In Chapter 2 we studied the purely mechanical actuation on the bistable beam structure. With the equivalent effort approach, the study of the PZ actuation also amounts to a purely mechanical study. The difference is that we will use a model that is based on Euler-Bernoulli's equation in a new form.

Equation and solving:

In the case of pure compression with an axial force P (see Figure 4.1), Euler-Bernoulli equation can also be written as:

$$\frac{d^4w}{dx^4} + \frac{P}{EI}\frac{d^2w}{dx^2} = 0 \tag{4.1}$$

where EI is the stiffness of the system's part (E is Young modulus and I is the quadratic moment) which varies depending on whether we are in the PZ patch bonding area or not.

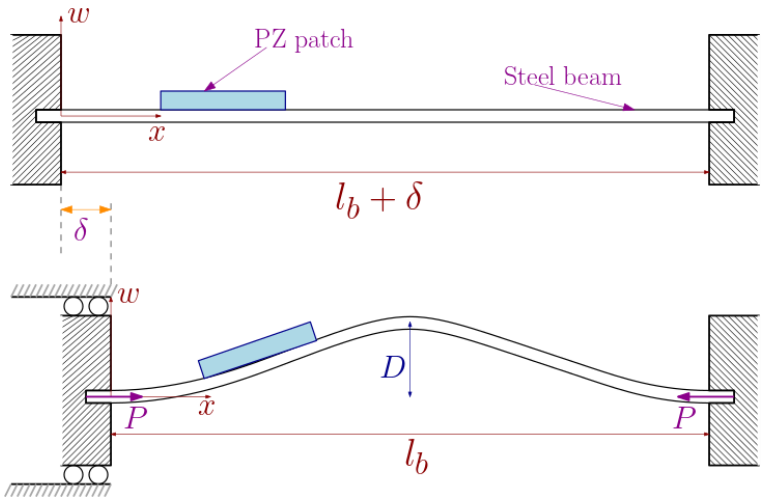

Figure 4.1: *Simple beam on which is bonded a PZ material: structure buckling to have the final configuration*

The general solution for this equation (4.1) is:

$$w(x) = Asin\,(kx) + Bcos\,(kx) + Cx + D \tag{4.2}$$

where $k^2 = \frac{P}{EI}$ and A, B, C and D are integration constants to be determined.

In this case of double-clamped beam, the equation (4.2) must satisfy the following boundary conditions:

$$w(0) = w(l_b) = 0 \quad and \quad \left(\frac{dw}{dx}\right)_{x=0} = \left(\frac{dw}{dx}\right)_{x=l_b} = 0 \tag{4.3}$$

These conditions give the four necessary equations to find integration constants:

$$\begin{aligned} B + D &= 0 \\ Ak + C &= 0 \\ Asin\,(kl_b) + Bcos\,(kl_b) + Cl_b + D &= 0 \\ Akcos\,(kl_b) - Bksin\,(kl_b) + C &= 0 \end{aligned} \tag{4.4}$$

To avoid the trivial zero solution, we set the determinant of these four equations,

where A, B, C and D are the unknowns, equal to zero. The determinant is:

$$\begin{vmatrix} 0 & 1 & 0 & 1 \\ k & 0 & 1 & 0 \\ sin\,(kl_b) & cos\,(kl_b) & l_b & 1 \\ kcos\,(kl_b) & -ksin\,(kl_b) & 1 & 0 \end{vmatrix}$$

After development, this determinant is zero if at least one of the two following conditions is met:

$$sin\left(\frac{kl_b}{2}\right) = 0 \tag{4.5a}$$

$$tan\left(\frac{kl_b}{2}\right) = \frac{kl_b}{2} \tag{4.5b}$$

Each of these conditions gives an infinite number of solutions of the deformation w as a function of the abscissa x. These are the buckling modes. The solution function could be written for the J first modes in the buckling mode basis as:

$$w(x) = \sum_{i=1}^{J} w_i(x) \tag{4.6}$$

The first condition (4.5a) gives all odd buckling modes $\{1, 3, 5, ...\}$. The second condition (4.5b) gives even modes $\{2, 4, 6, ...\}$.

$$w_i(x) = a_i\left(1 - cos\left((i+1)\pi\frac{x}{l_b}\right)\right), \quad i \in \{1, 3, 5, ...\} \tag{4.7a}$$

$$w_i(x) = a_i\left(1 - \frac{2x}{l_b} - cos\left(N_i\frac{x}{l_b}\right) + \frac{2}{N_i}sin\left(N_i\frac{x}{l_b}\right)\right), \quad i \in \{2, 4, 6, ...\}, N_i = 2.86\pi, 4.92\pi... \tag{4.7b}$$

We just need the expressions of the first and second modes (the reason behind this will be presented in the part where an external effort will be added):

$$w_1(x) = a_1\left(1 - cos\left(2\pi\frac{x}{l_b}\right)\right) \tag{4.8a}$$

$$w_2(x) = a_2\left(1 - \frac{2x}{l_b} - cos\left(N\frac{x}{l_b}\right) + \frac{2}{N}sin\left(N\frac{x}{l_b}\right)\right) \tag{4.8b}$$

where a_1 and a_2 are unknowns due to the fact that the determinant has been set to be equal to zero, and will be determined later by conducting an energy study. $N = kl_b$ is the first positive value that satisfies the condition $tan\left(\frac{N}{2}\right) = \frac{N}{2}$.

Solution if the buckled system is actuated by an external effort:

We have determined the solution of the equation (4.1), which is written for the J first modes in the buckling mode basis of the compressed beam as:

$$w(x) = \sum_{i=1}^{J} w_i(x) \tag{4.9}$$

The first two modes were taken. The reason behind this is as follows. For a compressed buckled beam actuated or not by an external effort, the form of the deflection can be written analytically as a sum of the first and second modes (for buckling behaviour) with the addition of a particular solution (for equilibrium) [Caz09] [Amo20]:

$$w(x) = w_1(x) + w_2(x) + w_p(x) \tag{4.10}$$

The interpretation of the two functions is different. $w_1(x)$ for the first buckling mode is responsible for bistability. Second mode function $w_2(x)$ has no effect on the initial state. It occurs to limit the snap-through energy. Sometimes, this mode does not appear.
The special feature of the particular solution $w_p(x)$ is that it is sought for a transverse buckling problem without axial compression. The axial compression force is not considered in the energy study for the determination of the special solution. This is because in the construction of the particular solution, it must contain only equilibrium solutions according to the applied transverse force. This is not the case when the system is buckled; not all positions are equilibrium positions.
We first start with the determination of the particular solution $w_p(x)$ under the conditions mentioned above.
The particular solution is also the sum of the buckling modes resulting from transverse actuation. We stop at mode 20 because it is enough to describe the behaviour of the buckled beam [Caz09]. The particular solution expression becomes:

$$w_p(x) = \sum_{j=1}^{20} w_j(x) \tag{4.11}$$

To determine the expression for the particular equilibrium solution, we use the explicit formula for the total energy of the system without compression $U_{tot}^{(p)}$:

$$U_{tot}^{(p)} = U_b^{(p)} + U_{ext}^{(p)} \tag{4.12}$$

where $U_b^{(p)}$ is the bending energy and $U_{ext}^{(p)}$ is the energy resulting from an external effort whether it is a force, a moment or a double moment. Their expressions are given in the Euler–Bernoulli model, in Cartesian coordinates and assuming small displacements, by:

$$U_b^{(p)} = \frac{EI}{2} \int_0^{l_b} w_p''(x)^2 \, dx \tag{4.13}$$

$$U_{ext_F}^{(p)} = -F.w_p(x_1) \tag{4.14a}$$
$$U_{ext_M}^{(p)} = -M.w_p'(x_1) \tag{4.14b}$$
$$U_{ext_{MM}}^{(p)} = -M.\left(w_p'(x_1) - w_p'(x_2)\right) \tag{4.14c}$$

where x_1 is the abscissa of application of the effort in the case of a single effort, and x_2 if there are two: F for one applied force, M for one applied moment and MM for two

applied moments.

The unknowns of the total energy $U_{tot}^{(p)}$ are the unknowns of the deflection expression $w_p(x)$. These unknowns are then a_j with $j \in \{1, 2, 3, 4...20\}$. It is therefore a question of twenty unknowns. This requires twenty equations in order to determine a particular solution. The particular solution is an equilibrium solution for all unknowns a_j. This is expressed analytically by the following twenty equations:

$$\left\{ \frac{\partial U_{tot}^{(p)}}{\partial a_j} = 0 \right\}_{j \in \{1,2,3,4...20\}} \tag{4.15}$$

The idea of this method is to minimise $U_{tot}^{(p)}$ with respect to the deformation amplitudes.

Once the particular solution is determined, we will put it into the expression of $w(x)$. $w(x) = w_1(x) + w_2(x) + w_p(x)$ now contains only two unknowns, those of $w_1(x)$ and $w_2(x)$, i.e. the a_i with $i \in \{1, 2\}$.
These two unknowns should give an equilibrium solution. They minimise therefore the total energy of the system U_{tot} for the case with compression this time.
There are three energy factors that must be used, the bending energy U_b, the compression energy U_c, and the work of externally applied efforts U_{ext} [CS15].

$$U_b = \frac{EI}{2} \int_0^{l_b} w''(x)^2 \, dx \tag{4.16}$$

$$U_c = \frac{AE}{8 \left(l_b + \delta\right)^2} \left(-2\delta + \int_0^{l_b} w'(x)^2 \, dx \right)^2 \tag{4.17}$$

where A is the section of the part with or without the PZ depending on the position x and δ is the free end displacement of the beam between the moment before buckling and the final position after buckling.

$$U_{ext_F} = -F.w(x_1) \tag{4.18a}$$
$$U_{ext_M} = -M.w'(x_1) \tag{4.18b}$$
$$U_{ext_{MM}} = -M.\left(w'(x_1) - w'(x_2)\right) \tag{4.18c}$$

The three cases for the actuation of the bistable beam, i.e. actuation by force, by moment or by double moment are given in the Figures 4.2a, 4.2b and 4.2c.

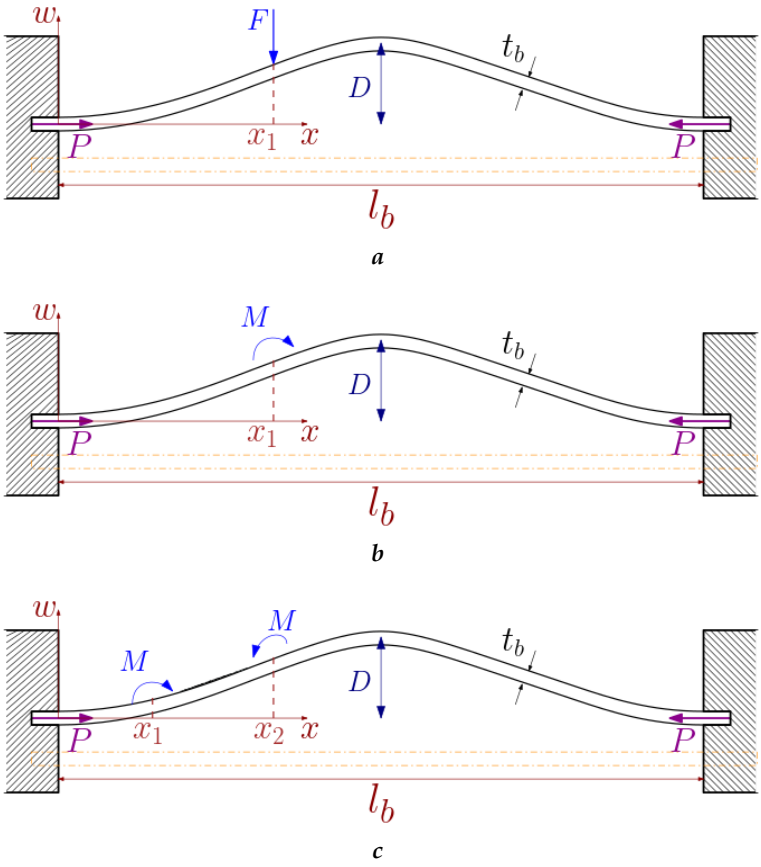

Figure 4.2: *Simple beam actuated by an external effort: (a) force actuation, (b) moment actuation and (c) two moments actuation*

The particular solution $w_p(x)$ is an equilibrium solution for a virtual buckled system without compression.
The next step is to obtain the global solution $w(x)$, witch is an equilibrium solution for the real compressed system.
The energy criterion for equilibrium can be written on the basis of minimisation with respect to the deformation amplitudes a_1 and a_2, and leads to the deflection shapes for a given external actuation. The energy criterion is as follows:

$$\left\{ \frac{\partial U_{tot}}{\partial a_1} = 0, \frac{\partial U_{tot}}{\partial a_2} = 0 \right\} \tag{4.19}$$

It is a system of two independent equations with two unknowns. These are two third-order equations. Many combinations of solutions are possible and only one doublet of solutions is retained that is physically valid.
It should be remembered that external efforts are so far unknown. They must be given as input to find the deflection solution $w(x)$.
The cases of actuation with a single force or moment have been extensively discussed in the literature [Caz+09] [CS15] [Amo20], and are not the cases we are interested in for actuation with PZ materials.
We have shown in Chapter 3 that the actuation of a PZ patch is equivalent to a double moment actuation, and this will be used to compare an actuation study with PZ patches

under FEM and an equivalent moment analytical model.
Analytically, we will study the influence of the actuation with two moments on the quantity $D = w\left(x = \frac{l_b}{2}\right)$. Numerically, we will study the influence of the action of one or two PZ patches on the transverse displacement D in the middle of the beam. The two results will be compared on the basis of the equivalence between the actuation moment and the supply voltage of the PZ patch.

Analytical modelling of PZ actuation on a bistable beam using moments equivalence:

The action of a voltage-fed PZ patch was previously modelled by either pin-forces or pin-moments. The second equivalence was chosen because of its consistency with the numerical result. The pin-moments are on both side of the ends of the PZ, around the same axis, in opposite directions and with equal module given by the formula:

$$M = bE_p\left(-K^f I_p + \left(K^e - 1 - z_n K^f\right) T - z_n\left(K^e - 1\right) t_p\right)\Lambda, \qquad \left(\Lambda = d_{31}\frac{V_0}{t_p}\right) \tag{4.20}$$

where $I_p = \frac{\left(\frac{t_b}{2}+t_p\right)^3 - \left(\frac{t_b}{2}\right)^3}{3}$ and $T = \frac{\left(\frac{t_b}{2}+t_p\right)^2 - \left(\frac{t_b}{2}\right)^2}{2}$,
where z_n defines the neutral axis of the beam (z position for which the strain ϵ_b is zero):

$$z_n = \frac{E_p\left(t_p^2 + t_p t_b\right)}{2\left(E_b t_b + E_p t_p\right)} \tag{4.21}$$

and where

$$K^f = \frac{2}{t_b + t_p}\left(1 - \frac{E_b E_p t_b^3 t_p + E_b^2 t_b^4 + E_p^2 t_p^4 + E_b E_p t_b t_p^3}{E_p^2 t_p^4 + E_b^2 t_b^4 + E_b E_p\left(4t_b^3 t_p + 6t_b^2 t_p^2 + 4t_b t_p^3\right)}\right)$$

$$K^e = \frac{t_p^4 + \frac{E_b}{E_p} t_b^3 t_p}{t_p^4 + \frac{E_b^2}{E_p^2} t_b^4 + \frac{E_b}{E_p}\left(4t_b^3 t_p + 6t_b^2 t_p^2 + 4t_b t_p^3\right)}$$

are introduced to simplify the moment formula.

We consider our study case, where actuation with piezoelectric patch supplied with voltage happens as if there is an internal double moment that actuates the system at the ends of the patch, with the patch kept passive (see Figure 4.3).
For the numerical applications, experimental work in the context of my internship concluded on the dimensions of the PZT patch and the steel beam to be used to achieve the proof of concept of the position feedback. Other tests with different dimensions (e.g. PZT of (10,10,0.5 mm) and steel beam of (70,10,0.3 mm)) were not successful.
In all the following, we use beam dimensions of (70,14,0.3 mm) and PZT actuator dimensions of (14,14,0.3 mm). The length of the PZT patch l_p gives the distance between the pin-moments.

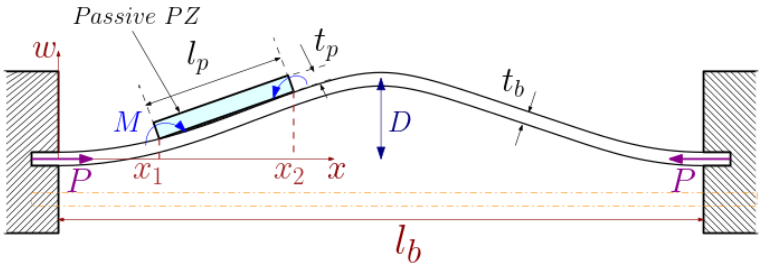

Figure 4.3: *Simple beam actuated by pin-moments at the ends of a passive PZ patch: pin-moments equivalence with PZ actuation*

Under the small displacement assumption, it is assumed that $x_2 = x_1 + l_p$.
With a constant PZ patch length l_p, changing the application position of the first moment means changing the position of the second moment as well. We can also define the middle position of the PZ patch x_0 between x_1 and x_2 as a characteristic parameter of the PZ position.
Based on the configuration in Figure 4.3, we change the values of the applied moments on the bistable beam, and the induced halfway point displacement is taken for each moment value. This allows us to draw the moment-displacement curves. As the application position is changeable, we can then change the application position of the pin-moments and see how this influences the shape of the resultant curves.

For an actuation with two moments on each side of the middle of the buckled beam ($\frac{l_b}{2} - \frac{l_p}{2}$ and $\frac{l_b}{2} + \frac{l_p}{2}$), the moment-displacement curve resembles that with an actuation using one applied force on the midpoint (see Figure 4.4a). The corresponding curve is a straight line with a negative slope (negative system stiffness): this is a passage by the second mode of buckling. The snap-through point corresponds to the local optima (around $\pm 0.3\ N.m$), either from bottom to top (local maximum) or from top to bottom (local minimum).
If we shift the point of application x_1 (and consequently the second point of application x_2 and the midpoint x_0), either to the right or to the left (the response is symmetrical), the force-displacement curve starts to change its shape.
Figure 4.4b, with a shifted actuation of 10%, shows a figure with a discontinuity at the point of unstable equilibrium (point of zero effort for zero displacement).
The code used traces all possible solutions. Some branches of curves are not physically interesting. In fact, only the branches given by the figure 4.5 are kept, with all the characteristic points presented before: snap-through points (local optima), stable equilibrium points (A and C) and unstable equilibrium points (B and its symmetry with respect to the ordinate axis).
Figure 4.4c, where the actuating moments position is offbeat by 20% from the middle position, has a different upward curve and reaches a high snap-through moment level compared to the two other cases.

We continue to change the positions of application of the two moments, keeping the spacing constant, and each time we take the value of the moment needed for the snap-through of the beam.

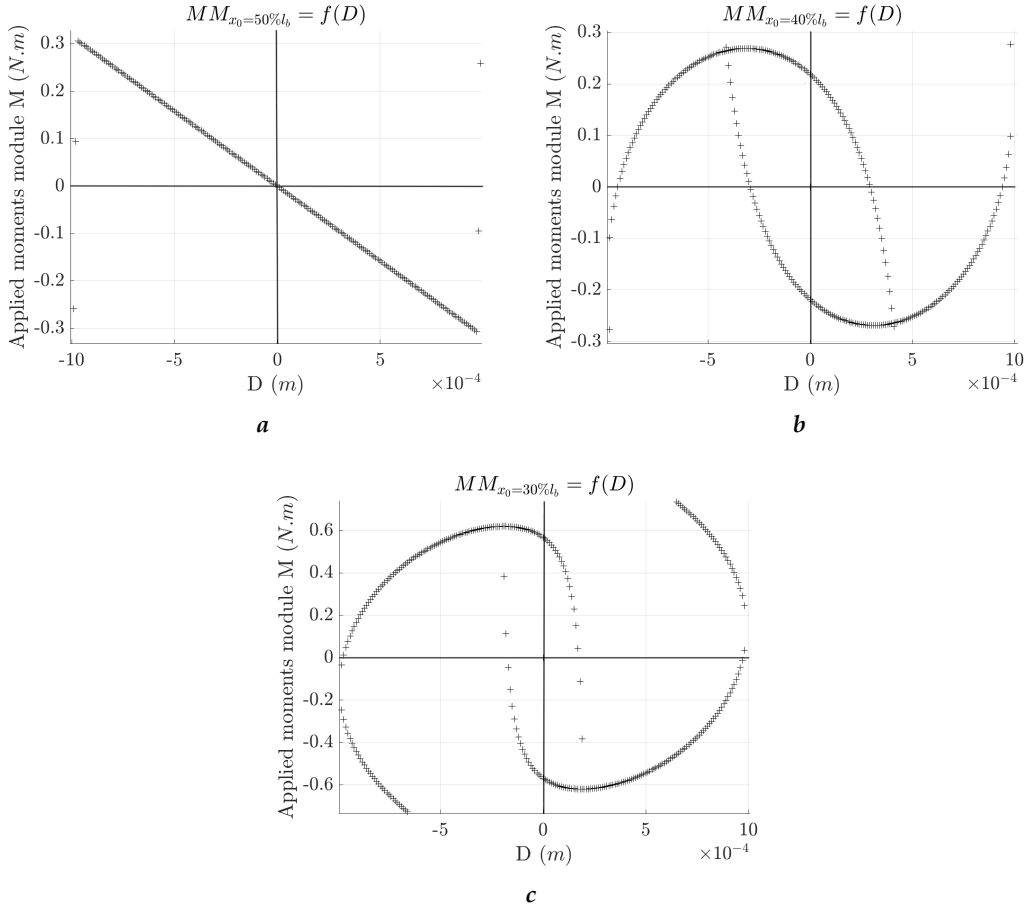

Figure 4.4: *Moment-displacement curves in the middle of bistable beams actuated by pin-moments in different positions. x_0 the midpoint between the position of application of the first moment x_1 and the second moment x_2: (a) $x_0 = 50\%.l_b$, (b) $x_0 = 40\%.l_b$ and (c) $x_0 = 30\%.l_b$*

This allows us to plot the critical snap-through curve which assembles the snap-through moment as a function of the position of the moments.
The shape of the analytical curve is given in Figure 4.6.

This curve of critical switching moments gives an idea of where two spaced moments by a distance of l_p apart should be applied for a low-effort snap-through.
Two positions stand out: close to the clamping bars or near the middle of the beam.
With the application of two moments, the position near the middle of the beam is more interesting with the smallest possible snap-through critical moment.
This analytical result will be compared with a numerical model where the beam is actuated with a voltage-supplied PZ patch. This will validate the accuracy of the moment model in this case of application and the snap-through model based on energy approach as well.

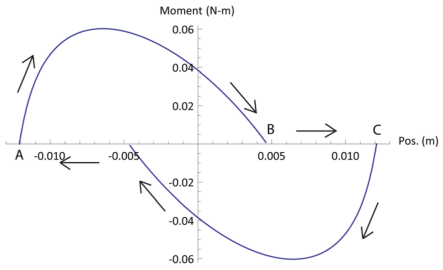

Figure 4.5: *Displacement vs moment curve for offset actuation from the middle position: actuation at 23.33% along the length of the beam [CS15]*

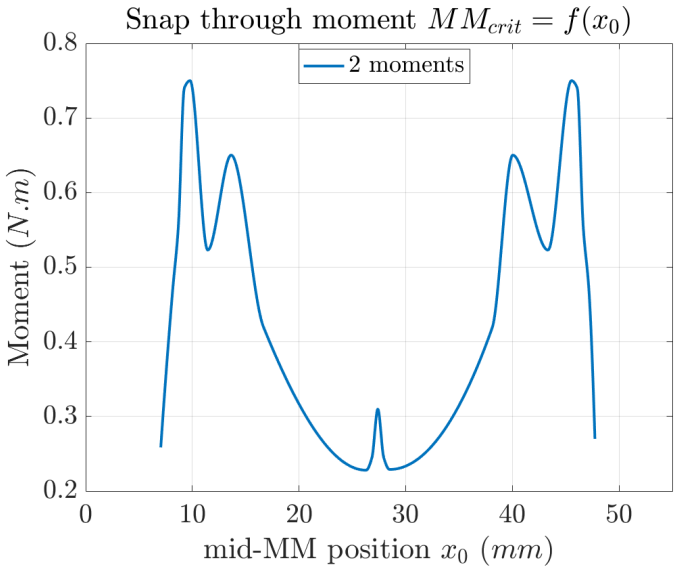

Figure 4.6: *Snap-through curve: snap-through moment vs moment position. Beam dimensions of (70,14,0.3 mm) and PZ actuator dimensions of (14,14,0.3 mm)*

FEM of PZ actuation on a bistable beam:

The idea of the numerical study is to design the structure, i.e. the beam, and a PZ actuator perfectly bonded on it. One end of the PZ patch is at the x_1 position, the other is at the x_2 position. The middle position of the PZ patch is noted x_0. Changing one position means changing the others because the length of the PZ is constant. We arbitrarily choose x_0 when we want to change the PZ patch position on the beam (see Figure 4.7).

For each position, the system is first buckled by applying the axial force on its moving end. Then, the PZ actuator is supplied with voltage and the snap-through point is determined, which is an optimum on the voltage vs beam middle displacement curve.
We change the position x_0 of the middle of the PZ patch, and get the switching voltage. This allows us to plot the switching voltage as a function of position.
To compare this result with the analytical study conducted earlier, the moment-voltage equivalence given by equation (4.20) is used.
The result of the comparison between the analytical model and the numerical model,

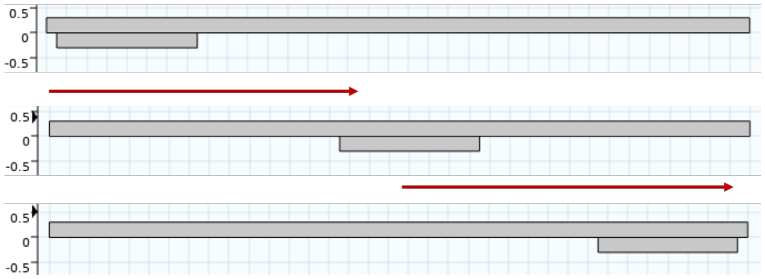

Figure 4.7: *Design of the system by numerical calculation software: changing of the position of one PZ actuator all along the beam structure*

concerning the snap-through voltage as a function of the actuator position, is given in Figure 4.8.

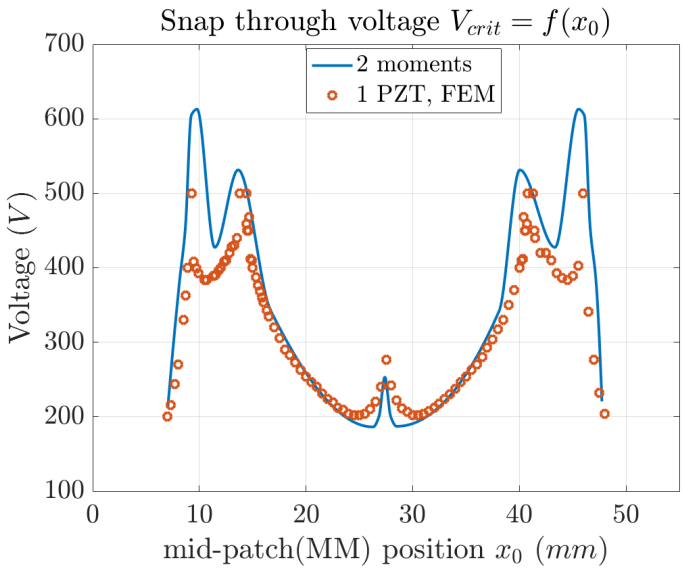

Figure 4.8: *Snap-through analytical and numerical curves: snap-through voltage vs PZ-patch/MM position. Beam dimensions of* (70,14,0.3 mm) *and PZ actuator dimensions of* (14,14,0.3 mm)

The two critical switching curves describe the same form of variation.
Some errors between the two models appear in some regions, especially when the actuator is on two regions of the beam surface, one in extension and the other in compression. This is mainly due to all the simplifications of the Euler-Bernoulli model which does not take the shear stress into account. Sometimes, the numerical code diverges at the snap-through or the unstable points, depending on the step and the fixed relative error of reference, which can introduce errors on the taken switching voltage value.
The two best bonding positions for the PZ actuator to easily switch the bistable system stand out again: next to the clamping bars and near the middle of the beam.
The choice between these two can be made on the basis of the mechanical limit of the PZ patch. In the middle of the beam, it can be demonstrated that the strain at the common surface between the PZ patch and the beam is relatively large compared to the surface

strain next to the clamping bars.
We therefore have more interest in gluing the PZ actuator next to the clamping bars rather than near the middle of the beam.

The two analytical and numerical studies on changing the position of a single PZ patch (Figure 4.7) to optimise the voltage required to switch the bistable were presented in this section, as well as their comparison which concludes on the accuracy of the analytical model.

We will extend the study to the case of two PZ actuators whose positions are changing using analytical and numerical modelling (Figure 4.9).

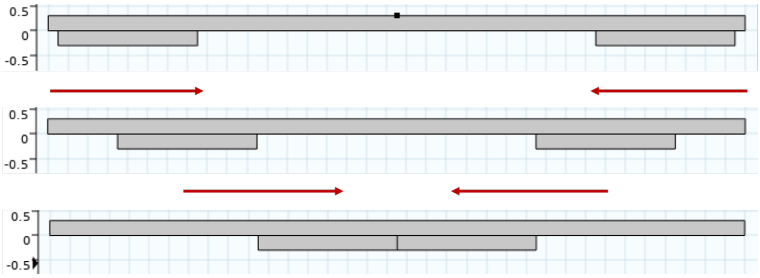

Figure 4.9: *Design of the system by numerical calculation software: changing of the position of two PZ actuators symmetrically all along the beam structure*

In the case of actuation with two PZs, we consider for the analytical model that it happens as if the two antagonistic moments are applied at x_1 and x_2, and two other moments are applied in the same way at x_3 and x_4.
Under the small displacement assumption, it is assumed that $x_2 = x_1 + l_p$, $x_3 = l_b - x_2$ and $x_4 = x_3 + l_p$.
The result of the comparison between the analytical model (4 moments application) and the numerical model (2 PZ actuation), concerning the snap-through voltage as a function of the actuator position, is given in Figure 4.10.

The results of the two models show a rather interesting and more significant consistency than for the comparison in the case of actuation with a single PZ.

To compare the impact of the use of several actuators on the voltage required to switch the bistable beam, we plot on the same figure the numerical results (a choice! we could have plotted the analytical results) of the two types of actuation.
Figure 4.11 shows the result of optimising the snap-through tension of the buckled beam from one stable state to the other by adjusting the position of one PZ actuator (as illustrated in Figure 4.7) and then the position of two PZ actuators (as illustrated in Figure 4.9).
(1 PZT, FEM) curve in Figure 4.11 is the same result as in Figure 4.8.
(2 PZT, FEM) curve in Figure 4.11 is the same result as in Figure 4.10.
They were put together to highlights the best bonding positions of the actuators and the

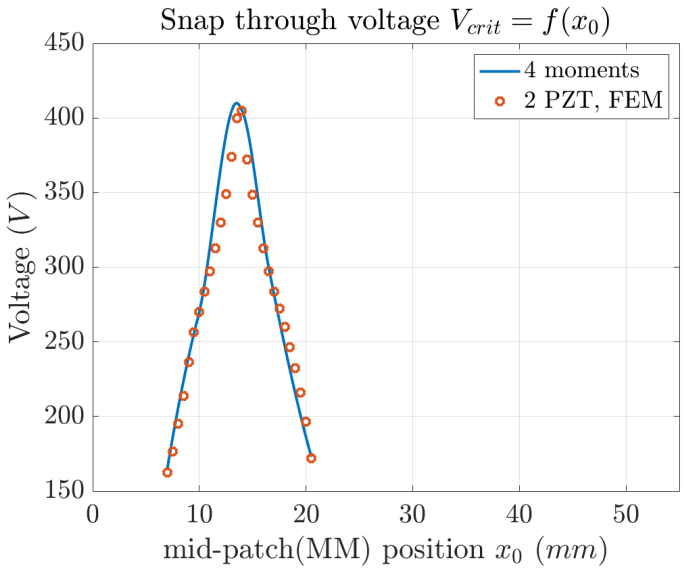

Figure 4.10: *Snap-through analytical and numerical curves in the case of two PZ actuators: snap-through voltage vs left PZ-patch/MM position. Beam dimensions of* (70,14,0.3 mm) *and PZ actuators dimensions of* (14,14,0.3 mm)

corresponding voltages.

Actuation with two PZ patches offers interesting positions for switching with minimum supply voltage. These are almost the same as for a single PZ actuator. However, the voltage for switching with two PZ patches is small compared to the case of a single PZ. The voltage required for switching is about 25% less in the two actuators case.
The use of two actuators may seem expensive, but much is gained as the switching voltage is minimised.

Now that we have dealt with the first topic of a bistable beam snap-through by piezoelectric actuators, we will move on to the case of 'U' shaped bistable clips.

4.2.2 Clips actuated by PZ actuators

As introduced in Chapter 2, we have characterised two types of 'U' shaped clips: one with dimensions (70,10,0.3 mm) and the other with dimensions (70,14,0.3 mm).
The characterisation focused on the bistability of the buckled 'U' shaped system and then on the levels of force needed for the snap-through of the buckled system.

In the same way as for the simple bistable beams, the actuation of the 'U' shaped systems in this part will be done by a PZ actuator.
We will try different actuation configurations: with one PZ patch or with two and in different positions. We can go to more than two PZ patches if the voltage levels are large compared to the breakdown voltage of the PZT ceramics we have.

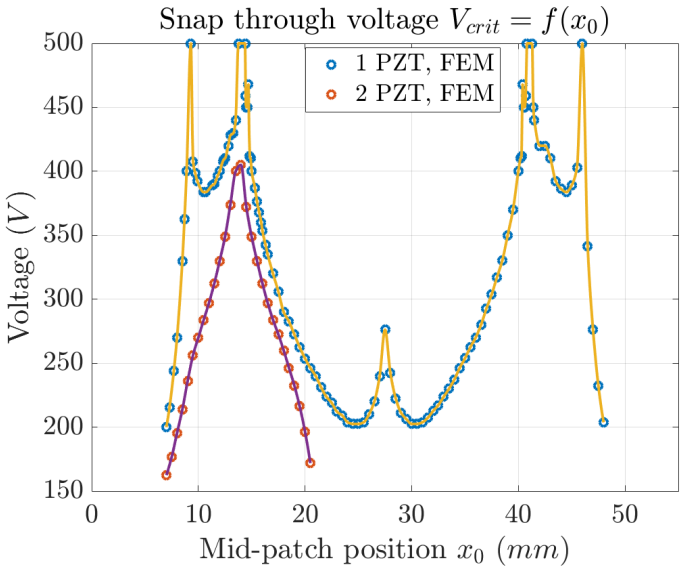

Figure 4.11: *Critical snap-through numerical curves: snap-through voltage vs one and two PZ-patch(es) position. (1 PZT, FEM) curve is the same as in Figure 4.8. Beam dimensions of* (70,14,0.3 mm) *and PZ actuator dimensions of* (14,14,0.3 mm)

Figure 4.12 shows the two 'U' shaped systems with dimensions (70,10,0.3 mm) and (70,14,0.3 mm). On each is perfectly bonded one PZ patch of dimensions (10,10,0.3 mm) and (14,14,0.3 mm) respectively.
Figure 4.13 also shows the two 'U' shaped systems with dimensions (70,10,0.3 mm) and (70,14,0.3 mm). On each is perfectly bonded, at the same position along the x axis on each arm of the 'U', two PZ patches of dimensions (10,10,0.3 mm) and (14,14,0.3 mm) respectively.
In each case in Figures 4.12 and 4.13, we change the PZ(s) position, we pre-stress the 'U' as described in the dedicated chapter. Once we have the bistable system, we supply voltage to the patch(es) so that it switches the system from one stable equilibrium state to the other.
We take the optimum on the curve of voltage vs displacement of the middle of the 'U' system. This allows to plot the snap-through voltage curve as a function of the position of the PZ patch(es).

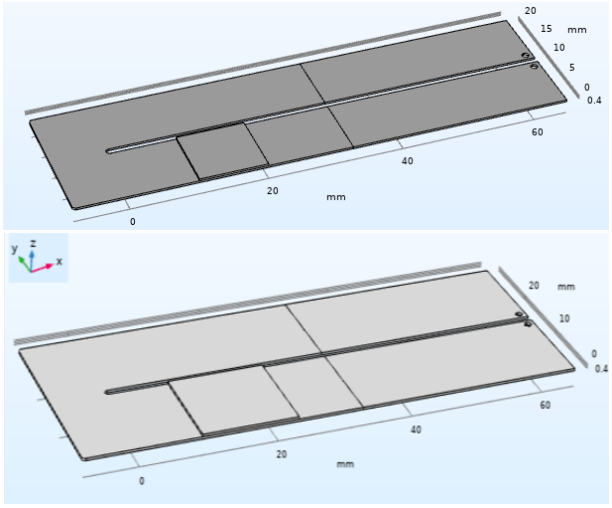

Figure 4.12: *Two 'U' shaped systems with dimensions* (70,10,0.3 mm) *and* (70,14,0.3 mm) *on which is bonded one PZ actuator of dimensions* (10,10,0.3 mm) *and* (14,14,0.3 mm) *respectively*

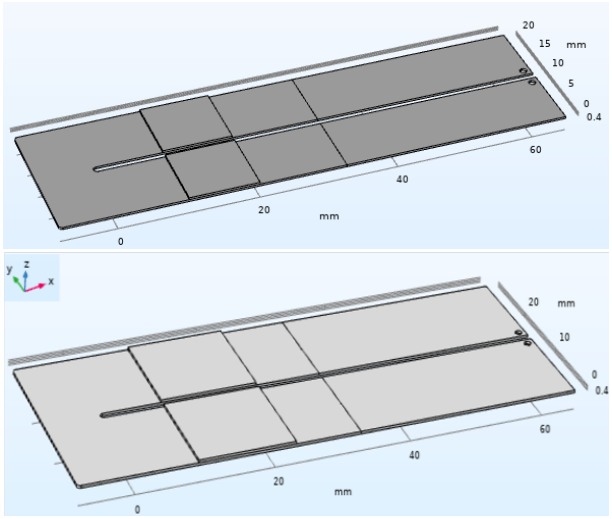

Figure 4.13: *Two 'U' shaped systems with dimensions* (70,10,0.3 mm) *and* (70,14,0.3 mm) *on which are bonded two PZ actuators of dimensions* (10,10,0.3 mm) *and* (14,14,0.3 mm) *respectively*

Figures 4.14 and 4.15 show the result of the snap-through voltage curve of the 'U' shaped bistables as a function of the position of the PZ actuator(s). The blue vertical lines indicate the range where the PZ patch can be bonded. Sometimes we stop before the ends because the tension increases significantly at the edge and we can no longer see the optimums of the curve.

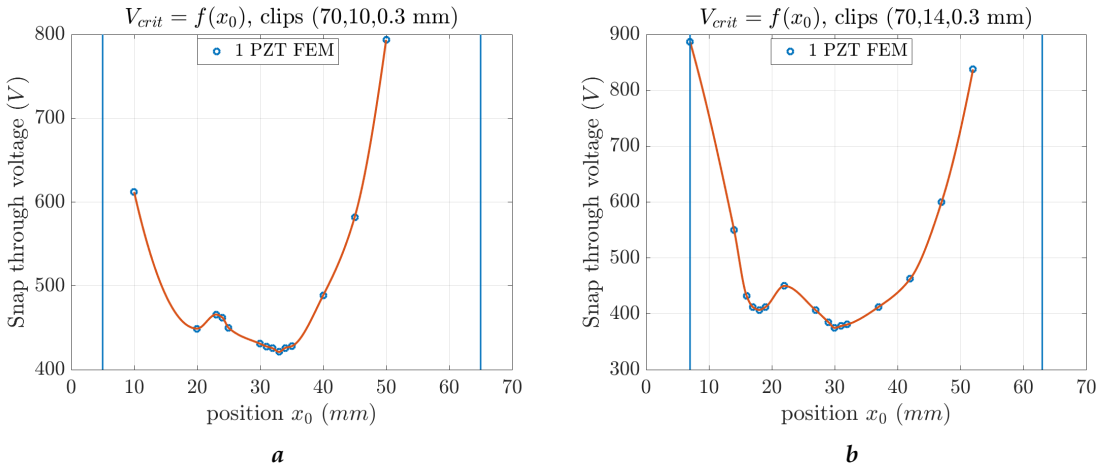

Figure 4.14: *Snap-through voltage of the 'U' shaped bistable clips vs the position of the PZ actuator: (a) 'U' arms of* (70,10,0.3 mm) *actuated by one PZ patch of* (10,10,0.3 mm) *and (b) 'U' arms of* (70,14,0.3 mm) *actuated by one PZ patch of* (14,14,0.3 mm)

For a single PZ patch actuation, we note first and this is also true for actuation with two PZ patches, that the voltage vs position curve is not symmetrical. This is expected because the bistable 'U' shaped system is not symmetrical in design. After buckling, two of its ends are brought together until they touch, while the other two are spaced apart.
For the 'U' system, the voltage versus position curve shows two local minima. It turns out that it is better to glue the PZ patch in the middle of the 'U' arm for a lower voltage switching.
For a PZ patch with dimensions (10,10,0.3 mm), the minimum switching voltage level is high compared to its rival with the dimensions (14,14,0.3 mm) (422 V vs 375 V).
It is therefore more interesting to use the 'U' with the larger dimensions, and the actuator with its associated PZ actuator when it is a single PZ patch actuation.

For two PZ patches actuation, the curve of switching voltage vs position of the PZ patches show two local minima, with this time more interest in bonding the PZ patches on the left part of the 'U' arms.
Again, using the 'U' with the large dimensions and associated PZ actuators has an advantage over the minimum snap-through voltage (363 V vs 324 V).

However, the voltage levels for switching the bistable 'U' remain high (over 300 V). Therefore, in addition to testing with a two-patch actuation, we will adjust the closeness of the ends of the 'U' to make it buckle with less transverse displacement, and try to add more PZ patches for actuation if necessary.

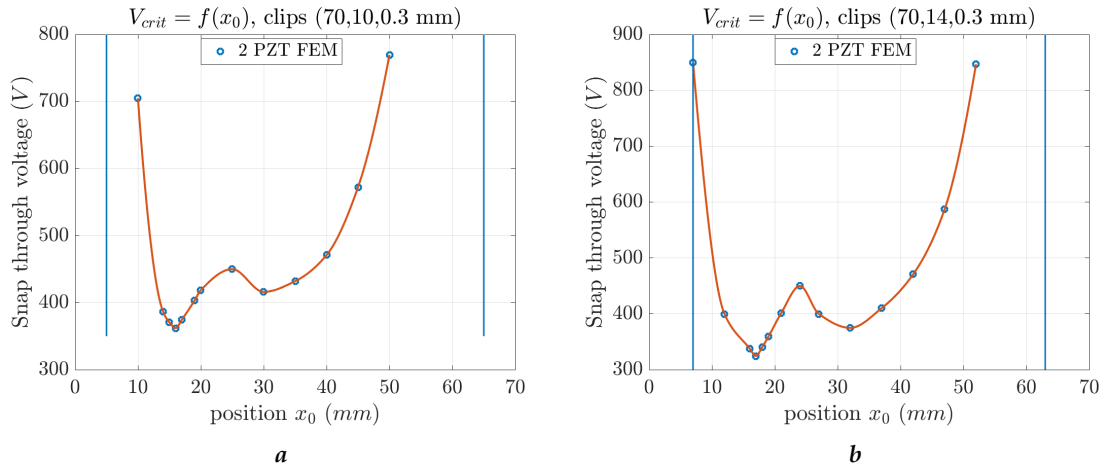

Figure 4.15: *Snap-through voltage of the 'U' shaped bistable clips vs the position of the PZ actuators: (a) 'U' arms of* (70,10,0.3 mm) *actuated by two PZ patches of* (10,10,0.3 mm) *and (b) 'U' arms of* (70,14,0.3 mm) *actuated by two PZ patches of* (14,14,0.3 mm)

4.3 Experiment: snap-through using PZ actuators

4.3.1 Prototyping

We contracted out the fabrication and cutting of the beams and 'U' shaped systems to a company as mentioned in Chapter 2.
The chosen material for both systems, which are bistable after pre-stressing, is steel (XC75 steel). This choice is due to some studies carried out in the laboratory before [Har12]. They concluded that the shear force transfer between the PZT ceramics (NCE41) and the host structure is maximum, for these thickness dimensions range, when the structure is made of steel.
The nature of the surface is very important as it determines the quality of the bonding. It is therefore necessary to prepare the surfaces.
The method used is that of surface preparation for the bonding of strain gauges. The first step is to polish and clean the surface: the PZ patch is gently polished at an angle of $+45°$ and $-45°$ with abrasive paper. The polished surface is cleaned with alcohol and degreaser and immediately wiped clean in one pass with a paper. Glue is added to the prepared surface and the PZ patch is placed on and tightened for more than eight hours to hold to the structure.
The adhesive used is Araldite (Figure 4.16), a two component epoxy paste adhesive provided by Huntsman International LLC.

To quickly discuss this choice, the adhesives are briefly presented bellow.
There are four common adhesives for bonding metal to metal and metal to other materials: Acrylic, Anaerobic, Cyanoacrylate and Epoxy.
Araldite has the feature of being a two components epoxy adhesive, which enables it to be one of the strongest adhesives for metal. The glue is a mixture of two parts that react

Figure 4.16: *Araldite, a two component epoxy paste adhesive provided by Huntsman International LLC*

with each other to initiate the curing process. The epoxy adhesive is suitable for bonding a wide range of materials: metal, ceramics, rubber, rigid plastics, etc. Its impact resistance is considerable, with good resistance to dynamic stresses. Its resistance to shear and peel is excellent. All these properties are interesting for such an application as ours, where a ceramic is bonded on a steel beam with static solicitations, and perhaps dynamic solicitations in the perspective of this work.

4.3.2 Simple beam actuated by PZ actuators

Numerical modelling of the PZ actuation of a bistable beam, using one PZT patch and two PZT patches, was carried out.
Some positions optimising the snap-through tension stood out.
In particular, these optimal points were tested experimentally for validation.
Figure 4.17 shows the two cases of bonding one PZT actuator to a beam in an optimal position. Figure 4.18 shows the two cases of bonding two PZT actuators to a beam in an optimal position.

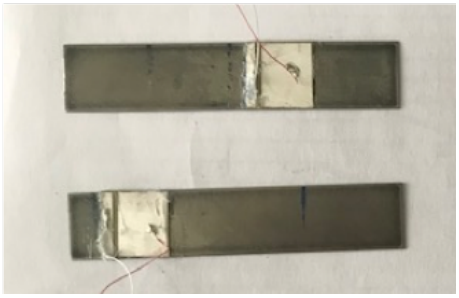

Figure 4.17: *Two cases of one PZT ceramic glued to a steel beam in two places that minimise the snap-through tension of the bistable beam system. Steel beam of* (70,14,0.3 mm) *and PZT ceramic of* (14,14,0.3 mm)

The beams are 70 mm long. The length used, whether in modelling or in experimentation, is just 60 mm to allow clamping the ends, and to validate experimentally some

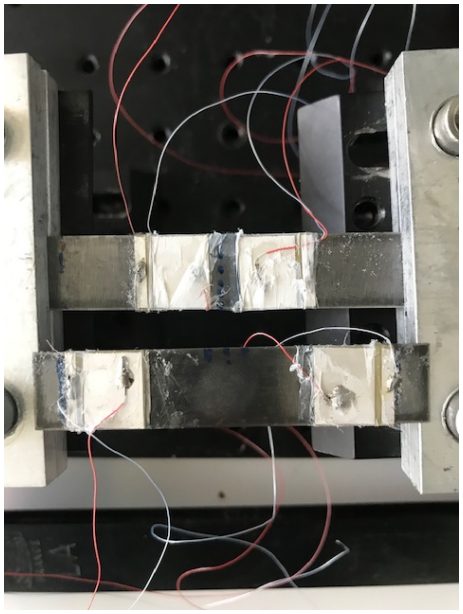

Figure 4.18: *Two cases of two PZT ceramics glued to a steel beam in two places that minimise the snap-through tension of the bistable beam system. Steel beam of* (70,14,0.3 mm) *and PZT ceramics of* (14,14,0.3 mm)

position of the PZ patch without having to glue a new one on a new beam, i.e. just to play on the part under the clamping bars.
Using these simple beam configurations with one or two PZ patches bonded to them, we axially compress the beams to buckling.
The PZ patches are then supplied with voltage, with twenty volt jumps. This allows an overview of the timing and measurement of the snap-through voltage from one stable state to another. This is repeated with different voltage starting points, allowing error bars to be drawn on the voltage. The possibility to clamp the beam at different points allows us to test a few points (tension, position), around the optimal points.
An error on the position of the PZ patch of $1\ mm$ is added.
Figures 4.19 and 4.20 show the numerical result of the snap-through voltage curves as a function of the position of the PZ patches, together with some experimentally tested points.

In the case of a single PZT ceramic bonded to the steel beam, we were able to take advantage of the tolerance in the clamped area to test the switching for actuator positions close to the edges (3 points) and also to the middle (2 points).
As shown in Figure 4.19, the errors on the switching voltage between the numerical model and the experiment do not exceed 45 volts (between $30\ V$ and $45\ V$).
Errors are mainly due to the sensitivity of the snap-through point, in particular the voltage and position to the boundary conditions and to the equipment used to apply the forces and apply the voltage. The adhesive layer between the PZT and the beam, used in the test bench and not taken into account in the model, is also a source of error.

In the case of two PZT ceramics bonded to the steel beam, the tolerance in the clamped

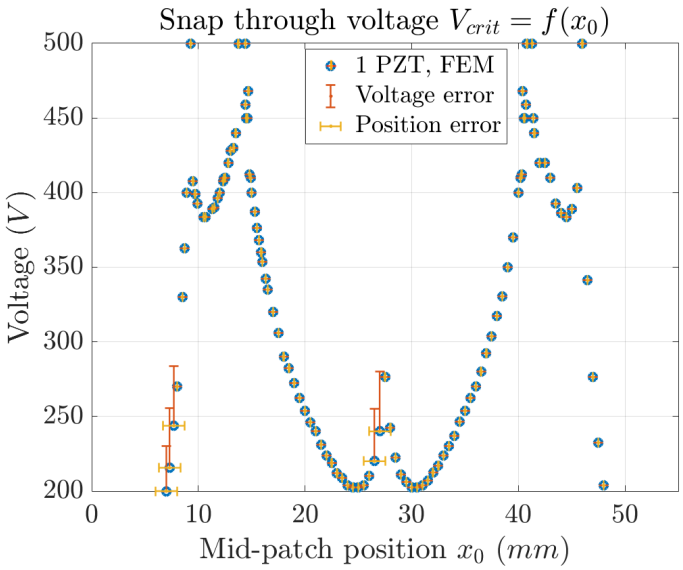

Figure 4.19: *Snap-through numerical curve with several experimentally validated points: snap-through voltage vs 1 PZT patch position. Steel beam of* (70,14,0.3 mm) *and PZT ceramic of* (14,14,0.3 mm)

area allows to test the switching for actuators positions (2 points close to the edges and 2 points close to the middle).
As shown in Figure 4.20, the errors on the switching voltage between the numerical model and the experiment do not exceed 25 volts (between 10 V and 25 V).
For the same reasons as the single PZ patch case, the errors, this time relatively small given the use of two PZ patches, are explained by the sensitivity of the snap-through point to boundary conditions and the used equipment. The adhesive layer is a source of error here too.

4.4 Conclusions

This chapter provided an opportunity to discuss the operating principle of the targeted application. Getting tactile feedback from the switching of a bistable system from the down to the up state based on PZ actuators is the objective of the study. It requires mechanical analysis of the buckling phenomenon, modelling of the actuation by piezoelectric materials and experimental validation work. This led to a proof of concept for the intended application, based on the buckled bistable beam actuated by PZ patches.
With the chosen deflection level ($D_0 = 1\ mm$), the PZT ceramics have indeed demonstrated their ability to switch a bistable buckled beam. This was proven for the steel beam of dimensions (70, 14, 0.3 mm) with PZT ceramics of dimensions (14, 14, 0.3 mm) glued on. An optimisation study was carried out to minimise the voltage required at switchover as a function of the position of a single PZ patch and then that of two PZ patches.
Promising bistable, 'U' shaped systems have been concerned with PZ actuation in modelling. The voltage to switch these 'U' shaped steel systems is large compared to the

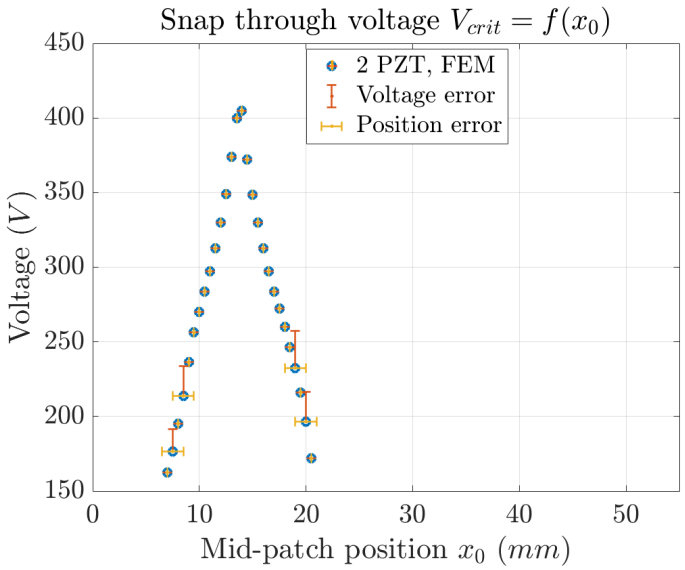

Figure 4.20: *Snap-through numerical curve with several experimentally validated points: snap-through voltage vs 2 PZT patches position. Steel beam of* (70,14,0.3 mm) *and PZT ceramics of* (14,14,0.3 mm)

breakdown voltage of PZT ceramics. This prevents experimental validation for the time being, but an alternative of bonding several actuators is being tested.

General conclusion

The objective of this work was to conduct a feasibility study to answer the following question: can contact detection and haptic feedback be guaranteed with a bistable host structure actuated by piezoelectric active materials?

To answer this, the conducted work addressed the modelling, understanding, design and proof of concept of the ability of piezoelectric actuators to provide haptic feedback, by means of switching a bistable system, leading to useful automotive applications. The concept has been filled for a patent.

Conclusions

The main contributions of the conducted work are summarised below:

- **Diversified state of the art that took into account all the elements building the whole picture of the work we want to achieve:** We have first dealt with all the terms that appear in the subject of the thesis, which means presenting in detail the notions of piezoelectricity, bistability, haptic feedback and finally mentioning the link that puts bistability at the service of haptics.
- **Proposition, design and characterisation of two types of bistable inactive structures:** Buckled beams and pre-stressed 'U' shaped double beams are systems that exhibit bistable behaviour. The dimensions of the structures, which are of the order of $70\ mm$ for the largest, give ideas on the levels of forces to be applied for buckling and making bistability appear. We have then the levels of transverse forces to make these bistable systems switch from one equilibrium state to another, which do not exceed $4\ N$. The snap-through phenomenon of a bistable system was modelled with numerical software, including all intermediate steps. The characterisation concerned numerically designed and experimentally prototyped structures.
- **Benchmark on piezoelectric analytical models in the literature, and parametric study to conclude on the validity of these models by comparing with the finite element model:** The comparison of the piezoelectric actuation models concluded on the validity of the pin-moment model with a relative error of the order of a few

percent compared to the numerical model of actuation by piezoelectric ceramics. This allowed us to use the analytical model of piezoelectric actuation, based on pin-moment, in our further study of the application of bistable switching using PZ actuators.

- **Proof of concept on bistable snap-through using piezoelectric actuators and experimental validation of the force and voltage levels involved:** The switching from one stable state to the other using the piezoelectric ceramics was demonstrated. This was done numerically to optimise the system with the given dimensions and experimentally by means of an experimental prototype at the scale of a single bistable system. Duplicating the bistable system into a matrix, with independently operated parts is a relatively difficult question that we tried to answer by introducing a new type of bistable system: the 'U' shaped clips.

- **A new concept for generating haptic feedback:** We have proposed an application to be integrated into the dashboard of a car, which aims to generate haptic feedback. The particularity of such a proposed invention is that it simulates the sensation of a button, that it exploits bistability, i.e. no power is required during switching, that it offers the possibility of hiding the button and that it guarantees a significant travel to feel the deformation of the surface (of the order of $1\ mm$).

Perspectives

A straightforward direction for the future work is to define a good technology transfer strategy. This is a project with experimentally demonstrated research results, for which a proof of concept on a target application has been established. In technology transfer jargon, it is a technical maturity (TRL level 3-5). An application is suspected but the market may not be fully identified. Work on market maturity remains to be done, to identify further specifications for technology transfer.

From a technical point of view, other suggested ideas for future studies can be proposed:

- **Chronological evolution of haptic feedback systems integrating piezoelectric materials:** We have carried out a state of the art study on how to exploit bistability and piezoelectric actuation for haptic feedback.
  We realised that there is a real gap in the picture that gives the chronology of appearance of haptic feedback systems based on intelligent materials.
  The state of the art lacks punctuality and updating on this type of applications.
  One proposal is to list in chronological order the developments in the field of intelligent material-based haptics, as well as their operating principles.

- **Experimental characterisation and validation perspective:** This experimental validation work is not a priority but it can be interesting to validate some points on

buckling models.
The aim is to define experimentally the levels of forces that must be applied to recover the deformed configurations.
For the simple beam for example, we could validate by experiment the levels of axial compression force to make the beam buckle, take the corresponding axial displacements and compare with the curve of axial force vs axial displacement or axial displacement vs transverse displacement. Similarly for the 'U' shaped clips, we can measure the force levels to be applied at the ends for it to buckle and compare with the lateral force curves vs displacement for instance (this has been done analytically and by finite elements).

- **Dynamic piezoelectric actuation models:** A parametric study of static piezoelectric actuation models where the action of piezoelectric patches is replaced by equivalent forces was carried out and compared with a numerical model with voltage-fed piezoelectric patches, and the result was published.
  An intermediate study that could have strengthened the analysis of the models could have been added: it is a hybrid study on the numerical calculation software that involves the analytical formulas of the equivalent forces, while leaving the piezoelectric patches unpowered.
  An other outlook of this part will be to model analytically, trying to have the exact formulas of the piezoelectric action in the case of the dynamic electric supply, then carry out a parametric study to validate the formulae by comparing with the numerical model for instance.

- **Technology, modelling of adhesive layer and the 'U' shaped bistable, miniaturisation:** After the proof of concept of the position and force feedback on a piezo-actuated bistable system, further work is required to achieve a quality level of performance. The feedback must be robust enough that it cannot be blocked by a relatively small force, from a finger.
  Technological questions concerning the power supplies to be used, the control electronics, the integration in the type of application targeted, etc. remain to be addressed.
  The modelling of the adhesive layer used and its impact on the transfer of stresses is a challenge to be met. There is also the possibility of thinking about printing the active material on the host structure, which may be closer to the modelling work we have carried out. Analytical modelling is also to be carried out on the buckling of 'U' shaped bars, as well as the study of their actuation by double moment and comparison with FEM.
  Thinking about miniaturising the system to the size of a finger is an interesting avenue that gives the application further potential for eventual technology transfer to industry.
  Another perspective is to integrate ageing aspects in the design of these devices, for a good understanding of the solicitations undergone by the piezoelectric elements and the system in general.

Appendix A

Equations of piezoelectric equivalent effort modelling

A.1 Pin-force model: uniform strain in the beam and the PZ [BU85; CA90]

Linear elasticity is assumed and the structures comply with Euler-Bernoulli's law (under the assumption of: straight and plane sections remain straight and plane after deformation).

Based on Figure 3.4, the stress on both cross sections is given by:

$$\sigma_p = \frac{F_0}{bt_p} \tag{A.1}$$

in the PZ patch, and

$$\sigma_b = \frac{-F_0}{bt_b} + \frac{F_k}{bt_b} \tag{A.2}$$

in the elastic beam, where F_k which models the general case of an added external force, for instance an axial tension or compression.

PZ patches are excited by the application of a voltage along their polarisation direction. In absence of constraint, the patch strains by the PZ deformation Λ, proportional to the applied voltage. Strains across the surfaces of the perfectly bonded PZ actuator and the beam, supposed constant and equal ($\epsilon_b = \epsilon_p$), are given by:

$$\begin{cases} \epsilon_b = \dfrac{\sigma_b}{E_b} \\ \epsilon_p = \dfrac{\sigma_p}{E_p} + \Lambda \end{cases} \tag{A.3}$$

Substituting equations (A.1) and (A.2) in (A.3), and solving for the force gives:

$$\frac{F_0}{b} = \frac{1}{1+\psi}\frac{F_k}{b} - \frac{1}{1+\psi}E_b t_b \Lambda \qquad \left(\psi = \frac{E_b t_b}{E_p t_p}\right) \tag{A.4}$$

$F_k = 0$ in our case, we find then the expression:

$$\frac{F_0}{b} = -\frac{1}{1+\psi} E_b t_b \Lambda \qquad \left(\psi = \frac{E_b t_b}{E_p t_p}\right) \tag{A.5}$$

A.2 Pin-force model: uniform strain in the PZ, Euler-Bernoulli assumption on the beam [BU85; CA90]

A.2.1 Without flexural stiffness of the PZ actuator

In this bending case (Figure 3.5, the stiffness of the PZ is not considered), we write the moment curvature equation, in Euler-Bernoulli assumption (straight and plane sections remain straight and plane after deformation) as follows:

$$M = F_1 \frac{t_b}{2} = E_b I_b C \tag{A.6}$$

where M is the bending moment of the beam, $I_b = \frac{b t_b^3}{12}$ the second moment of area of the beam, about its neutral axis, and C is the curvature induced in the beam whose expression is given hereafter.

The strain continuity is ensured on the contact surface between the PZ patch and the beam, and can be expressed as follows:

$$-\frac{t_b}{2} C = \epsilon_p = \frac{F_1}{E_p A_p} + \Lambda \tag{A.7}$$

where $A_p = b.t_p$ the PZ actuator section.

Solving for the force from equations (A.6) and (A.7):

$$F_1 = -\frac{b E_b t_b}{3+\psi} \Lambda \tag{A.8}$$

A.2.2 With flexural stiffness of the PZ actuator

The weakness of the previous model as mentioned before, is due to not considering the flexural stiffness of the actuator: the moment curvature equation (A.6) is therefore inaccurate. Besides the beam, the actuator also bends along, and its flexural stiffness should be taken into account in the equation.
In this case (Figure 3.5, the stiffness of the PZ is added), we can rewrite the moment curvature equation, in Euler-Bernoulli assumption, which includes the flexural stiffness of the PZ actuator:

$$F_2 \frac{t_b}{2} = \left(E_b I_b + E_p I_p\right) C \tag{A.9}$$

where

$$I_p = b \frac{(\frac{t_b}{2} + t_p)^3 - (\frac{t_b}{2})^3}{3}$$

the second moment of area of the actuator, about its own neutral axis.
The strain continuity on the contact surface between the PZ and the beam gives:

$$-\frac{t_b}{2}C = \epsilon_p = \frac{F_2}{E_p A_p} + \Lambda \tag{A.10}$$

Solving for the force from equations (A.9) and (A.10):

$$F_2 = -\frac{bE_b t_b}{3 + \psi + \frac{1}{3\widetilde{T}^2}}\Lambda \qquad \widetilde{T} = \frac{t_b}{t_p} \tag{A.11}$$

A.3 Moments model: variant plane deformation assumption along the sections of the beam and the PZ actuator [GF98]

The neutral axis of the beam z_n, defined by zero strain in this case, is modified by the presence of the PZ patch. The force equilibrium in the x direction gives its expression:

$$\int_{-\frac{t_b}{2}}^{\frac{t_b}{2}} \sigma_b b \, \mathrm{d}z + \int_{\frac{t_b}{2}}^{\frac{t_b}{2}+t_p} \sigma_p b \, \mathrm{d}z = 0 \tag{A.12}$$

$$\begin{cases} \sigma_b = E_b \epsilon_x \\ \sigma_p = E_p \left(\epsilon_x - \Lambda\right) \end{cases} \tag{A.13}$$

$$\epsilon_x = -\left(z - z_n\right) \frac{\partial^2 w}{\partial x^2} \tag{A.14}$$

where w is the transverse displacement at the neutral plane of the beam, and $\epsilon_x = \epsilon_x(x, z)$ the strain across the system section.
By combining equations (A.13) and (A.14) in case of no voltage application on the active patch ($\Lambda = 0$), and replacing in equation (A.12), we find:

$$\int_{-\frac{t_b}{2}}^{\frac{t_b}{2}} -E_b(z - z_n)\frac{\partial^2 w}{\partial x^2} \, \mathrm{d}z + \int_{\frac{t_b}{2}}^{\frac{t_b}{2}+t_p} -E_p(z - z_n)\frac{\partial^2 w}{\partial x^2} \, \mathrm{d}z = 0 \tag{A.15}$$

which we solve for z_n, the new position of the neutral axis relative to $z = 0$:

$$z_n = \frac{E_p \left(t_p^2 + t_p t_b\right)}{2\left(E_b t_b + E_p t_p\right)} \tag{A.16}$$

Taking into account the assumptions of Figure 3.7, the strain distribution in the z direction $\epsilon(z)$, within the cross section can be written as:

$$\epsilon(z) = Cz + \epsilon_0 \tag{A.17}$$

where C is the curvature of the beam and ϵ_0 is the $z = 0$ intercept.

Using the new strain distribution (equation (A.17)) and Hooke's law, the stress distribution within the beam and the PZ patch are given as below:

$$\begin{cases} \sigma_b(z) = E_b\left(Cz + \epsilon_0\right) \\ \sigma_p(z) = E_p\left(Cz + \epsilon_0 - \Lambda\right) \end{cases} \tag{A.18}$$

Moment equilibrium about the center of the beam and force equilibrium in the x direction are two equations, in which two unknowns C and ϵ_0 can be determined:

$$\int_{-\frac{t_b}{2}}^{\frac{t_b}{2}} \sigma_b b \,\mathrm{d}z + \int_{\frac{t_b}{2}}^{\frac{t_b}{2}+t_p} \sigma_p b \,\mathrm{d}z = 0 \tag{A.19}$$

$$\int_{-\frac{t_b}{2}}^{\frac{t_b}{2}} \sigma_b z b \,\mathrm{d}z + \int_{\frac{t_b}{2}}^{\frac{t_b}{2}+t_p} \sigma_p z b \,\mathrm{d}z = 0 \tag{A.20}$$

Making the necessary calculations and simplifications leads to:

$$\begin{aligned} C &= K^f \Lambda \\ \epsilon_0 &= K^e \Lambda \end{aligned} \tag{A.21}$$

K^f and K^e are constants, depending on the dimensions and Young modulus of the beam and the PZ patch, their expressions are:

$$\begin{aligned} K^f &= \frac{2}{t_b + t_p}\left(1 - \frac{E_b E_p t_b^3 t_p + E_b^2 t_b^4 + E_p^2 t_p^4 + E_b E_p t_b t_p^3}{E_p^2 t_p^4 + E_b^2 t_b^4 + E_b E_p\left(4t_b^3 t_p + 6t_b^2 t_p^2 + 4t_b t_p^3\right)}\right) \\ K^e &= \frac{t_p^4 + \frac{E_b}{E_p} t_b^3 t_p}{t_p^4 + \frac{E_b^2}{E_p^2} t_b^4 + \frac{E_b}{E_p}\left(4t_b^3 t_p + 6t_b^2 t_p^2 + 4t_b t_p^3\right)} \end{aligned} \tag{A.22}$$

Fanson *et al.* [FC87] and Crawley *et al.* [CL87] show in their works that a voltage-powered patch actually applies moment lines at its ends, on the elastic structure on which it is glued.

The moment applied by the patch on the beam, about a point on the neutral axis of the system, is defined by:

$$\begin{aligned} M &= \int_{\frac{t_b}{2}}^{\frac{t_b}{2}+t_p} -(z - z_n)\sigma_p b \,\mathrm{d}z \\ &= -bE_p \int_{\frac{t_b}{2}}^{\frac{t_b}{2}+t_p} (z - z_n)(Cz + \epsilon_0 - \Lambda) \,\mathrm{d}z \end{aligned} \tag{A.23}$$

Making the necessary calculations and simplifications leads to:

$$\frac{M}{bE_p} = \left(-K^f I_p + \left(K^e - 1 - z_n K^f\right) T - z_n\left(K^e - 1\right) t_p\right) \Lambda \tag{A.24}$$

where $I_p = \frac{\left(\frac{t_b}{2}+t_p\right)^3-\left(\frac{t_b}{2}\right)^3}{3}$ and $T = \frac{\left(\frac{t_b}{2}+t_p\right)^2-\left(\frac{t_b}{2}\right)^2}{2}$ to simplify the formula.

List of Figures

Bibliography

[Tim36] S. Timoshenko. “Theory of Elastic Stability”. In: 1936.

[RS74] J. Van Randeraat and R. Setterington. *Piezoelectric Ceramics*. London, UK, 2nd edn.: Mullard Ltd, 1974.

[Pop76] Egor Paul Popov. *Mechanics of Materials*. 2nd. Englewood Cliffs, N.J. : Prentice-Hall, 1976.

[JV77] R S Johansson and A B Vallbo. “Tactile sensibility in the human hand: relative and absolute densities of four types of mechanoreceptive units in glabrous skin”. In: *J. Physiol* 286 (1977), pp. 283–300. URL: 10.1113/jphysiol.1979.sp012619.

[BU85] T. Bailey and J.E. Ubbard. “Distributed piezoelectric-polymer active vibration control of a cantilever beam”. In: *Journal of Guidance, Control, and Dynamics* 8.5 (1985), pp. 605–611. DOI: 10.2514/3.20029.

[WL85] G. Zorn W. Wersing and K. Lubitz. “Comparison of Piezoelectric Constants of PZT Ceramics with Values Calculated from Electrostrictive Coefficients”. In: *Japanese Journal of Applied Physics* 24 (1985), pp. 721–723. URL: http://iopscience.iop.org/1347-4065/24/S2/724.

[ZWG85] G. Zorn, W. Wersing, and H. Göbel. “Electrostrictive tensor components of PZT-ceramics measured by X-ray diffraction”. In: *Japanese Journal of Applied Physics* 24 (1985), pp. 724–726.

[CL87] E.F. Crawley and J. De Luis. “Use of piezoelectric actuators as elements of intelligent structures”. In: *AIAA JOURNAL* 25 (1987), pp. 1373–1385.

[FC87] J.L. Fanson and J.C. Chen. “Structural control by the use of piezoelectric active members”. In: *CSIC* 87 (1987), pp. 809–829.

[CL89] E.F. Crawley and K.B. Lazarus. “Induced Strain Actuation of Isotropic and Anisotropic Plates”. In: *AIAA Journal* 29(6) (1989), pp. 944–951.

[CA90] E.F. Crawley and E.H. Anderson. “Detailed Models of Piezoceramic Actuation of Beams”. In: *Journal of Intelligent Material Systems and Structures* 1(1) (1990), pp. 4–25.

[EF90] D. M. Moore E. H. Anderson and J. L. Fanson. "Development of an active member using piezoelectric and electrostrictive actuation for control of precision structures". In: *American Institute of Aeronautics and Astronautics* 61 (1990), pp. 2221–2233. URL: http://iopscience.iop.org/0034-4885/61/9/002.

[DFR91] E.K. Dimitriadis, C.R. Fuller, and C.A. Rogers. "Piezoelectric Actuators for Distributed Vibration Excitation of Thin Plates". In: *J. of Vibration and Acoustics* 113(1) (1991), pp. 100–107.

[WR91] B.T. Wang and C.A. Rogers. "Modelling of Finite Length Spatially Distributed Induced Strain Actuators for Laminate Beams and Plates". In: *AIAA Journal* 2(1) (1991), pp. 1511–1520.

[Y91] Xu Y. *Ferroelectric Materials and Their Applications*. North-Holland, 1991.

[CR94] Z. Chaudhry and C.A. Rogers. "The Pin-Force Model Revisited". In: *Journal of Intelligent Material Systems and Structures* 5 (1994), pp. 347–354.

[WF95] Toshio Watanabe and Shigehisa Fukui. "A method for Controlling Tactile Sensation of Surface Roughness Using Ultrasonic Vibration". In: *IEEE International Conference on Robotics and Automation* 6 (1995), pp. 1134–1139.

[YK95] Y. Yang and C. J. Kim. "Testing and characterization of a bistable snapping microactuator based on thermo-mechanical analysis". In: *Proc. Solid-State Sensors Actuators* (1995), pp. 337–340.

[Wag+96] B. Wagner et al. "Bistable microvalve with pneumatically coupled membranes". In: *Proc. IEEE MEMS* (1996), pp. 384–388.

[Dam98] Dragan Damjanovic. "Ferroelectric, dielectric and piezoelectric properties of ferroelectric thin films and ceramics". In: *Reports on Progress in Physics* 61 (1998), pp. 1267–1324. URL: http://iopscience.iop.org/0034-4885/61/9/002.

[GF98] G.P. Gibbs and C.R. Fuller. "Excitation of thin beams using asymmetric piezoelectric actuators". In: *Acoustical Society of America* 89 (1998), pp. 3221–3227. DOI: 10.1121/1.404172. URL: http://acousticalsociety.org/content/terms..

[KP98] E. Kruglick and K. Pister. "Bistable MEMS relays and contact characterization". In: *Solid-state Sensors and Actuators Workshop* (1998), pp. 333–337.

[SSM98] M. Shinohara, Y. Shimizu, and A. Mochizuki. "Three-dimensional tactile display for the blind". In: *IEEE TRANSACTIONS ON REHABILITATION ENGINEERING* 6.3 (1998), pp. 249–256. URL: DOI:%2010.1109/86.712218.

[SFC98] X. Sun, K. Farmer, and W. Carr. "A bistable microrelay based on twosegment multimorph cantilever actuators". In: *IEEE MEMS, Cleveland, OH* (1998), pp. 154–159.

[Van98] Mattias Vangbo. "An analytical analysis of a compressed bistable buckled beam". In: *Sensors and Actuators, A: Physical* 69.3 (1998), pp. 212–216. ISSN: 09244247. DOI: 10.1016/S0924-4247(98)00097-1.

[HKV99] M. Hoffmann, P. Kopka, and E. Voge. "All-silicon bistable micromechanical fiber switch based on advanced bulk micromachining". In: *IEEE J. Select. Topics Quantum Electron* 5.1 (1999), pp. 46–51.

[Bel00] Yves Bellouard. "Conception de dispositifs en alliage à mémoire de forme en microtechnique". PhD thesis. LSRO, EPFL, 2000. URL: 10.5075/epfl-thesis-2308.

[HC00] V. Hayward and M. Cruz-Hernandez. "Tactile Display Device Using Distributed Lateral Skin Stretch". In: *Proc. of the Haptic Interfaces for Virtual Environment and Teleoperator Systems Symposium, ASME IMECE2000, Orlando, Florida, USA* DSC-69-2 (2000), pp. 1309–1314.

[Tah00] M. Taher. "On a tunable bistable MEMS-theory and experiment". In: *Journal of MEMS* 9.2 (2000), pp. 157–170.

[Hay01] Vincent Hayward. "Survey of haptic interface research at mc gill university". In: *Workshop in Interactive Multimodal Telepresence Systems. TUM, Munich, Allemagne* (2001), pp. 91–98.

[Jen+01] B. Jensen et al. "Design optimization of a fully-compliant bistable micromechanism". In: *ASME International Mechanical Engineering Congress and Exposition* (2001), pp. 1–7.

[Pie01] Vincent Piefort. "Finite Element Modelling of Piezoelectric Active Structures". PhD thesis. Université Libre de Bruxelles, 2001. URL: http://scmero.ulb.ac.be/Publications/Thesis/Piefort01.pdf.

[Bor+04] D. Borro et al. "A large haptic device for aircraft engine maintainability". In: *IEEE Computer Graphics and Applications* 24.6 (2004), pp. 70–74. DOI: 10.1109/MCG.2004.45.

[CS04] J. Casals-Terre and A. Shkel. "Dynamic analysis of a snap-action micromechanism". In: *IEEE Sensors* (2004), pp. 1245–1248.

[GG04] Diana A. Galletly and Simon D. Guest. "Bistable composite slit tubes. II. a shell model". In: *International Journal of Solids and Structures* 41 (2004), pp. 4503–4516.

[QLS04] Jin Qiu, Jeffrey H. Lang, and Alexander H. Slocum. "A Curved-Beam Bistable Mechanism". In: *Journal of microelectromechanical systems* 13.2 (2004), pp. 137–146.

[Zha+04] D. Zhang et al. "Piezoelectric 1–3 Composites for High Frequency Ultrasonic Transducer Applications". In: *Ferroelectrics* 304.1 (2004), pp. 201–205. URL: 10.1080/00150190490456781.

[Pig05] François Pigache. "Modélisation causale en vue de la commande d'un translateur piézoélectrique plan pour une application haptique". PhD thesis. L2EP, Université de Lille, 2005.

[Zha+05] Shujun Zhang et al. “Piezoelectric materials for high power, high temperature applications”. In: *Materials Letters* 59 (2005), pp. 3471–3475. URL: 10.1016/j.matlet.2005.06.016.

[RSM06] Jonathan Rossiter, Boyko Stoimenov, and Toshiharu Mukai. “A Bistable Artificial Muscle Actuator”. In: *2006 IEEE International Symposium on Micro-NanoMechanical and Human Science*. 2006, pp. 1–6. DOI: 10.1109/MHS.2006.320317.

[Win+07] Laura Winfield et al. “T-PaD: Tactile Pattern Display through Variable Friction Reduction”. In: *Second Joint EuroHaptics Conference and Symposium on Haptic Interfaces for Virtual Environment and Teleoperator Systems* (2007), pp. 421–426.

[CBB08] R. Corcolle, F. Bouillault, and Y. Bernard. “Modeling of a plate structure with piezoelectric patches: Damping application”. In: *IEEE Transactions on Magnetics* (2008). ISSN: 00189464. DOI: 10.1109/TMAG.2007.916591.

[Cor+08] R. Corcolle et al. “Modeling of a beam structure with piezoelectric materials: introduction to SSD techniques”. In: *COMPEL* 27(1) (2008), pp. 205–214.

[CDB08] Romain Corcolle, Laurent Daniel, and Frédéric Bouillault. “Generic formalism for homogenization of coupled behavior: Application to magnetoelectroelastic behavior”. In: *Phys. Rev. B* 78 (21 Dec. 2008), p. 214110. DOI: 10.1103/PhysRevB.78.214110. URL: https://link.aps.org/doi/10.1103/PhysRevB.78.214110.

[NSG08] A.D. Norman, K.A. Seffen, and S.D. Guest. “Multistable textured shell structures”. In: *3rd CIMTEC conference on smart materials* Acireale, Sicily, Italy, 54 (2008), pp. 168–173. URL: doi:10.4028/www.scientific.net/AST.54.168.

[Sal+08] E. Salaün et al. “Modélisation de structures de type plaque contenant des matériaux piézoélectriques”. In: *RIGE* 11.6 (2008), p. 730. DOI: 10.3166/RIGE.11.717-730.

[CPT09] Luciano C., Banerjee P., and DeFanti T. “Haptics-based virtual reality periodontal training simulator”. In: *Virtual Reality* 13 (2009), pp. 69–85. URL: doi.org/10.1007/s10055-009-0112-7.

[Caz09] Paul Cazottes. “Actionnement des systèmes bistables : modélisation et études expérimentales”. PhD thesis. Institut Jean le Rond d’Alembert, CNRS-UMR 7190 Université Pierre et Marie Curie, 2009.

[Caz+09] Paul Cazottes et al. “Bistable Buckled Beam: Modeling of Actuating Force and Experimental Validations”. In: *Journal of Mechanical Design* 131 (2009), pp. 101001-1–10. URL: 10.1115/1.3179003.

[Duc09] Julien Ducarne. “Modélisation et optimisation de dispositifs non-linéaires d’amortissement de structures par systèmes piézoélectriques commutés”. PhD thesis. Conservatoire National des Arts et Métiers, 2009.

[HH09] Chris Harrison and Scott E. Hudson. "Providing Dynamically Changeable Physical Buttons on a Visual Display". In: *Proceedings of the SIGCHI Conference on Human Factors in Computing SystemsApril* (2009), pp. 299–308. URL: https://doi.org/10.1145/1518701.1518749.

[VSL09] Roman Vitushinsky, Sam Schmitz, and Alfred Ludwig. "Bistable Thin-Film Shape Memory Actuators for Applications in Tactile Displays". In: *Journal of Microelectromechanical Systems* 18.1 (2009), pp. 186–194. DOI: 10.1109/JMEMS.2008.2009816.

[JKB10] Yvonne Jansen, Thorsten Karrer, and Jan Borchers. "MudPad: Tactile Feedback and Haptic Texture Overlay for Touch Surfaces". In: *ACM International Conference on Interactive Tabletops and Surfaces* (2010), pp. 11–14. URL: DOI:%2010.1145/1936652.1936655.

[Def11] Emmanuel Defaÿ. *Integration of Ferroelectric and Piezoelectric Thin Films: Concepts and Applications for Microsystems*. UK: ISTE Ltd, 2011.

[Kaj11] Hiroyuki Kajimoto. "Enlarged electro-tactile display with repeated structure". In: *2011 IEEE World Haptics Conference*. 2011, pp. 575–579. DOI: 10.1109/WHC.2011.5945549.

[SY11] Zhang Shujun and Fapeng Yu. "Piezoelectric Materials for High Temperature Sensors". In: *The American Ceramic Society* 94 (2011), pp. 3153–3170. URL: 10.1111/j.1551-2916.2011.04792.x.

[Har12] Hassan Hariri. "Design and realization of a piezoelectric mobile for cooperative use". Theses. Université Paris Sud - Paris XI, Nov. 2012. URL: https://tel.archives-ouvertes.fr/tel-01124059.

[Fin13] Bruce A. Finlayson. *The Method of Weighted Residuals and Variational Principles*. RICHARD BELLMAN, University of Southern California, 2013. URL: https://doi.org/10.1137/1.9781611973242.

[TMM14] Stephen C. Thompson, Richard J. Meyer, and Douglas C. Markley. "Performance of tonpilz transducers with segmented piezoelectric stacks using materials with high electromechanical coupling coefficient". In: *Acoustical Society of America* 135.1 (2014), pp. 155–164. URL: http://dx.doi.org/10.1121/1.4837217.

[CS15] Jonathon Cleary and Hai-Jun Su. "Modeling and Experimental Validation of Actuating a Bistable Buckled Beam Via Moment Input". In: *ASME. J. Appl. Mech.* 82.5 (2015), pp. 051005-1–7. URL: doi.org/10.1115/1.4030074.

[POH15] Wiwattananon Peerawan, Bergsma Otto K, and Bersee HEN. "Understanding piezoelectric composite–based actuators with nonlinear and 90° domain walls effects". In: *Journal of Intelligent Material Systems and Structures* 27.13 (2015), pp. 1738–1754. URL: https://doi.org/10.1177/1045389X15610900.

[WI15] Jung-Han Woo and Jeong-Guon Ih. "Vibration rendering on a thin plate with actuator array at the periphery". In: *Journal of Sound and Vibration* 349 (2015), pp. 150–162. URL: https://doi.org/10.1016/j.jsv.2015.03.031.

[Ghe16] Sofiane Ghenna. "Approche multimodale pour la conception d'interfaces à retour tactile à plusieurs doigts". PhD thesis. L2EP, Université de Lille, 2016.

[MBL16] Wael Ben Messaoud, Marie-Ange Bueno, and Betty Lemaire-Semail. "Textile Fabrics' Texture: From Multi-level Feature Extraction to Tactile Simulation". In: *International Conference on Human Haptic Sensing and Touch Enabled Computer Applications* 9775 (2016), pp. 294–303. URL: doi.org/10.1007/978-3-319-42324-1_29.

[Vez+16] Eric Vezzoli et al. "Texture Rendering Strategies with a High Fidelity - Capacitive Visual-Haptic Friction Control Device". In: *Proceedings, part I, 10th International Conference on Haptics: Perception, Devices, Control and Applications* 9774 (2016), pp. 251–260. URL: doi.org/10.1007/978-3-319-42321-0_23.

[Bra17] Mouhanned Brahim. "Modeling and Position Control of Piezoelectric Motors". Theses. Université Paris Saclay (COmUE), Oct. 2017. URL: https://tel.archives-ouvertes.fr/tel-01689921.

[HW17] Ryan L. Harne and K.W. Wang. *Harnessing Bistable Structural Dynamics: For Vibration Control, Energy Harvesting and Sensing*. John Wiley Sons Ltd, 2017.

[Maa17] Seifeddine Maaroufi. "Conception et réalisation d'un banc pour l'étude de fiabilité des micros dispositifs piézoélectriques de récupération d'énergie dédiés aux implants cardiaques". PhD thesis. Université Paris-Saclay, 2017. URL: https://tel.archives-ouvertes.fr/tel-01563105/document.

[GB18] James M. Goodman and Sliman J. Bensmaia. "The Neural Basis of Haptic Perception". In: *Stevens' Handbook of Experimental Psychology and Cognitive Neuroscience* Fourth Edition (2018), pp. 1–39. URL: doi.org/10.1002/9781119170174.epcn205.

[Seg18] Valentin Segouin. "Développement d'un outil de Corrélation d'Images Numériques pour la caractérisation du comportement piézoélectrique et ferroélectrique". PhD thesis. CentraleSupelec, Université Paris-Saclay, 2018. URL: https://hal-centralesupelec.archives-ouvertes.fr/tel-01943036v2/document.

[Shc+18] Alexander V. Shchagin et al. "Ceramic Piezoelectric Transformer in Vacuum for Acceleration of Electrons and Production of X-Rays". In: *Acoustical Society of America* 11, 1188 (2018), pp. 1–7. URL: http://dx.doi:10.3390/ma11071188.

[WAN+19] Dangxiao WANG et al. “Haptic display for virtual reality: progress and challenges”. In: *Virtual Reality & Intelligent Hardware* 1.2 (2019), pp. 136–162. URL: DOI:%2010.3724/SP.J.2096-5796.2019.0008.

[Amo20] Achref Amor. “Actionnement des poutres bistables : modélisations statique et dynamique, optimisations et études expérimentales”. Theses. Sorbonne Université, June 2020. URL: https://tel.archives-ouvertes.fr/tel-03135799.

[Kac20] Anis Kaci. “Méthodologie de commande de vibrations multimodales par modulation-démodulation synchrone : application au retour tactile "multi-touch"”. PhD thesis. L2EP, Université de Lille, 2020.

[Ajn+21] Taha Ajnada et al. “Equivalent pin-forces or equivalent moments for the modelling of piezoelectric patches: a parametric study”. In: *Journal of Intelligent Material Systems and Structures* (2021).

[BTS21] Andrew J. Bell, P. Comyn Tim, and Timothy J. Stevenson. “Expanding the application space for piezoelectric materials”. In: *APL Materials* 9.010901 (2021), pp. 1–6. URL: https://doi.org/10.1063/5.0035416.

[SLZ21] Yunlai Shi, Chengshu Lou, and Jun Zhang. “Investigation on a Linear Piezoelectric Actuator Based on Stick-Slip/Scan Excitation”. In: *Actuators 2021* 10.39 (2021), pp. 1–12. URL: https://doi.org/10.3390/act10020039.

Abstract

université PARIS-SACLAY

ÉCOLE DOCTORALE
Physique et ingénierie : électrons, photons, sciences du vivant (EOBE)

Titre : Activation de surfaces bistables par des matériaux piézoélectriques, application au retour haptique

Mots clés : flambement, basculement bistable, actionnement piézoélectrique, modèles équivalents, approche énergétique, modélisation analytique, modélisation numérique

Résumé : L'objectif de cette thèse est de modéliser, concevoir et réaliser un système à retour haptique, basé sur l'activation d'une surface bistable par actionnement piézoélectrique.

L'activation de surface est un enjeu technologique majeur. Parmi les fonctions recherchées, la détection et le positionnement d'un contact sont des défis d'ampleur. Les matériaux piézoélectriques sont particulièrement bien positionnés pour relever ce défi. Ils intègrent par nature les fonctions capteur et actionneur, permettent une conversion électrique-mécanique efficace dans un volume restreint et, moyennant un dimensionnement optimal, peuvent permettre d'obtenir des amplitudes de déplacement intéressantes.

La surface réalisée est constituée d'une structure passive de type poutre rendue bistable, sur laquelle sont collés ou imprimés des actionneurs piézoélectriques. Ces actionneurs sont placés de façon optimale pour minimiser la tension de basculement d'un état d'équilibre stable à l'autre de la structure bistable.

Ce travail fait appel à un large éventail de connaissances dans le domaine de l'ingénierie mécanique et électrique. Deux types de systèmes bistables sont modélisés, prototypés et caractérisés mécaniquement pour comprendre les niveaux de force caractéristiques qu'ils doivent subir pour le basculement bistable. Les modèles d'actionnement piézoélectrique de la littérature sont comparés entre eux, par le biais d'une étude paramétrique, puis comparés à un modèle numérique pour conclure sur leur validité d'usage dans le cas de notre système. Ce résultat est par la suite utilisé pour modéliser l'actionnement des matériaux piézoélectriques sur les structures passives et l'optimiser, afin de réaliser une preuve de concept.

Le travail réalisé incorpore à la fois des aspects 'Matériaux' pour la compréhension des mécanismes physiques à l'œuvre, et des aspects 'systèmes' pour une bonne compréhension des sollicitations subies par les structures.

université PARIS-SACLAY
ÉCOLE DOCTORALE
Physique et ingénierie : électrons, photons, sciences du vivant (EOBE)

Title: Bistable surfaces activation by piezoelectric materials, application to haptic feedback

Keywords: buckling, bistable snap-through, piezoelectric actuation, equivalent models, energy approach, analytical modeling, numerical modeling

Abstract: The objective of this thesis is to model, design and realise a haptic feedback system, based on the activation of a bistable surface by piezoelectric actuation.

Surface activation is a major technological challenge. Among the functions sought, the detection and positioning of a contact are a major issue. Piezoelectric materials are particularly well positioned to meet this defiance. They inherently integrate the sensor and actuator functions, allow efficient electrical-mechanical conversion in a small volume and, with optimal sizing, can achieve interesting displacement ranges.

The surface is made of a passive beam structure made bistable, on which piezoelectric actuators are glued or printed. These actuators are optimally placed to minimise the snap-through voltage from one stable equilibrium state to another of the bistable structure.

This thesis work involves a wide range of knowledge in the field of mechanical and electrical engineering. Two types of bistable systems are modelled, prototyped and mechanically characterised to understand the characteristic force levels they have to endure in bistable snap-through. Piezoelectric actuation models from the literature are compared to each other, through a parametric study, and then compared to a numerical model to conclude on their validity for our system. This result is then used to model and optimise the actuation of piezoelectric materials on passive structures in order to achieve a proof of concept of the intended haptic feedback application.

The work carried out incorporates both 'Materials' aspects for the understanding of the physical mechanisms involved, and 'Systems' aspects for a good understanding of the stresses endured by the structures.

Université Paris-Saclay
Espace Technologique / Immeuble Discovery
Route de l'Orme aux Merisiers RD 128 / 91190 Saint-Aubin, France